Manuscript prepared for Biogeosciences
with version 2014/09/16 7.15 Copernicus papers of the LaTeX class copernicus.cls.
Date: 7 September 2015

New insights into the organic carbon export in the Mediterranean Sea from 3D modeling

A. Guyennon[1], M. Baklouti[1], F. Diaz[1], J. Palmieri[2], J. Beuvier[3,4], C. Lebaupin-Brossier[4], T. Arsouze[5,6], K. Béranger[5], J.-C. Dutay[7], and T. Moutin[1]

[1]Aix Marseille Université, CNRS/INSU, Université de Toulon, IRD, Mediterranean Institute of Oceanography (MIO) UM110, 13288, Marseille, France
[2]Southampton University – National Oceanography Center (NOC), Waterfront Campus, European Way, Southampton SO14 3ZH, UK
[3]Mercator Ocean, Ramonville Saint-Agne, France
[4]CNRM-GAME, Météo-France/CNRS, Toulouse, France
[5]UME, ENSTA-ParisTech, Palaiseau, France
[6]Laboratoire de Météorologie Dynamique, École Polytechnique, Palaiseau, France
[7]LSCE/IPSL, Laboratoire des Sciences du Climat et de l'Environnement, CEA-CNRS-UVSQ, Gif-sur-Yvette, France

Correspondence to: melika.baklouti@mio.osupytheas.fr

Abstract. The Mediterranean Sea is one of the most oligotrophic regions of the oceans, and nutrients have been shown to limit both phytoplankton and bacterial activities, resulting in a potential major role of dissolved organic carbon (DOC) export in the biological pump. Strong DOC accumulation in surface waters is already well-documented, though measurements of DOC stocks and export flux are still sparse and associated with major uncertainties. This study provides the first basin-scale overview and analysis of organic carbon stocks and export fluxes in the Mediterranean Sea through a modeling approach based on a coupled model combining a mechanistic biogeochemical model (Eco3M-MED) and a high-resolution (eddy-resolving) hydrodynamic simulation (NEMO-MED12). The model is shown to reproduce the main spatial and seasonal biogeochemical characteristics of the Mediterranean Sea. Model estimations of carbon export are also of the same order of magnitude as estimations from in situ observations, and their respective spatial patterns are mutually consistent. Strong differences between the western and eastern basins are evidenced by the model for organic carbon export. Though less oligotrophic than the eastern basin, the western basin only supports 39 % of organic carbon (particulate and dissolved) export. Another major result is that except for the Alboran Sea, the DOC contribution to organic carbon export is higher than that of particulate organic carbon (POC) throughout the Mediterranean Sea, especially in the eastern basin. This paper also investigates the seasonality of DOC and POC exports as well as the differences in the processes involved in DOC and POC exports in the light of intracellular quotas. Finally, according to the model, strong phosphate limitation of both bacteria and phytoplankton growth is one of the main drivers of DOC accumulation and therefore of export.

1 Introduction

The biological pump is recognized as a major component of carbon export in the ocean and plays a significant role in the carbon cycle as a whole (Siegenthaler and Sarmiento, 1993). The sinking of organic particles has long been identified as the main process involved in the biological pump, thereby sustaining the vertical carbon and nutrient gradients in the ocean (Eppley and Peterson, 1979; Sarmiento and Gruber, 2006). Considerable attention has therefore been paid to the export of organic carbon in its particulate form.

Advances in the characterization of dissolved organic pools have led to a better knowledge of the role of the dissolved organic carbon (DOC) compartment in the ocean carbon cycle. As a non-sinking tracer, the fate of DOC is strongly linked to physical processes and its export occurs via vertical mixing and/or downwelling when it lies in intermediate waters, and via oceanic overturning circulation in deep water (Hansell et al., 2002, 2009). If the early works of Copin-Montégut and Avril (1993) in the Mediterranean Sea and Carlson et al. (1994) in the Sargasso Sea were the first attempts to quantify DOC export flux below the euphotic zone, estimation of detrital particulate organic carbon (POC) export began years before with the deployment of sediment traps and isotopics measurements (Buesseler, 1991).

The seasonal variability of DOC in the euphotic zone has been widely recorded in the sub-tropical and temperate areas of the ocean (Carlson et al., 1994; Avril, 2002; Hansell and Carlson, 2001; Santinelli et al., 2013). The results of these studies indicate a time lag between DOC production and consumption, causing summer accumulation in the upper layers due to both biotic and abiotic processes, which either alter DOC bioavailability or reduce bacterial activity. The inefficiency of the microbial loop in organic carbon mineralization - the so-called malfunctioning microbial loop (Thingstad et al., 1997) - induces an accumulation of bioavailable DOC. This inefficiency is directly related to low phosphate availability in the upper waters of the Mediterranean Sea (Moutin et al., 2002; Van Wambeke et al., 2002; Thingstad et al., 2005; Santinelli et al., 2013).

In this paper, our aim is to investigate the pathways of organic carbon (OC) at the scale of the Mediterranean Sea, and more specifically to characterize OC export fluxes since this is crucial to determine the efficiency of the biological pump. High resolution 3D modeling using the biogeochemical mechanistic model Eco3M-MED (Alekseenko et al., 2014) forced by the physical model NEMO-MED12 (Beuvier et al., 2012b) was chosen to address this question. Major modeling work has already been done to estimate organic carbon export using box models (e.g. Toggweiler et al., 2003), ocean carbon-cycle models (e.g. Bopp et al., 2001; Sarmiento et al., 1998; Maier-Reimer et al., 1996; Sarmiento and Gruber, 2006) and ecosystem models coupled with hydrodynamic models (e.g. Le Quéré et al., 2010). Several coupled models have also been developed to study the whole of the Mediterranean Sea, starting with the early simulation by Crispi et al. (1998) and Crise et al. (1998). The number of models designed for this purpose is increasing (Lazzari et al., 2013; Mattia et al., 2013; Macías et al., 2014), but to our knowledge, no modeling work has yet focused on or-

ganic carbon fluxes for the entire Mediterranean Sea. Here, our aim is to focus on OC export in the Mediterranean Sea by characterizing and quantifying the associated fluxes, studying their temporal and spatial variability, and providing the first estimations at this scale of the respective contributions of DOC and POC (which refers to the detrital particulate organic carbon only in the present paper) to carbon export. We also aim to analyze the processes involved in DOC and POC production export in the light of the intracellular quotas of planktonic organisms calculated by Eco3M-MED. The paper is organized as follows: After the introduction (Sec. 1), a succinct overview (Sect. 2) of the hydrodynamical model NEMO-MED12 (Sec. 2.1) and the biogeochemical model Eco3M-MED (Sec. 2.2) is provided, given that they are described in detail in the aforementioned papers. Simulation set-up and datasets used for model comparison are also presented. Sect. 3 first focuses on the results related to organic carbon inventory and export at the scale of the Mediterranean Basin, and for the purpose of discussion results on intracellular quotas in phytoplankton and bacteria as well as on exudation fluxes are also presented. In Sect. 4 results on export are discussed in the context of previous POC and DOC export evaluations in the Mediterranean Sea, and in the light of processes and intracellular quotas in phytoplankton and bacteria. Finally, an appendix is associated with this paper containing the assessment of the biogeochemical model outputs (nutrients, chlorophyll, primary production and DOC) through comparison with available data and analysis of the main discrepancies.

2 Material and methods

2.1 The hydrodynamic model

The physical run used in this work is described in Beuvier et al. (2012b). It has been simulated by the regional circulation model NEMO-MED12 Beuvier et al. (2012a) which is part of a suite of Mediterranean regional versions of OPA and NEMO (Madec and The-NEMO-Team, 2008) as OPAMED16 (Béranger et al., 2005), OPAMED8 (Somot et al., 2006) and NEMO-MED8 (Beuvier et al., 2010).

Model resolution is 1/12 ° ($\approx$ 8 km) which means that most of the mesoscale features are explicitely resolved, and the domain includes the whole of the Mediterranean Sea as well as the Atlantic Ocean West of 11°W (Fig. 2). More details of the model and its parametrization are given in Beuvier et al. (2012a).

The simulation was initiated in October 1958 with temperature and salinity data representative of the 1955–1965 period using the MEDATLAS dataset (MEDAR/MEDATLAS-Group 2002, Rixen et al., 2005). Atmosphere forcings are applied daily and come from the ARPERA dataset (Herrmann and Somot, 2008), a 55-year simulation at 50 km and daily resolutions. SST-relaxation and water-flux correction terms, as well as fresh water input from rivers and the Black Sea and Atlantic exchanges are the same as described in Beuvier et al. (2010, 2012a).

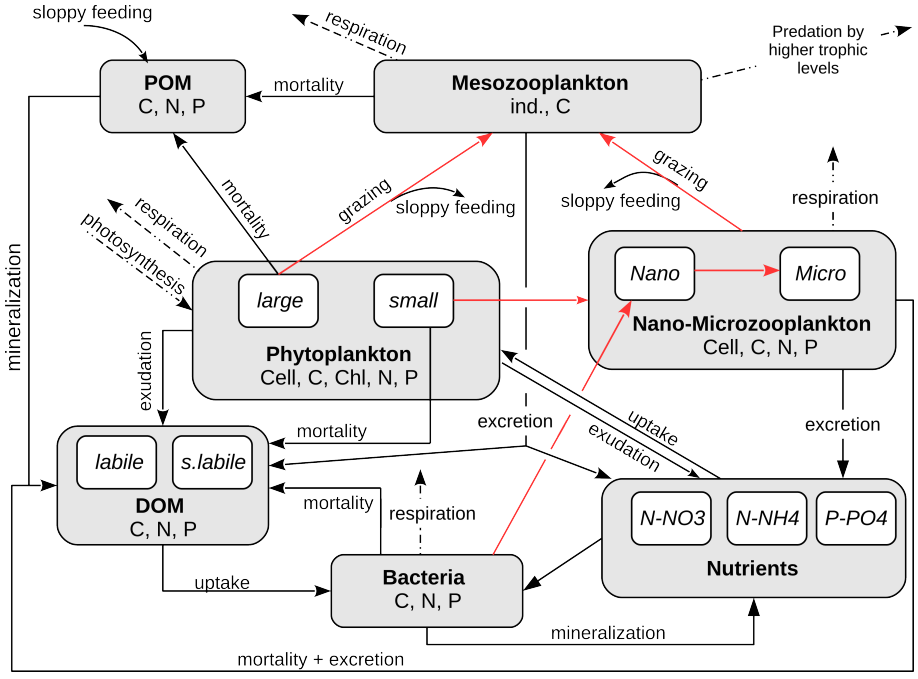

Figure 1. Conceptual diagram of the biogeochemical model Eco3M-MED. Grey boxes represent major compartments and white boxes sub-compartments. State variables for each sub-compartment are listed at the bottom of compartment boxes. Red arrows indicate grazing processes from the prey to the predator.

2.2 The biogeochemical model

The biogeochemical model Eco3M-MED is embedded in the Eco3M modular numerical tool (Baklouti et al., 2006b), and its structure is similar to the model presented in Alekseenko et al. (2014). Fig. 1 summarizes the interactions between the state variables through the biogeochemical processes. We chose to represent three different element cycles C, N and P in order to reproduce the different limitations and co-limitations observed in the Mediterranean Sea. Silicium, potentially limiting in some regions (Leblanc et al., 2003) is not represented in the model, as P and N limitations are the most common ones in the Mediterranean Sea. Six different planktonic functional types (P.F.T., see Le Quéré et al. (2005) for a proper definition) are represented : 2 primary producers (phytoplankton), 1 decomposer (heterotrophic bacteria) and 3 consumers (nano-, micro- and meso-zooplanktons). The structure of the trophic web thereby includes the main P.F.T.s of the Mediterranean Sea (Siokou-Frangou et al., 2010).

Each P.F.T. of the model is represented through several state variables, namely C, N, P (and Chl for producers) concentrations and a cell number (i.e. an abundance), except for meso-zooplankton which is only represented through its C concentration and its abundance (in individuals per unit volume). Intracellular ratios (i.e. the ratio between two elemental concentrations) as well as intracellular quotas (i.e. the quantity of a given element per cell) can therefore be calculated dynamically

by the model. Intracellular ratios are indicators of plankton stoichiometry, i.e. of its C:N:P elemental composition. Early biogeochemical models (NPZD models) have considered a constant C:N:P ratio in plankton given by the canonical Refield ratio of 106:16:1 (Redfield, 1958). Based on Droop's work (e.g. Droop, 1968, 1975), an increasing number of biogeochemical models (e.g. Baretta et al., 1995; Geider et al., 1998) have in recent decades assumed flexible plankton stoichiometry. Though Droop's original quota function relating growth rate to the intracellular quota of the limiting element was based on cell quotas, these biogeochemical models have used intracellular ratios instead of quotas to regulate the rate of biomass synthesis (and other process rates) with quota functions similar to that of Droop. These flexible stoichiometry models have been widely used in the framework of theoretical batch or chemostat studies (e.g. Geider et al., 1998; Baklouti et al., 2006b) or for large-scale studies with ERSEM (Baretta et al., 1995), BFM (Vichi et al., 2007) or others (e.g. Moore et al., 2002) models. In such models, substrate uptake and biomass synthesis are decoupled, but cell division is not explicitly represented.

Intracellular quotas (or cell quotas) as they are defined in the present paper are indicators of the C, N and P cellular content of plankton. They are an original feature of the Eco3M-MED model in the category of 3D coupled physical-biogeochemical models. This model is based on the assumption that there are a minimum ($Q_X^{\min}$) and a maximum ($Q_X^{\max}$) intracellular content for each element X among (C, N, P). $Q_X^{\min}$ can be interpreted as the amount of element X used in cellular structure and machinery, and the accumulated surplus as storage for future growth (Klausmeier et al., 2008). The variability in cell quotas has indeed been widely evidenced through several experimental and in situ studies (e.g. Brown and Harris, 1978; Fukuda et al., 1998; Lovdal et al., 2008; Heldal et al., 2003; Bertilsson et al., 2003; Wilhelm et al., 2013).

The use of cell numbers as state variables and of the associated intracellular quotas offers several advantages: firstly, it makes it possible to distinguish between cell division, which is described by a specific equation, see Eq. 1), biomass synthesis, and uptake. Second, intracellular quotas are indicative of the actual internal status of cells, i.e. they indicate whether cells are rich or depleted in a given element, while intracellular ratios only provide relative values. In other words, a given value of intracellular ratio Q_{XY} can correspond to several different cell statuses (for example, a given C:N ratio can be obtained with an infinity of pairs of C and N intracellular concentration values). Thus, intracellular ratios can only provide information on the internal relative quantity of X as compared to that of Y, while intracellular quotas inform on intracellular absolute quantities. The latter information is very useful for the analysis of plankton dynamics since it is informative about the nutritional status of each P.F.T. of the trophic web (see the Discussion section). It is also a good proxy of the quality of the prey available for zooplankton (i.e. whether prey are rich or depleted in a given element). Thirdly, the parameters determined at cell level can be used without using conversion factors. For example, uptake rate measured at cell level (Talarmin et al., 2011), or grazing parameters expressed

in number of prey per predator per unit time, such as the ones provided in Christaki et al. (2009) for HNF and ciliates can be used directly.

Intracellular quotas have already been used in previous modeling studies to study phytoplankton growth (Klausmeier et al., 2004) or the dynamics of the planktonic food web (Thingstad et al., 2005). In the latter study, however, cell quotas of carbon were assumed to be fixed in the protozoa, while fixed C:N-ratios were assumed for bacteria and phytoplankton. Moreover, this model was used without being coupled with a physical model (i.e. for the simulation of microcosm and lagrangian experiments).

In the model, the producers are split into two different P.F.T.s according to their theoretical size, i.e. large phytoplankton (> 10 μm) mainly encompassing diatoms, and small phytoplankton (< 10 μm) which includes picophytoplankton and the remaining nanophytoplankton. The two P.F.T.s have different parameters, distinct predators and fuel different detritic pools (Fig. 1). Decomposers are represented by heterotrophic bacteria and are responsible for the organic matter mineralization, including hydrolysis of particles. Zooplankton is divided into three different size groups, heterotrophic nanoflagellate (HNF) which feeds on bacteria and small phytoplankton, ciliate which feeds on small phytoplankton and HNF, and mesozooplankton (copepods) which feeds on ciliate, HNF and large phytoplankton. Copepods are the only metazoans in the model, and mechanisms such as individual growth, egg production or reproduction are implicitely represented (Alekseenko et al., 2014).

The processes used in the model are extensively described in the aforementioned reference. However, for the purposes of the present paper, we recall that POC is fueled by the natural mortality of largest organisms (mesozooplankton, diatoms and ciliates) and by the egestion of fecal pellets and sloppy feeding by mesozooplankton, and consumed by POC hydrolysis to DOC. The DOC pool has many inputs (phytoplankton exudation, zooplankton excretion, mortality of small organisms, POC hydrolysis) and a single output (uptake by bacteria). The formulations of most of the biogeochemical processes, for which details are extensively given in Baklouti et al. (2006a, 2011); Mauriac et al. (2011), and Alekseenko et al. (2014), follow cell level mechanistic considerations. Intracellular ratios (Q_{XY}) and intracellular quotas (Q_X) are used to regulate growth via Droop's quota function (Droop, 1968) and net uptake and grazing rates via Geider's limitation formulation (Geider et al., 1998). For example, the specific growth rate (i.e. the division rate) μ of all unicellulars in the model is given by the following equation:

$$\mu = \mu^{\max} \min_{X \in \{\mathrm{C,\,N,\,P}\}} \left(1 - \frac{Q_X^{min}}{Q_X}\right) \tag{1}$$

where $\mu^{\max}$ is the maximum division rate and $Q_X^{\min}$ the minimum intracellular X quota.

Grazing, primary production and uptake rates are controlled firstly by the organism's environment (either prey or nutrient concentration, or light availibility). Secondly, the internal cell status represented by intracellular quotas and ratios drives a feedback regulation of the net incorporated biomass

through quota functions. Hence, the uptaken surplus (which becomes more and more significant as the intracellular quota approaches Q^{max}) is either released in its initial form or exuded in the form of DOM. In the same way, excretion and fecal pellet production fluxes are proportional to the grazing flux and to a quota function the value of which increases as the quota approaches Q^{max}. Furthermore, 10 % of the material grazed by mesozooplankton directly fuels the particulate organic matter stock, to represent sloppy feeding. Respiration rates are estimated via energy costs for every plankton activity (Alekseenko et al., 2014). Nitrification is represented through first order kinetics while particulate hydrolysis function depends on bacteria intracellular quotas (POC hydrolysis increases with bacterial C-limitation). Grazing by higher trophic levels is implicitely taken into account via quadratic mortality affecting only mesozooplankton. Grazing function is a Holling II type (Holling, 1959; Kooijman, 2000) for multiple prey. The only difference with the configuration of Alekseenko et al. (2014) lies in the formulation used to represent predator preferences for multiple prey. We here used the "Kill The Winner" (KTW) formulation depicted in Vallina et al. (2014), which combines active-switching (i.e. the preference of a predator for a given prey depends on prey density) and an ingestion rate always increasing with the total biomass of prey. This active-switching formulation was used to preserve foodweb diversity (e.g Prowe et al., 2012) and to prevent unrealistic predator-prey oscillations.

Since the model relies on a mechanistic basis, parameters are mainly physiological (and measurable) and they were either taken from literature or derived from other parameters on the basis of physiological considerations and in the interests of greater consistency between parameters. For example, maximum intracellular quotas are inferred from minimum ones as done in Thingstad et al. (2005). Another example lies in the relationship between the maximum uptake rate of a given element, which is the product of the maximum specific growth rate and the maximum intracellular quota in that element. Other examples as well as the whole set of parameters are given in Alekseenko et al. (2014).

2.3 Model coupling

The models NEMO and Eco3M-MED have been associated for the first time. The coupling between the hydrodynamic and biogeochemical models is offline, i.e. biological retroaction on the physics is not taken into account. Daily-averaged water velocities were used for the advection of biogeochemical tracers, using a MUSCL scheme (horizontal and vertical diffusion fluxes are calculated according to a centered scheme). The time-step used for the numerical integration of the tracer conservation equations equals 1200 s. A sinking velocity of 2 m d^{-1} is applied only on the particulate organic pool (i.e. the detrital compartment). The aim of this compartment is to represent particles with different sizes and sinking velocities and the value of 2 m d^{-1} is within the usual range found in the litterature (Vichi et al., 2007; Fasham et al., 2006). Light attenuation in the water column is modeled via the formulation of Morel (1988).

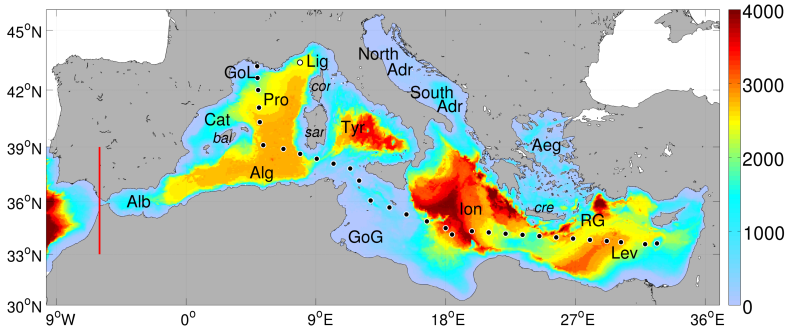

Figure 2. Bathymetry of the grid in meters, black dots represent the BOUM cruise stations (Moutin et al., 2012a) while white dot is DyFaMed position (Marty and Chiavérini, 2010). The area west of the red line constitutes the buffer-zone. Acronyms indicate different sub-basin names and islands (in italic). Terminology is taken from Millot and Taupier-Letage (2005). From west to east, **Alb** stands for Alboran Sea, **Cat** for Catalan Sea, **GoL** for Gulf of Lions, **Pro** for Provencal sub-basin, **Alg** for Algerian basin, **Lig** for Ligurian Sea, **Tyr** for Tyrrhenian Sea, **GoG** for Gulf of Gabes, **North Adr** and **South Adr** for north and south Adriatic Sea respectively, **Ion** for Ionian sub-basin, **Aeg** for Aegean Sea, **Lev** for Levantine sub-basin and **RG** for Rhodes Gyre. Major islands names are also plotted, *bal* stands for the Balearic islands, *sar* for Sardinia, *Cor* for corsica, *cre* for Crete.

2.4 Initial and boundary biogeochemical conditions

Initial nutrient and chlorophyll fields are derived from annual means of Mediterranean Sea climatological data (Schaap and Lowry, 2010). The remaining biogeochemical variables are derived from chlorophyll using conversion factors derived from published works (see Alekseenko et al. (2014) for details).

A "buffer-zone" has been defined between the domain western boundary and the Gibraltar Strait (from 11°W to 6°W), in which a damping procedure towards Atlantic conditions has been applied. The restoring time is 2 days west of 7.5°W, linearly increasing to 90 days from 7.5°W to 6°W (Fig. 2). Atlantic nutrient concentrations come from the World Ocean Atlas monthly climatology (Garcia et al., 2006), so that the nutrients damping in the "buffer-zone" takes into account the nutrients' monthly variability. Given the inaccuracies in phosphate measurements, we decided to compute phosphate profiles from that of nitrate by imposing a redfield ratio of 16 in order to be more consistent with observed NO_3:PO_4 ratios in this region (Gómez, 2003). Chlorophyll concentrations were not provided in this database. We therefore used in situ data from the SeaDataNet database to create a mean vertical chlorophyll profile for the Atlantic, and then used a climatology of surface chlorophyll from the GlobColour product in this region to represent an annual cycle of the chlorophyll vertical

profile. The remaining Atlantic biogeochemical variables were derived from chlorophyll using the same procedure as for initial conditions.

Nutrient (NO_3 and PO_4) inputs from riverine influx and coastal runoffs are derived from Ludwig et al. (2009), following the same procedure as for the riverine freshwater inputs in the circulation model (Beuvier et al., 2010, 2012b). The nutrient influx of the 29 rivers included in the RivDis database (Vörösmarty et al., 1996) are taken into account in the simulation, while the nutrients of the remaining rivers from the Ludwig et al. (2009) database are averaged for every sub-basin and distributed along their respective sub-basin's coast as coastal runoffs. Dissolved organic carbon inputs in the Mediterranean Sea are distributed in every sub-basin according to the riverine DOC estimates of Ludwig (1996) (a total of $\sim$ 1.8 Tg C y^{-1} in the whole of the Mediterranean Sea). Sub-basin DOC inputs were then distributed among fluvial estuarine and coastal runoffs to match circulation model freshwater geographical distribution (Palmiéri, 2014; Palmiéri et al., in prep).

Mass exchanges with the Black Sea in the Dardanelles Strait are treated as river inputs, with nutrients and DOC input concentrations provided by the SESAME project (Tugrul and Besiktepe, 2007; Meador et al., 2010). But, since NO_3 budget indicates a negative net flux of NO_3 the Dardanelles Strait (i.e. exiting from the Mediterranean), NO_3 flux at Dardanelles is set to zero and the outcome is transferred on the Aegean sub-basin's runoffs. These runoffs are artificially reduced in order to keep the riverine budget of NO_3 in the Aegean sub-basin realistic.

2.5 Simulation set-up

Using the biogeochemical initial conditions defined in Sect. 2.4, we have conducted a 5 years simulation using physical forcings from the years 1973-1977. This first simulation was considered as a 'spin-up', in order to reduce the impact of state variables adjustment in the simulations. It has deliberately been done long enough before the Eastern Mediterranean Transient period (starting around 1991) which is not stable enough to be chosen as a spin-up period. Moreover, due to high computational costs, it was not possible to run this first simulation until the year 1996. We therefore used the final biogeochemical state of this spin-up as initial conditions for a second simulation running from 1996 to 2012. In this second simulation, only the years following 1998 are considered, since the first 3 years were treated as an additional spin-up beyond which the stability of the run was ensured (i.e. no drift could be observed).

2.6 Data description

The aim of the present work is to study and to quantify organic carbon export fluxes using a 3D physical-biogeochemical model. For this purpose, our first aim was to assess the reliability of our model by examining the agreement between different model outputs and corresponding available data : chlorophyll, nutrients, DOC concentrations and primary production rates.

Three type of comparisons were undertaken : (i) at basin scale, using surface chlorophyll fields provided by satellite for comparisons (ii) at basin scale, using BOUM cruise transect as a "snapshot" to compare nutrients and DOC vertical profiles during the stratified period (iii) at a local scale using the time series data collected at DyFaMed station

2.6.1 Chlorophyll data derived from satellite

Among the specificities of the Mediterranean Sea, its strong oligotrophy and the major influence of colored dissolved organic matter, make the use of classical satellite chlorophyll products difficult (e.g. Claustre et al., 2002). Several algorithms have already been developed (Bosc et al., 2004; D'Ortenzio et al., 2002; Volpe et al., 2007), using different satellite reflectances and datasets. Here, we used a daily surface chlorophyll product delivered by the Myocean project (http://www.myocean.eu). In this product, chorophyll concentrations have been derived using the MEDOC4 algorithm developped by Volpe et al. (2007). This algorithm was built using a large dataset of chlorophyll concentrations collected in situ and reflectance measurements from 3 satellites (Seawifs, MERIS and MODIS), constituting a homogeneous series from September 1997 to March 2012.

2.6.2 The BOUM cruise data

The BOUM cruise took place during summer 2008 (from June 16 to July 20) and traversed both the western and eastern basins of the Mediterranean Sea (Moutin et al., 2012a). The data acquired during this cruise provide a unique picture of the biogeochemical status of the Mediterranean Sea since many biogeochemical variables were observed. Measurements of nutrients and DOC concentrations were used to perform a basin-scale comparison during the summer stratified period with the model outputs obtained at the same dates as the cruise, and averaged over this period.

2.6.3 The DyFaMed station data

The DyFaMed station is located in the Ligurian Sea at 7.9°E and 43.4°N (Fig. 2) and is isolated from coastal inputs by the Mediterranean Northern Current. A strong winter mixing is observed in this area, although it is less intensive than the deep convection occuring in the Provencal sub-basin (Marshall and Schott, 1999). Nutrients (Pasqueron de Fommervault et al., 2015), chlorophyll (Marty et al., 2008), dissolved organic carbon (Avril, 2002) and primary production rates (Marty et al., 2008) time series were used for comparison. The comparison of the model outputs with DyFaMed time series can be done through different methods. The simplest consists in using a single grid point which is the nearest to the DyFaMed station location. This implies that the model perfectly reproduces spatial patterns in this region, which is obviously never the case. On the other hand, the use of model outputs averaged on several grid points around the DyFaMed station amounts to dampening signal variability. We finally chose to use the nearest gridpoint to the DyFaMed station, while assessing spatial variability in the 8 neighbouring grid points (Table 2).

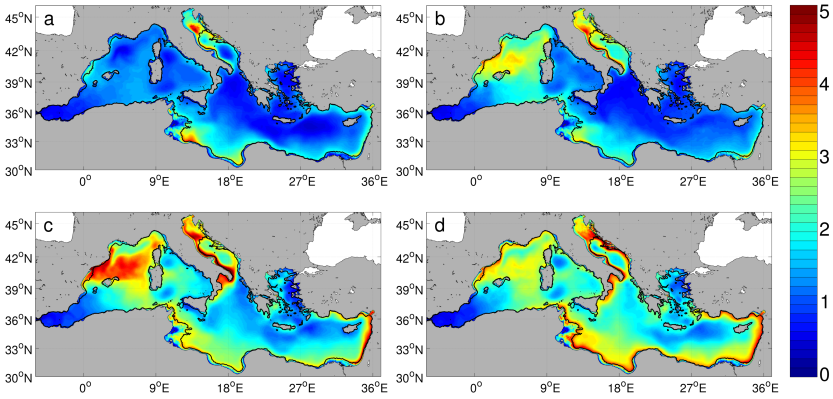

Figure 3. Modeled dissolved organic carbon inventory (mol m^{-2}) integrated over the first 100 m. Maps are averaged over the 2000-2012 period in (a) winter (Dec.-Feb.), (b) spring (Mar.-May), (c) summer (Jun.-Aug.), (d) autumn (Sept.-Nov.).

3 Results

3.1 Organic carbon inventory and export

3.1.1 Dissolved organic carbon inventory

In the following section, mDOC refers to the modeled dissolved organic carbon integrated over the first 100 m of the water column. Seasonal variations of mDOC are given in Fig. 3. Low mDOC values (< 1 mol m^{-2}) are observed throughout the year in the Alboran Sea (and up to the Balearic Islands), the North Levantine basin, and in some well marked structures in the Tyrrhenian Sea. In contrast, very high mDOC values (up to 5 mol m^{-2}) can be found throughout in the North Adriatic Sea and along the Lybian Coast. Apart from these regions, mDOC is low everywhere (below 2 mol m^{-2}) in winter (Fig. 3 a), and this is also true in spring except in the region of the spring bloom in the Provencal sub-basin. In the western basin, highest DOC concentrations are generally observed in summer, with values reaching 4 mol m^{-2} in the bloom region of the Liguro-Provencal sub-basin. In the eastern basin, they are reached in autumn and mostly concern the Adriatic Sea, and the regions along the southern and eastern coasts.

3.1.2 Particulate organic carbon inventory

In what follows, mPOC refers to the modeled particulate organic carbon integrated over the first 100 m of the water column. Seasonal variations of mPOC are given in Fig. 4. Unlike mDOC, mPOC highest values are observed in winter and spring. This is mostly true for the western basin since, in the eastern basin, mPOC remains low (< 0.05 mol m^{-2}) all over the year, except for the Adriatic

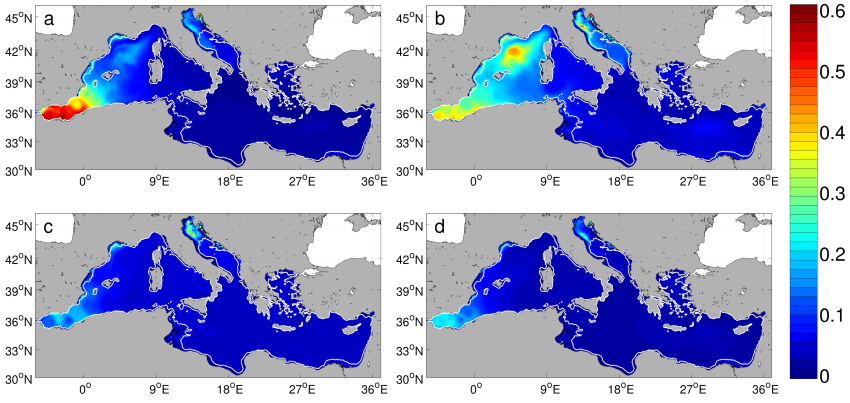

Figure 4. Modeled particulate organic carbon inventory (mol m^{-2}) integrated over the first 100 m. Maps are averaged over the 2000-2012 period in (a) winter (Dec.-Feb.), (b) spring (Mar.-May), (c) summer (Jun.-Aug.), (d) autumn (Sept.-Nov.). White lines are the 0 m and 100 m isolines.

Sea and a local maximum in the Rhodes Gyre distinguishable in spring. During winter (Fig. 4 a), the highest values of mPOC (> 0.5 mol m^{-2}) are found in the region of the Alboran Sea and the surrounding Balearic Islands and also in the Liguro-Provencal sub-basin though with much lower concentrations. In the Adriatic Sea, mPOC is in the range [0.1;0.2] mol m^{-2}. Elsewhere, mPOC is low (< 0.2 mol m^{-2}). During spring (Fig. 4 b), the maximum mPOC is observed in the region of the bloom in the Provencal sub-basin (≈ 0.4 mol m^{-2}) and the North Adriatic Sea. During summer and autumn (Fig. 4 c and d), overall values are low (< 0.05 mol m^{-2}), except in the Alboran Sea (where values reach 0.3 mol m^{-2}) and in the North Adriatic Sea.

3.1.3 Dissolved and particulate organic carbon export

Organic carbon fluxes are computed by adding the contribution of advection (vertical velocity and settling velocity for POC) and vertical diffusion (implicitly representing turbulent and convective mixing) fluxes across an horizontal section of the grid. Negative fluxes account for downward fluxes. For clarity, modeled fluxes will be referred to as F_{DOC} , F_{POC} and F_{OC} as the sum of the latter two. F_{DOC} and F_{POC} have been computed at 100 m and 200 m so as to include most of the productive layer and to allow the comparison in space and time between regions. These depths are also used in several other modeling studies (Lévy et al., 1998; Bopp et al., 2001).

The yearly amount of mOC export at 100 m is equal to 48.4 MtC y^{-1}. The eastern basin is the main contributor to this export with a total export of 28.7 against 19.7 MtC y^{-1} for the western basin. mDOC export is equal to 38.8 MtC y^{-1}, and comparatively, river inputs of mDOC are equal to 1.8 MtC y^{-1}, thereby representing less than 5% of the exported mDOC. mDOC contribution to the total organic carbon flux is dominant. In the western basin, the total amounts of exported mPOC

and mDOC below 100 m are respectively 7.0 MtC y^{-1} and 12.7 MtC y^{-1}, meaning that 64 % of this export is due to DOC. In the eastern basin, DOC is responsible for 90 % of the organic carbon export below 100 m, with an annual flux of 26.1 (against 2.6 for POC) MtC y^{-1}.

3.1.4 Spatial variability of export fluxes

Mean F_{OC} over the whole basin equals -22.8 gC m^{-2} y^{-1}, but a wide spatial variability can be observed in Fig. 5. Hence, the main regions of mOC export are the Liguro-Provencal sub-basin, the Alboran Sea, the southern continental slopes and the Adriatic Sea.

In the western basin, high positive values (i.e. upward) of F_{DOC} are simulated along the French and Spanish coasts, the entrance to the Sicilian Strait and north-eastern Excluding these areas, the highest downward fluxes of DOC are calculated in the Provencal sub-basin (especially in the region of deep convection), the north of the Balearic Islands and along the Algerian slope, where downward F_{DOC} can be higher than 60 gC m^{-2} y^{-1}.

In the eastern basin, the complexity of topography and hydrodynamic regimes in the Aegean Sea may explain the high heterogeneity of the fluxes calculated in this region that are difficult to interpret. Highest downward F_{DOC} values are located along the continental slope from the Libyan to the Turkish coasts and in the Adriatic Sea. Elsewhere (i.e. in the open sea), F_{DOC} distribution is more homogeneous, with a median of -17 gC m^{-2} y^{-1}.

A strong difference exists between the western and eastern basins regarding F_{POC} at 100 m. The mean value of downward F_{POC} throughout the western basin is -9.8 gC.m^{-2}.y^{-1} against -2.4 gC m^{-2} y^{-1} in the eastern basin (Fig. 5 bottom).

In the western basin, F_{POC} is the highest in the Alboran Sea, particularly in the south east of the easily identifiable anticyclonic eddies. Following the pathway of the Atlantic waters, downward F_{POC} values decrease to reach absolute values lower than 5 gC m^{-2} y^{-1} in the Tyrrhenian Sea. In the Provencal basin high POC fluxes linked to the deep convection, with values ranging from -15 to -30 gC m^{-2} y^{-1} have been modeled. Throughout the eastern basin, F_{POC} is low except in the Adriatic Sea.

Finally, as suggested in Fig. 5, the spatial correlation between POC and DOC fluxes is weak almost everywhere. Regions of high POC or DOC export generally do not match. The only areas associated with both high POC and DOC exports are the Algerian coast, the Adriatic coast, the regions of deep convection and a band east of the Balearic Islands.

3.1.5 Seasonal variability

The seasonal variability and the spatial distribution of F_{DOC} and F_{POC} differ significantly (Fig. 6 and 7). In winter (Fig. 6a), F_{DOC} values are high in almost all of the Mediterranean Basin except the Alboran Sea, with maximum values that can be observed in the Provencal sub-basin and along the continental slopes, especially along the southern and eastern coasts of the eastern basin. F_{DOC}

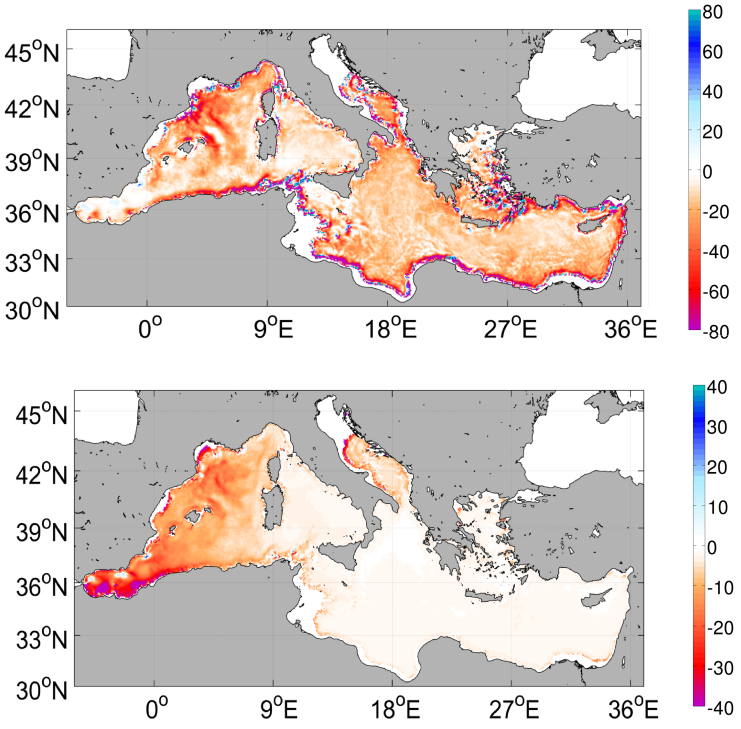

Figure 5. Maps of modeled annual DOC fluxes (top) and POC fluxes (bottom) below the 100 m layer in gC m^{-2} y^{-1}. Note the colorscale differences. Negative (red) means a downward flux.

distribution is quite similar in autumn, though with values that are significantly lower everywhere. During the rest of the year, F_{DOC} values are very low in spring nearly everywhere, and almost null in summer. In several areas (Tyrrhenian and Adriatic Seas, Levantine and Ionian basins), high downward F_{DOC} values are observed in winter while they are almost null during the rest of the year.

High downward POC fluxes at 100 m were calculated from winter to spring west of 7°E, namely in the Alboran Sea and the Provencal sub-basin (Fig. 7). In these regions, maximum values are reached in late winter (February-March) in the Alboran Sea, and in spring (March-April) in the Algerian Sea and the Provencal sub-basin. POC export in the eastern basin (excluding the Adriatic Sea) is very weak (even in the Rhodes Gyre) all year long. Maximum values can however be identified in spring in the Tyrrhenian Sea, the Levantine basins (except for the Rhodes Gyre where the maximum is earlier in winter) and in the Adriatic Sea.

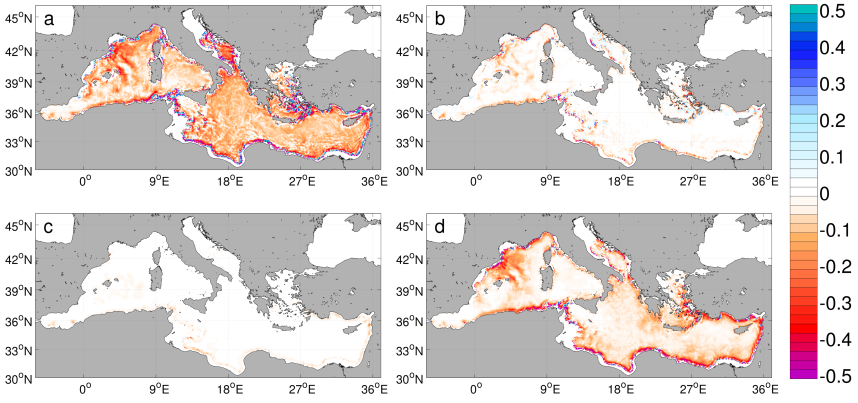

Figure 6. Maps of modeled DOC fluxes across the 100 m layer (F_{DOC}) in gC m^{-2} d^{-1} in (a) winter (Dec.-Feb.), (b) spring (Mar.-May), (c) summer (Jun.-Aug.), (d) autumn (Sept.-Nov.). Negative (red) means a downward flux.

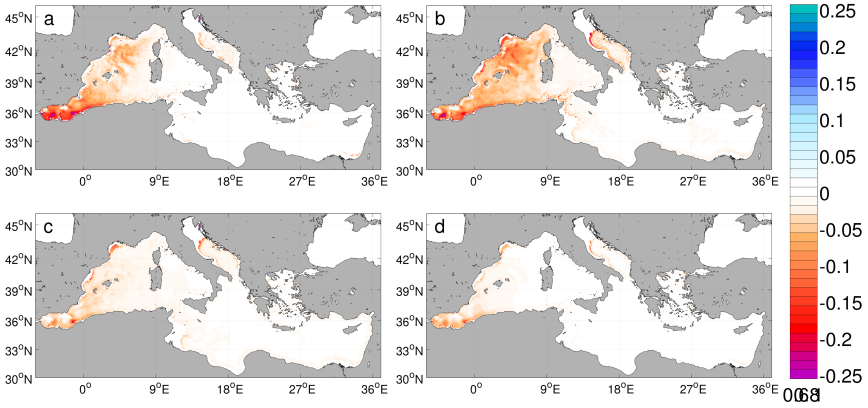

Figure 7. Maps of modeled POC fluxes across the 100 m layer F_{POC} in gC m^{-2} d^{-1} in (a) winter (Dec.-Feb.), (b) spring (Mar.-May), (c) summer (Jun.-Aug.), (d) autumn (Sept.-Nov.). Negative (red) means a downward flux.

3.1.6 Export below 200 m

Below 100 m, organic carbon is progressively consumed via the bacterial activity and respiration. At 200 m, the calculated mean export fluxes of total organic carbon are reduced by almost 87 % and 64 % compared to those at 100 m, respectively in the western and eastern basins. However, the ratio between export at these two depths is highly variable, depending on the region (see Fig. 8).

For POC (Fig. 8 a), if we consider first the regions where the annual F_{POC} values are significant, i.e. west of 7°E, (see Fig. 5 bottom), the 200 m to 100 m ratio is lower than 0.25 (i.e. only 25 % of

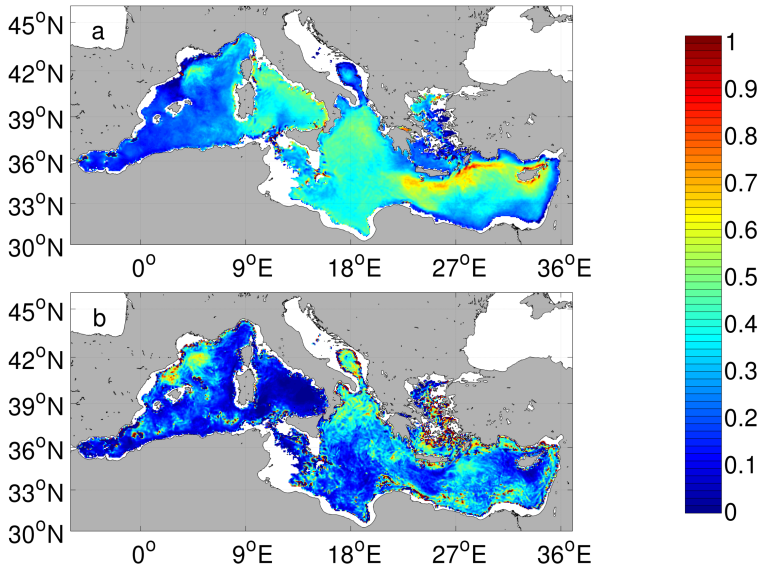

Figure 8. Ratio between export fluxes at 200 m and at 100 m (a) for POC, (b) for DOC.

the carbon exported at 100 m goes below 200 m) in a region including the Alboran Sea, the western Algerian Sea and the Balearic Sea. This ratio is slighly higher but still below 0.3 for the central Algerian Sea and the Adriatic Sea. The Provencal sub-basin is the only region of high export below 200 m with a ratio about 0.4. In regions of low annual POC export (i.e. east of 7°E), the ratio ranges between 0.4 and 0.8 in the Tyrrhenian Sea, the Ionian and Levantine basins.

For DOC (Fig. 8 b), the ratio is more spatially variable, and in some regions the ratio is higher than 0.4, namely in the Provencal sub-basin, along the coasts of the Levantine basin, in the North Ionian basin, the Rhodes Gyre and the Adriatic Sea. Some patches of high ratios are also visible close to the Algerian Coast. Elsewhere the ratio ranges from almost zero (Tyrrhenian Sea, the Alboran Sea) to 0.2 in the eastern basin.

3.2 Intracellular quotas in bacteria and phytoplankton

Intracellular quotas in phytoplankton and bacteria are required for a further analysis of POC and DOC export fluxes and are presented in the following section. Carbon quota (Q_C) in small phytoplankton is maximum (> 0.7) in spring and summer in almost all of the Mediterranean Sea, though Q_C values are slightly lower in spring than in summer in the western basin, especially in the bloom region (Fig. 9). In autumn, though Q_C has decreased in nearly all of the Mediterranean Sea, Q_C values along the southern and eastern coasts of the eastern basin are significantly higher than in the rest of the open sea. In winter, Q_C values are even lower, with local maximum located in the Balearic Sea and in the south of the eastern basin.

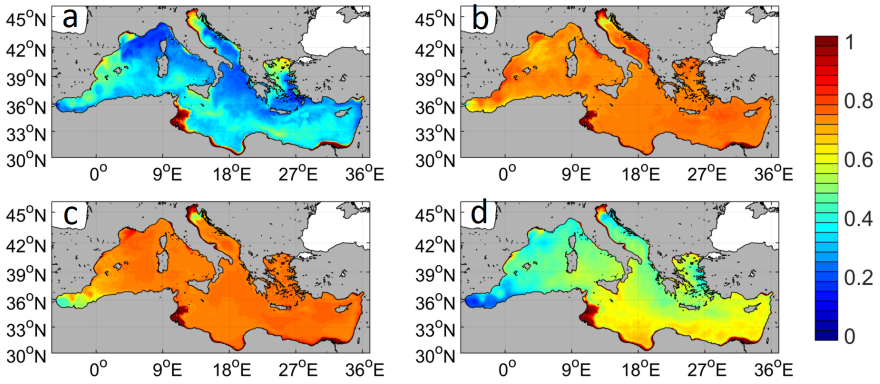

Figure 9. Seasonal variations of mean 0-50 m carbon relative quotas in small phytoplankton: (a) winter (Dec.-Feb.), (b) spring (Mar.-May), (c) summer (Jun.-Aug.), (d) autumn (Sept.-Nov.). Relative quotas are equal to 0 when the quota is mimimum (i.e. when Q_C = Q_C^{min}) and equal to 1 when the quota is maximum (i.e. when Q_C = Q_C^{max})

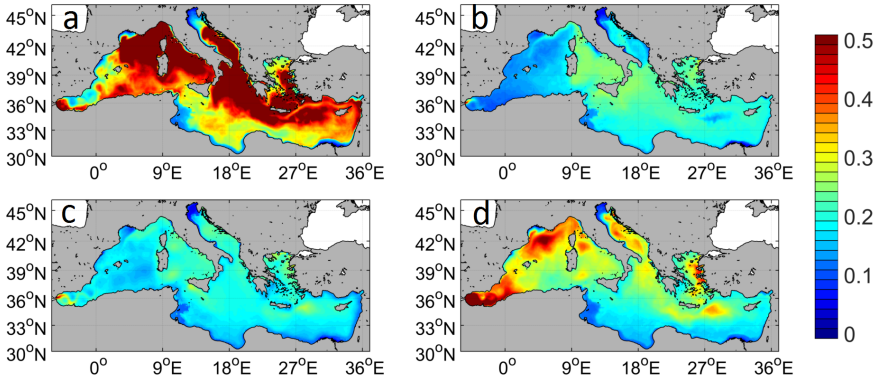

Figure 10. Seasonal variations of mean 0-50 m phosphorous relative quotas in small phytoplankton: (a) winter (Dec.-Feb.), (b) spring (Mar.-May), (c) summer (Jun.-Aug.), (d) autumn (Sept.-Nov.). Relative quotas are equal to 0 when the quota is mimimum (i.e. when Q_P = Q_P^{min}) and equal to 1 when the quota is maximum (i.e. when Q_P = Q_P^{max})

The seasonal signal of the P quota (Q_P) in small phytoplankton is nearly the opposite of that of Q_C values in autumn and mostly in winter in nearly the whole of the Mediterranean Basin, and the lowest ones in spring and summer (Fig. 10). All year long, Q_P values are lower along the southern and eastern coasts than in the rest of the eastern basin.

Bacteria Q_C generally increases from winter to summer in most of the Mediterranean Basin (Fig. 11). In autumn, the decrease in Q_C is observed everywhere except throughout the same already identified region (namely along the southern and eastern coasts of the eastern basin). All year round,

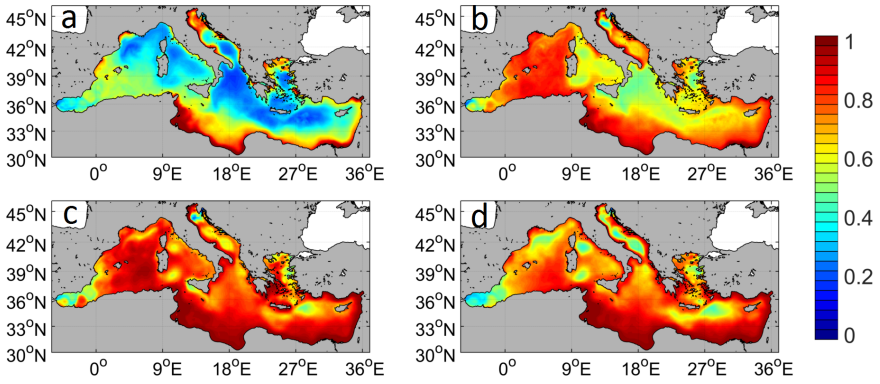

Figure 11. Seasonal variations of mean 0-50 m carbon relative quotas in bacteria: (a) winter (Dec.-Feb.), (b) spring (Mar.-May), (c) summer (Jun.-Aug.), (d) autumn (Sept.-Nov.). Relative quotas are equal to 0 when the quota is mimimum (i.e. when $Q_C = Q_C^{min}$) and equal to 1 when the quota is maximum (i.e. when $Q_C = Q_C^{max}$)

Q_C values are higher in this region than in the rest of the basin and even reach the $Q_C^{\max}$ value in summer and autumn thus indicating that carbon needs for bacteria growth are fully satisfied. In the deep convection regions (Liguro-Provencal sub-basin, Adriatic, Rhodes Gyre region), and in some eddies well identified in the Alboran and Tyrrhennian seas, the carbon quota is generally lower than in the surrounding waters, especially in autumn.

Bacteria Q_P values are very low everywhere in spring and summer except in the latter regions. The minimum Q_P values (i.e. the highest bacterial P-limitation) are observed in spring in the western basin, while they are reached in summer in the eastern basin. As for phytoplankton, Q_P values are lower all year round along the southern and eastern coasts than in the rest of the eastern basin.

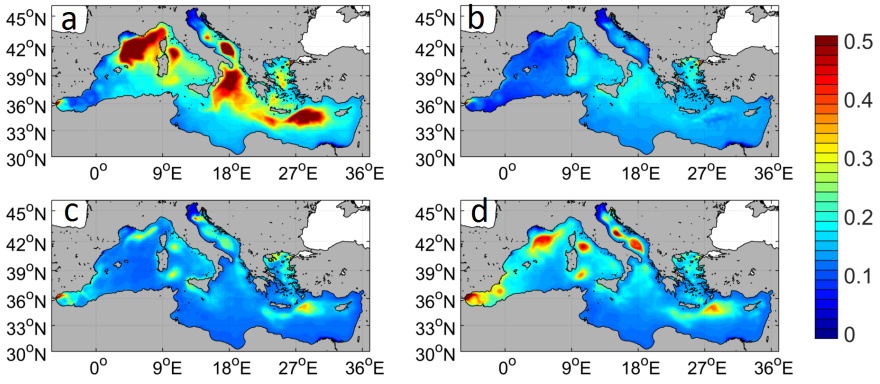

Figure 12. Seasonal variations of mean 0-50 m phosphorous relative quotas in bacteria: (a) winter (Dec.-Feb.), (b) spring (Mar.-May), (c) summer (Jun.-Aug.), (d) autumn (Sept.-Nov.). Relative quotas are equal to 0 when the quota is mimimum (i.e. when $Q_P = Q_P^{min}$) and equal to 1 when the quota is maximum (i.e. when $Q_P = Q_P^{max}$)

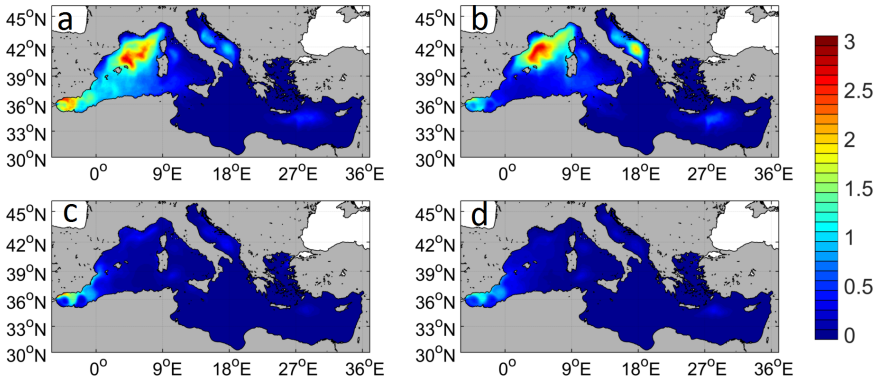

Figure 13. Seasonal variations of DOC mean 0-100 m exudation accumulated flux by large phytoplankton (in mol C.m^{-2}).

3.3 DOC exudation by phytoplankton

DOC exudation by large phytoplankton mainly occurs in the bloom region of the western basin (especially in the deep convection zone), in (late) winter and spring where accumulated fluxes are up to 2.8 mol C.m^{-2} (Fig. 13). Elsewhere, exudation fluxes are very low throughout the year, except in the Alboran Sea, two eddies of the Adriatic Sea and in the Rhodes gyre region.

The seasonality and the spatial patterns of DOC exudation flux by small phytoplankton are rather different. The highest mDOC exudation fluxes are modeled in spring in the western basin, especially in the Gulf of Lions and the deep convection zone where accumulated fluxes up to 3 mol C.m^{-2} are calculated. In the eastern basin, the highest fluxes are observed in spring and summer. During these seasons, apart from the Adriatic Sea (especially in the north and along the eastern coast where accumulated fluxes also reach 3 mol C.m^{-2}) and some hot spots (Rhodes gyre, Nile plume), mDOC exudation seems homogeneous though a north-south gradient is present. Hot spots of mDOC exudation are also present nearly all year long in the plumes of the main rivers.

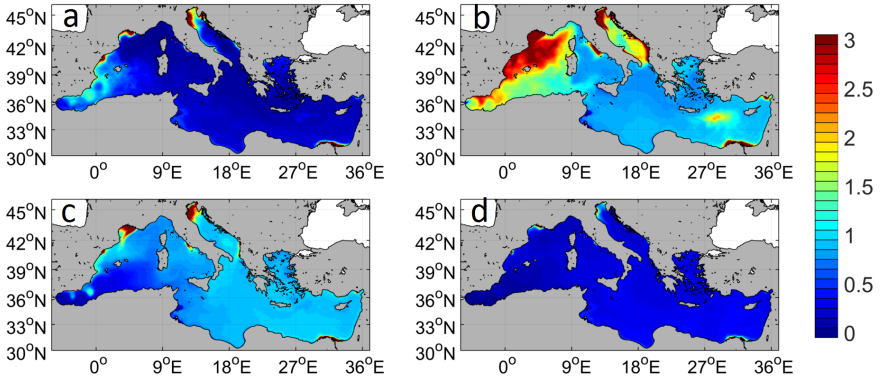

Figure 14. Seasonal variations of mDOC mean 0-100 m exudation accumulated flux by small phytoplankton (in mol C.m^{-2}).

4 Discussion

4.1 The dissolved fraction in the organic carbon export is predominant at the scale of the Mediterranean Sea

One of the main results of this study is that mDOC export exceeds mPOC export in the whole of the Mediterranean Basin, with the exception of the Alboran Sea (west of 3°W). This is consistent with the comparisons between POC and DOC exports performed in the Tyrrhennian, North Ionian and Ligurian seas by Copin-Montégut and Avril (1993); Santinelli et al. (2013) or by Lefèvre et al. (1996) who estimated that DOC was the main source of remineralization processes in the aphotic layer. In the western basin, the ratio of mDOC over mPOC export fluxes ranges between 2 and 5, and is approximately equal to 4 at the DyFaMed grid point. Observations at the DyFaMed station led to a oDOC export estimation of about 11.9 gC $m^{-2}.y^{-1}$, markedly higher than oPOC export estimations at 200 m (Avril, 2002, and references herein). Moreover, oPOC fluxes calculated by Miquel et al. (2011) during the 2001-2005 period ranged from 1.6 to 2.6 gC $m^{-2}.y^{-1}$. For comparison, mPOC export flux was in the range [1.5;3.1] gC $m^{-2}.y^{-1}$ during the same period. In the northwestern basin, the modeled ratio is about 2 at 100 m and 200 m, while in the same area a modeling study (Herrmann et al., 2014) led to a ratio at 200 m which ranged from 0.9 to 1.8, even though the corresponding export fluxes were higher than in the present study.

The ratio between modeled DOC and POC exports at 100 m ranges from 2 to 8 in the Adriatic Sea. In the same region, a oDOC flux of 15.4 (against 23 for mDOC) gC $m^{-2}.y^{-1}$ was estimated from observations by Santinelli et al. (2013). This is nearly 5 times higher than the measured oPOC export flux estimated by Boldrin et al. (2002) under the euphotic zone of 3.3 (against 4.5 for mPOC export at 100 m) gC $m^{-2}.y^{-1}$. These oDOC and oPOC fluxes were however estimated at different periods.

In the eastern basin, mDOC export is regularily more than 10 times that of mPOC, due to the very weak mPOC export and to the high mDOC export along the coasts and in the open sea. Few observations and estimations are available for this region. In the northern Ionian Sea, Boldrin et al. (2002) reported annual oPOC fluxes at 150 m of 2.4 gC $m^{-2}.y^{-1}$, which are in the same order of magnitude as the annual mPOC fluxes calculated in the same area but for a different period (1.2 gC $m^{-2}.y^{-1}$ and 0.6 gC $m^{-2}.y^{-1}$ at 100 m and 200 m, respectively).

DOC predominance in the OC export flux is first due to the higher DOC gross production fluxes as compared to those of POC, and this still holds if the POC to DOC hydrolysis flux is ruled out (i.e. if the DOC inputs due to POC hydrolysis are not taken into account). At the scale of the Mediterranean Basin as a whole, mDOC and mPOC gross production fluxes are indeed respectively equal to 20 10^{12} and 2.7 10^{12} molC.y^{-1}. In the western basin, mDOC predominance in the export of OC still holds though to a lesser extent, with mDOC and mPOC gross production fluxes respectively equal

to 8.7 10^{12} and 1.9 10^{12} molC.y^{-1}. In the following section, the reasons for these differences will be further analyzed in the light of the processes associated with DOC and POC production.

4.2 POC and DOC exports are characterized by different processes and timing

Strong disparities can be identified between the spatial patterns of the annual DOC and POC export fluxes (figure 5), with rather homogeneous DOC export fluxes across the Mediterranean Sea (though with well identified regions of maximum export that will be analyzed later), contrasting with the high east-west gradient in POC export. This is consistent with in situ measurements of daily POC export across the Mediterranean Sea at 200 m that showed much lower POC export in the eastern basin than in the western basin (Moutin and Raimbault, 2002).

There are also considerable differences in the seasonality of DOC and POC export fluxes (Fig. 6 and 7). Over the whole of the Mediterranean Sea, 88 % of DOC export occurs between November and February, which is consistent with observations at the DyFaMed station where 90% of annual DOC export was linked to winter mixing (Avril, 2002). By contrast, POC export is more even throughout the year, and during the same period only 23 % of POC is exported.

In the model, only the detrital compartment (POC) is allowed to sink. The sinking process is therefore the only source of explicit distinction between POC and DOC exports, but it is probably not sufficient to explain the strong aforementioned differences. The main source of difference lies in the biogeochemical processes that fuel or consume POC and DOC pools (see section 2.2). In the model, POC is fueled by the natural mortality of the largest organisms (mesozooplankton, diatoms and ciliates) and by the egestion of fecal pellets and sloppy feeding by mesozooplankton. Thus, higher concentrations of large organisms in the western basin, primarily due to the spring bloom in the Liguro-Provencal sub-basin associated with high primary production rates is the main reason for the higher POC production and export in this basin. Hence, POC export is at a maximum in spring (i.e. from March to May in figure 7) since it is the period including the maximum and the end of the bloom during which detrital concentrations of large organisms are highest. Moreover, according to the model, mortality is the main process that fuels the POC pool, far ahead of the egestion and sloppy feeding processes. More generally, a strong correlation between annual primary production and POC export has been evidenced at basin scale (Spearman's rank correlation coefficient is 0.84), while this is not the case for DOC export (correlation below 0.01).

As shown in the Results section, the regions of high POC or DOC export are generally not the same, except for the regions characterized by high primary production rates during the spring bloom, namely the Alboran Sea, the bloom region in the NW Mediterranean Sea and the south of the Adriatic Sea (see also section 4.3). Apart from these regions, the annual DOC export at 100 m is relatively high in almost all of the Mediterranean Basin, particularly in autumn and winter, and is the consequence of DOC accumulation in the 0-100 m layer during summer and autumn (Fig. 3). DOC export

does indeed take place when DOC rich surface waters plunge or are mixed with poorer deeper waters.

This accumulation of DOC is primarily due to water stratification that results in nutrient depletion in the 0-100 m layer. As a result, the pool of DOC in phytoplankton is saturated with newly synthesized organic compounds since photosynthesis (i.e. carbon production), which is not controlled by P-availability, takes place more rapidly than is required to supply the needs of growth (cell division being limited by the intracellular quota of P). This results in high DOC exudation by phytoplankton, which is the main source of DOC in the model. The contribution of zooplankton excretion is at a maximum in spring in the bloom region of the NW Mediterranean, but remains always much lower than that of exudation (results not shown). Similarly, the annual contribution of POC hydrolysis to the DOC production flux is weak (around 10 %). Bacteria are the first consumers of DOC, and the second ingredient for DOC accumulation is therefore a strong nutrient limitation that will highly restrict the bacteria growth rate (see Eq. 1). In this situation, DOC availability may exceed bacteria needs and result in DOC accumulation when DOC production by phytoplankton exceeds DOC uptake by bacteria. This process is enhanced in hydrodynamic situations where the surface layers are isolated from the deep waters (i.e. stratification period). Such a mechanism of DOC accumulation due to a malfunctioning microbial loop has already been described in Thingstad et al. (1997) and is also the main driver of DOC accumulation in the model. Destratification in autumn leads to a net export as well as an increase of DOC consumption through bacterial activity, driven by nutrient supply from deep water.

4.3 DOC accumulation in the light of intracellular quotas

The regions of highest DOC export fluxes correspond to the regions where the highest DOC accumulation occurs. It is therefore informative to analyze the occurrence of DOC accumulation in the light of intracellular quotas. Geographical and hydrological considerations are indeed not sufficient for a full understanding of the DOC accumulation pattern at the scale of the Mediterranean Sea.

It has already been said that, according to the model, phytoplankton exudation is the primary source of DOC. High DOC exudation by phytoplankton occurs in nutrient-depleted waters. In such a situation N and/or P phytoplankton nutrient quotas are low and limit growth rate (i.e. the cell division rate). In the model, phytoplankton (and bacteria) cell division rate is indeed controlled by the most strongly limiting element among C, N and P (see Eq. 1). In other words, the intracellular quota which is the closest to its minimum value controls the division rate. When P (and/or N) are the most strongly limiting, growth will proceed at low rate and the carbon input due to photosynthesis will rapidly meet phytoplankton needs, thus resulting in an increase in the carbon quota Q_C. Since DOC exudation flux per cell increases with Q_C through a Geider et al. (1998) non-linear quota function, DOC exudation flux will highly increase as the quota approaches its maximum value $Q_C^{\max}$. Phytoplankton carbon quota is therefore a good indicator of DOC exudation.

In the oligotrophic Mediterranean Sea, nutrient (and mostly P in the model) depletion is at a maximum at the end or just after the spring bloom, or under well established conditions of water stratification, thus leading to maximum exudation fluxes (see Fig. 13 and 14). In the rest of the Mediterranean, DOC exudation is at a maximum in (late) spring and summer, and mainly due to small phytoplankton. The latter is indeed characterized by low phosphorous quotas (see Fig. 10) and high carbon quotas (see Fig. 10).

The driving processes of DOC accumulation are not the same in the western and the eastern Mediterranean. In the western Mediterranean, and especially in the enlarged bloom region, large phytoplankton blooms first and is rapidly P-limited (as early as February) and the same occurs for small phytoplankton though later (i.e. only in spring, see Fig. 10). This is consistent with observations performed in the NW Mediterranean Sea (Gulf of Lions) (Diaz et al., 2001). In this situation, the high phytoplankton exudation fluxes are not only due to phytoplankton carbon quotas that are relatively high (around 50-60%, see the small phytoplankton carbon quota in Fig. 9), resulting in relatively high exudation flux per cell, but to the high phytoplankton abundance. Though exudation fluxes are high in (late) winter due to large phytoplankton (Fig. 13a), the high bacteria P-quotas (Fig. 12a) combined with winter mixing prevents DOC accumulation (Fig. 3a). In spring, and mostly in late spring, bacteria are strongly P-limited (Fig. 12b) since the bloom has rapidly consumed the available nutrients and vertical mixing has stopped. As a result, DOC accumulation starts in this region (Fig. 3b) and reaches its maximum in summer (Fig. 3c) during the stratification period since DOC exudation by phytoplankton still proceeds (though at a lower rate) and bacteria are still strongly P-limited (Fig. 12c). Finally, the end of the stratification in autumn will not only dilute the DOC-rich surface concentrations with DOC-poor deep waters, but allow the P-enrichment of surface waters (see the increase in bacteria Q_P in Fig. 12d).

In the eastern Mediterranean, DOC accumulation is mainly visible along the southern and eastern coasts. Moreover, it starts later than in the western Mediterranean (i.e. in summer against spring for the west), and is at a maximum in autumn. In the model, the Atlantic waters that flow along the coast are less dense (with densities slightly underestimated as compared to in situ measurements (Beuvier, 2011)) and therefore strongly isolated from the rest of the water column. As a result, their nutrient content will be progressively consumed and these waters become more and more oligotrophic as they flow along the southern coast of the basin, and always remain more oligotrophic than the rest of the eastern basin. In summer and autumn, they can even be considered as ultra-oligotrophic (see the phytoplankton Q_P in Fig. 10c and d). Moreover, they extend over a layer of around 100 m in thickness in which concentrations are roughly homogeneous. During summer and autumn, bacteria are also strongly P-limited but more and more carbon-rich (see Fig. 11) since phytoplankton exudation still proceeds (though at extremely low rates in autumn). Moreover, the vertical mixing that starts in autumn is not sufficiently deep to reach the nutrient-rich waters since the MLD is shallower than the bottom of these Atlantic waters. In addition, since DOC concentration is high over the

whole layer, DOC surface concentrations are not diluted by the mixing. As a result, accumulation still proceeds until winter during which higher MLD will allow the P-enrichment in surface waters and dilute surface DOC concentrations as well.

Furthermore, DOC concentrations (as well as DOC annual export flux though this is more difficult to see in Fig.5) are negligeable throughout the year in some well-identified regions, namely the two cyclonic structures in the Tyrrhenian Sea, the south of the Adriatic Sea (excluding the coastal zones), and the region of the Rhodes Gyre in the Levantine basin. All these structures are characterized by regular input of nutrients from deep waters, resulting in an absence of strong P-limitation in bacteria. Under such conditions, the bacteria carbon quota is rather low and DOC accumulation and export cannot occur.

Finally, the strong link between low phosphate availability in the upper surface water of the Mediterranean Sea and DOC accumulation due to nutrient limitation of bacterial production that is evidenced in this modeling study is consistent with previous in situ (Moutin et al., 2002; Van Wambeke et al., 2002) and modeling (Thingstad et al., 1997) studies and is shown to apply at the scale of the whole of the Mediterranean Sea, with the exception of the aforementioned specific regions.

4.4 Robustness of results

Though difficult to achieve in a rigorous way, the robustness of our main results will be discussed in the following section. As shown in section (2.2), the model includes many DOC and POC production and consumption processes. A sensitivity study on all the parameters they involve is obviously impossible to achieve, though some steps towards this goal have already been made in Baklouti et al. (2006b). Moreover, accounting for the fact that most of the parameters used have a physiological significance (including cell size considerations), and constitute a coherent set that remains unchanged for the different studies undertaken with Eco3M-MED (even outside the Mediterranean), we consider that their values are reasonably reliable. However, the POC to DOC degradation (i.e. hydrolysis) rate and the sinking velocity are not physiological parameters and their impact on the results will be discussed later.

The comparison of DOC stocks with the few available results (see section A4 in Appendix) showed that, though the shape of the modeled DOC vertical profiles were quite different (but the values were in the same order of magnitude) from those measured, modeled and measured integrated DOC stocks over the 0-100 m layer showed much better agreement. Furthermore, when compared to in situ estimations of DOC export from the DyFaMed station (Avril, 2002) and the Adriatic and Tyrrhenian seas (Santinelli et al., 2013), the model always provides higher DOC export values. These differences in DOC export may be partly attributable to the model failures discussed in section (A4) but, as already mentioned, in situ estimations also involve considerable uncertainties. Hence, according to Santinelli et al. (2013), DOC export computations from stock differences below the euphotic layer probably underestimate the real flux. This is also the conclusion we came to by using model

outputs to compute export fluxes with our method and with the in situ method. If we assume, however, that the different in situ estimations are consistent with each other, it appears that the highest DOC export occurs in the Adriatic Sea, followed by the DyFaMed station (Ligurian Sea) and then by the Tyrrhenian Sea, and the same order can be inferred from the model outputs.

Two parameters are essential in POC export, namely POC to DOC degradation rate and the sinking velocity.

Since our model includes a single detrital compartment, an intermediate value of 2 m d^{-1} has been used for the sinking velocity. This value is intended to be representative of the high sinking rates (> 100 m/day) of very large particles as well as the very low sinking rates of small particles. It may however reflect an underestimation of the actual mean value though this is difficult to verify. In several other models (e.g. Lévy et al., 1998; Lacroix and Gregoire, 2002; Herrmann and Somot, 2008), two detrital compartments are used, thus making it possible to differentiate between low and high sinking rates of detrital particules. However, in these models, the large detrital compartment (to which high sinking rates are affected) is only fueled by zooplankton fecal pellets (Lévy et al., 1998; Herrmann and Somot, 2008) and by mesozooplankton mortality in Lacroix and Gregoire (2002). These fluxes, except the latter, are probably weak compared to the other POC sources in our model (which is dominated by the mortality of the largest organisms). Finally, in these models, the remaining sources of POC fuel the small detrital compartment for which the sinking velocities are lower than that used in our model.

More importantly, it can be considered that the likely underestimated sinking velocity used in the present model is compensated by the very low POC degradation rate. In our model, its maximum value is set at 0.03 d^{-1} but it is modulated by the bacteria carbon quota. In substance, the higher the carbon quota, the more the degradation rate decreases and eventually becomes 0 when the bacteria carbon quota is maximum. As a result, the effective POC degradation rate is always less than 0.03 d^{-1} in the model, and it is lower in the surface layers since bacteria are more rich in carbon than in deep waters. It is also lower than all the values used in the aforementioned models. Concerning in situ data for the degradation rate, Sempéré et al. (2000) have determined values at 50 and 200 m for labile and less labile POC in three regions of the Mediterranean Sea, showing that, for the labile POC (which represent a significant part in the latter study), the degradation rate can be up to 100 times higher than that used in the present study.

Apart from these two parameters, it has been seen that the model underestimates Chl concentrations at the DCM (mainly due to a lack of large phytoplankton) and this may also lead to an underestimation of POC export. However, the 0-100 m mIPP values are consistent with oIPP thereby suggesting that this DCM underestimation has only a limited impact on carbon production. Overall, the annual POC export flux at 100 m provided by the model is around 8% of the annual primary production, a value that is consistent with in situ estimations (Miquel et al., 1994).

Between 100 m and 200 m, however, the mean bacteria carbon quota is lower since POC hydrolysis and bacteria and heterotrophic nanoflagellate mortalities are the only sources of DOC, resulting in higher hydrolysis rates and in lower POC export at 200 m. Looking at the vertical attenuation of POC fluxes, it is common to use a power law expressed as $F(z) = F(z = z_0) * (\frac{z}{z_0})^{-b}$, where F(z) is the depth-dependent POC flux and b a positive coefficient whose values may vary according to the location or the period. In regions of significant export, b values inferred from the model outputs fluctuate between 0.9 in the Provencal sub-basin and 2.3 for the Algerian basin. Values of b derived from observations tend to be lower, i.e. respectively equal to 0.92 and 1.0 for the western and eastern moorings (Gogou et al., 2014), or 0.75 in the Alboran Sea (Zúñiga et al., 2007). This again suggests that the attenuation of POC export flux between 100 m and 200 m is too great in the model. Furthermore, when compared to the few available data for POC export fluxes, the model always underestimates the export flux in the eastern basin. However, all the in situ estimations we could find in the literature were done at 150 m or 200 m depth, which means in the 100-200 m layer where the modeled POC export is more likely to be underestimated. In summary, all this suggests that the underestimation of POC export fluxes is more to be the case at 200 m than at 100 m depth though the comparison at the DyFaMed station shows that the mean mPOC export rate (5.6 gC.m^{-2}.y^{-1} and 2.2 gC.m^{-2}.y^{-1} at 100 m and 200 m respectively) is within the range of the measured rate at 200 m (i.e. [1.6;2.6] gC.m^{-2}.y^{-1} (Copin-Montégut and Avril, 1993; Miquel et al., 2011)). Finally, it is very unlikely that these uncertainties could shed doubt on the predominance of DOC in the OC export in the eastern basin. This conclusion also applies in the western basin (though with less certainty), all the more so in that in situ measurements allow the same conclusion to be drawn in the sampled stations of the NW Mediterranean (Copin-Montégut and Avril, 1993; Avril, 2002; Miquel et al., 2011).

5 Conclusions

A 14-year simulation combining a high resolution physical model (NEMO-MED12) and a mechanistic biogeochemical model (Eco3M-MED) has been developed to study carbon organic production and fate at the scale of the Mediterranean Sea.

A preliminary work presented in the Appendix focused on the Model Skill Assessment through an extensive comparison of different model outputs (i.e. chlorophyll, nutrients, primary production and DOC profiles) with available data at various time and space scales. This work allowed to verify the model's ability to represent the main features of the biogeochemical functioning of the Mediterranean Sea. In the Results section, carbon export fluxes are investigated. Previous estimations of DOC export in the Mediterranean Sea were restricted to specific regions of the Mediterranean (e.g. the Ligurian, Adriatic, Tyrrhenian Seas). We here propose the first Mediterranean-scale view of an-

nual DOC and POC export fluxes, as well as an analysis of their spatial and seasonal variations in the light of plankton intracellular quotas.

The two major results of this modeling study lie in (i) the predominance of the eastern basin in OC export (with nearly 60 % of the OC export occuring in the eastern basin), and (ii) in the crucial role of the dissolved fraction in the total organic carbon export. At Mediterranean scale, DOC export represents about four fifths of total organic carbon fluxes, thereby attesting to its major role in the carbon cycle and the biological pump in the Mediterranean Sea. The concept of a malfunctioning microbial loop (Thingstad et al., 1997), due to high P-limitation of both phytoplankton and bacteria leading to high DOC exudation fluxes beyond bacterial needs, also applies in the present study though it is generalized to the whole of the Mediterranean Basin, except for some specific P-rich regions (see Results and Discussion). Export in the eastern basin is markedly high despite its lower productivity compared to the western basin. By contrast, POC export is closely associated with regions characterized by high productivity. As a consequence, total carbon export in the eastern basin is considerably higher than expected as regards its low primary productivity. Results also show high spatial variability in organic carbon fluxes and a temporal uncoupling between POC and DOC exports. This is attributable to the differences in the processes involved in the production and export of POC and DOC.

Further comparisons with observations are clearly necessary to confirm these results, which emphasizes the need for in situ temporal monitoring to properly quantify organic carbon export. This study also highlights the need to examine the microbial food web in detail in order to further investigate the carbon cycle in the Mediterranean Sea. Furthermore, the implementation of an explicit inorganic carbon compartment in the biogeochemical model would close the carbon budget and help in the full characterization of the biological pump.

In conclusion, the strong link between low phosphate availability in the upper surface water of the Mediterranean Sea and DOC accumulation due to nutrient limitation of bacterial production already identified by previous modeling (Thingstad et al., 1997) and in situ (Moutin et al., 2002; Van Wambeke et al., 2002) studies, is confirmed by this modeling study, which may therefore be of interest for other oceanic regions. The low phosphate availability of the upper waters has been identified in other oceanic regions such as the Sargasso Sea (Wu et al., 2000), the North Pacific and the South West Pacific (Van Den Broeck et al., 2004), and high DOC accumulation has also been reported in some of these areas (Carlson et al., 1994). This work may therefore be of interest for these oceanic regions. Finally, in the context of climate change, the enhanced stratification and the probable geographical extension of low phosphate availability in upper waters (Karl et al., 1997; Moutin et al., 2008) is expected to result in an increase in DOC production (Santinelli et al., 2013; Lazzari et al., 2013), and thereby further increase the importance of DOC in the biological carbon pump.

Acknowledgements. The authors are grateful to the various organisations that funded this work. This includes the French PACA Region (which funded the PhD thesis of A. Guyennon), the Mercator Ocean group (which funded the SiMED project that provided an efficient framework for this work), the MED-ICCBIO project (funded by the *Groupement d' Intérêt Scientifique* "Climat, Environnement et Société"), and the OT-MED Labex. This work is a contribution to the MerMEx and the OT-MED programs and it was granted access to the HPC resources of IDRIS (Institut du Développement et des Ressources en Informatique Scientifique) of the Centre National de la Recherche Scientifique (CNRS). The DYFAMED time series was provided by the Oceanological Observatory (CNRS-UPMC) of Villefranche-sur-Mer (L.Coppola). This project is funded by CNRS-INSU and ALLENVI through the MOOSE observation network. The satellite data used in this is study are MyOcean Products. Authors are also grateful to Jean-Michel André for his help and valuable advice, and to L. Coppola for his very efficient assistance in obtaining in situ data from the DyFaMed station.

References

Alekseenko, E., Raybaud, V., Espinasse, B., Carlotti, F., Queguiner, B., Thouvenin, B., Garreau, P., and Baklouti, M.: Seasonal dynamics and stoichiometry of the planktonic community in the NW Mediterranean Sea: a 3D modeling approach, Ocean Dynamics, 64, 179–207, 2014.

Antoine, D., Morel, A., and André, J.: Algal pigment distribution and primary production in the eastern Mediterranean as derived from coastal zone color scanner observations, Journal of Geophysical Research, 100, 16 193–16, 1995.

Avril, B.: DOC dynamics in the northwestern Mediterranean Sea (DYFAMED site), Deep Sea Research Part II: Topical Studies in Oceanography, 49, 2163–2182, 2002.

Baklouti, M., Diaz, F., Pinazo, C., Faure, V., and Quéguiner, B.: Investigation of mechanistic formulations depicting phytoplancton dynamics for models of marine pelagic ecosystems and description of a new model, Progress in Oceanography, 71, 1–33, 2006a.

Baklouti, M., Faure, V., Pawlowski, L., and Sciandra, A.: Investigation and sensitivity analysis of a mechanistic phytoplankton model implemented in a new modular numerical tool (Eco3M) dedicated to biogeochemical modelling, Progress in Oceanography, 71(1), 34–58, 2006b.

Baklouti, M., Chevalier, C., Bouvy, M., Corbin, D., Pagano, M., Troussellier, M., and Arfi, R.: A study of plankton dynamics under osmotic stress in the Senegal River Estuary, West Africa, using a 3D mechanistic model, Ecological Modelling, 222, 2704–2721, 2011.

Baretta, J., Ebenhoh, W., and Ruardij, P.: The European Regional Seas Ecosystem Model, a complex marine ecosystem model, J. Sea Res., 33, 233–246, 1995.

Béranger, K., Mortier, L., and Crépon, M.: Seasonal variability of water transport through the Straits of Gibraltar, Sicily and Corsica, derived from a high-resolution model of the Mediterranean circulation, Progress in Oceanography, 66, 341–364, 2005.

Bertilsson, S., Berglund, O., Karl, D. M., and Chisholm, S. W.: Elemental composition of marine Prochlorococcus and Synechococcus: Implications for the ecological stoichiometry of the sea, Limnol. Oceanogr., 48, 1721–1731, 2003.

Beuvier, J.: Modélisation de la variabilité climatique de la circulation et des masses d'eau en mer Méditerranée: impact des échanges océan-atmosphére, Ph.D. thesis, Ecole Polytechnique, 2011.

Beuvier, J., Sevault, F., Herrmann, M., Kontoyiannis, H., Ludwig, W., Rixen, M., Stanev, E., Béranger, K., and Somot, S.: Modeling the Mediterranean Sea interannual variability during 1961–2000: focus on the Eastern Mediterranean Transient, Journal of Geophysical Research: Oceans (1978–2012), 115, doi:10.1029/2009JC005950, 2010.

Beuvier, J., Béranger, K., Brossier, C., Somot, S., Sevault, F., Drillet, Y., Bourdallé-Badief, R., Ferry, N., Lyard, F., et al.: Spreading of the Western Mediterranean Deep Water after winter 2005: Time scales and deep cyclone transport., Journal of Geophysical Research, 117, doi:10.1029/2011JC007679, 2012a.

Beuvier, J., Lebeaupin Brossier, C., Béranger, K., Arsouze, T., Bourdallé-Badie, R., C., D., Drillet, Y., Drobinski, P., Lyard, F., Ferry, N., Sevault, F., and Somot, S.: Oceanic component for the modeling of the regional Mediterranean Eart System., Mercator Ocean Quarterly Newsletter, 46, 60–66, 2012b.

Boldrin, A., Miserocchi, S., Rabitti, S., Turchetto, M., Balboni, V., and Socal, G.: Particulate matter in the southern Adriatic and Ionian Sea: characterisation and downward fluxes, Journal of Marine Systems, 33, 389–410, 2002.

Bopp, L., Monfray, P., Aumont, O., Dufresne, J., Le Treut, H., Madec, G., Terray, L., and Orr, J.: Potential climate change on marine export production, Global Biogeochemical Cycles, 15, 81–99, 2001.

Bosc, E., Bricaud, A., and Antoine, D.: Seasonal and interannual variability in algal biomass and primary production in the Mediterranean Sea, as derived from 4 years of SeaWiFS observations, Global Biogeochemical Cycles, 18, GB1005, doi:10.1029/2003GB002034, 2004.

Brown, E. J. and Harris, R. F.: Kinetics of algal transient phosphate uptake and the cell quota concept, Limnol. Oceanogr., 23, 35–40, 1978.

Buesseler, K.: Do upper-ocean sediment traps provide an accurate record of particle flux ?, Nature, 353, 420–423, 1991.

Carlson, C., Ducklow, H., and Michaels, A.: Annual flux of dissolved organic carbon from the euphotic zone in the northwestern Sargasso Sea, Nature, 371, 405–408, 1994.

Christaki, U., Courties, C., Joux, F., Jeffrey, W. H., Neveux, J., and Naudin, J.: Community structure and trophic role of ciliates and heterotrophic nanoflagellates in Rhone River diluted mesoscale structures (NW Mediterranean Sea), Aquat Microb Ecol, 57, 263–277, 2009.

Claustre, H., Morel, A., Hooker, S., Babin, M., Antoine, D., Oubelkheir, K., Bricaud, A., Leblanc, K., Queguiner, B., and Maritorena, S.: Is desert dust making oligotrophic waters greener ?, Geophysical Research Letters, 29, 107–1–107–4, 2002.

Copin-Montégut, G. and Avril, B.: Vertical distribution and temporal variation of dissolved organic carbon in the North-Western Mediterranean Sea, Deep Sea Research Part I: Oceanographic Research Papers, 40, 1963–1972, 1993.

Crise, A., Crispi, G., and Mauri, E.: A seasonal three-dimensional study of the nitrogen cycle in the Mediterranean Sea: Part I. Model implementation and numerical results, Journal of Marine Systems, 18, 287–312, 1998.

Crispi, G., Crise, A., and Solidoro, C.: Three-dimensional oligotrophic ecosystem models driven by physical forcing: the Mediterranean Sea case, Environmental Modelling Software, 13, 483–490, 1998.

Diaz, F., Raimbault, P., Boudjellal, B., Garcia, N., and Moutin, T.: Early spring phosphorus limitation of primary productivity in a NW Mediterranean coastal zone (Gulf of Lions), Marine Ecology Progress Series, 211, 51–62, 2001.

D'Ortenzio, F. and Ribera d'Alcalà, M.: On the trophic regimes of the Mediterranean Sea: a satellite analysis, Biogeosciences, 6, 139–148, 2009.

D'Ortenzio, F., Marullo, S., Ragni, M., Ribera d'Alcalà, M., and Santoleri, R.: Validation of empirical SeaWiFS algorithms for chlorophyll-a retrieval in the Mediterranean Sea: A case study for oligotrophic seas, Remote Sensing of Environment, 82, 79–94, 2002.

Droop, M.: Vitamin B12 and marine ecology. IV. The kinetics of uptake, growth and inhibition in Monochrysis lutheri, J. Mar. Biol. Assoc. UK, 48, 689–733, 1968.

Droop, M.: The nutrient status of algal cells in batch culture, J. Mar. Biol. Assoc. UK, 55, 541–555, 1975.

Eppley, R. and Peterson, B.: Particulate organic matter flux and planktonic new production in the deep ocean, Nature, 282, 677–680, 1979.

Fasham, M., Flynn, K., Pondaven, P., Anderson, T., and Boyd, P.: Development of a robust marine ecosystem model to predict the role of iron in biogeochemical cycles: A comparison of results for iron-replete and iron-limited areas, and the SOIREE iron-enrichment experiment, Deep Sea Research Part I: Oceanographic Research Papers, 53, 333–366, 2006.

Fukuda, R., Ogawa, H., Nagata, T., and Koike, I.: Direct Determination of Carbon and Nitrogen Contents of Natural Bacterial Assemblages in Marine Environments, Appl Environ Microbiol, 64, 3352–3358, 1998.

Garcia, H. E., Locarnini, R., Boyer, T., and Antonov, J.: World Ocean Atlas 2005. Vol. 4, Nutrients (phosphate, nitrate, silicate), 2006.

Geider, R., MacIntyre, H., and Kana, T.: A dynamic regulatory model of phytoplankton acclimation to light, nutrients, and temperature, Limnology and Oceanography, 43, 679–694, 1998.

Gogou, A., Sanchez-Vidal, A., Durrieu de Madron, X., Stavrakakis, S., Calafat, A. M., Stabholz, M., Psarra, S., Canals, M., Heussner, S., Stavrakaki, I., et al.: Carbon flux to the deep in three open sites of the Southern European Seas (SES), Journal of Marine Systems, 129, 224–233, 2014.

Gómez, F.: The role of the exchanges through the Strait of Gibraltar on the budget of elements in the Western Mediterranean Sea: consequences of human-induced modifications, Marine Pollution Bulletin, 46, 685–694, 2003.

Hansell, D. and Carlson, C.: Marine Dissolved Organic Matter and the Carbon Cycle, Oceanography, 14, 685–716, 2001.

Hansell, D., Carlson, C., and Suzuki, Y.: Dissolved organic carbon export with North Pacific Intermediate Water formation, Global Biogeochemical Cycles, 16, 7–1–7–8, 2002.

Hansell, D., Repeta, D., Carlson, C., and Schlitzer, R.: Dissolved organic matter in the ocean: A controversy stimulates new insights, Oceanography, 22, 202–211, 2009.

Heldal, M., Scanlan, D. J., Norland, S., Thingstad, F., and Mann, N. H.: Elemental composition of single cells of various strains of marine Prochlorococcus and Synechococcus using X-ray microanalysis, Limnol. Oceanogr., 48, 1732–1743, 2003.

Herrmann, M. and Somot, S.: Relevance of ERA40 dynamical downscaling for modeling deep convection in the Mediterranean Sea, Geophysical Research Letters, 35, doi:10.1029/2007GL032442, 2008.

Herrmann, M., Diaz, F., Estournel, C., Marsaleix, P., and Ulses, C.: Impact of atmospheric and oceanic interannual variability on the Northwestern Mediterranean Sea pelagic planktonic ecosystem and associated carbon cycle, Journal of Geophysical Research: Oceans, 118, 1–22, 2014.

Holling, C.: Some characteristics of simple types of predation and parsitism, The Candian Entomologist, 91, 385–398, 1959.

Karl, D. M., Letelier, R. M., Tupas, L., Dore, J., Christian, J., and Hebel, D.: The role of nitrogen fixation in biogeochemical cycling in the subtropical North Pacific Ocean, Nature, 387, 533–538, 1997.

Klausmeier, C., Litchman, E., and Levin, S.: Phytoplankton growth and stoichiometry under multiple nutrient limitation, Limnology and Oceanography, 49, 1463–1470, 2004.

Klausmeier, C., Litchman, E., Daufresne, T., and Levin, S.: Phytoplankton stoichiometry, Ecol. Res., 23, 479–485, 2008.

Kooijman, S. A. L. M.: Dynamic Energy and Mass Budgets in Biological Systems, Cambridge University Press, Cambridge, UK, 2000.

Lacroix, G. and Gregoire, M.: Revisited ecosystem model (MODECOGeL) of the Ligurian Sea: seasonal and interannual variability due to atmospheric forcing, Journal of Marine Systems, 37, 229–258, 2002.

Lavigne, H., D'Ortenzio, F., Migon, C., Claustre, H., Testor, P., d'Alcalà, M., Lavezza, R., Houpert, L., and Prieur, L.: Enhancing the comprehension of mixed layer depth control on the Mediterranean phytoplankton phenology, Journal of Geophysical Research: Oceans, 118, 3416–3430, 2013.

Lazzari, P., Solidoro, C., Ibello, V., Salon, S., Teruzzi, A., Béranger, K., Colella, S., and Crise, A.: Seasonal and inter-annual variability of plankton chlorophyll and primary production in the Mediterranean Sea: a modelling approach, Biogeosciences, 8, 5379–5422, 2012.

Lazzari, P., Mattia, G., Solidoro, C., Salon, S., Crise, A., Zavatarelli, M., Oddo, P., and Vichi, M.: The impacts of climate change and environmental management policies on the trophic regimes in the Mediterranean Sea: Scenario analyses, Journal of Marine Systems, 2013.

Le Quéré, C., Takahashi, T., Buitenhuis, E., Rödenbeck, C., and Sutherland, S.: Impact of climate change and variability on the global oceanic sink of CO2, Global Biogeochemical Cycles, 24, 2016–2040, 2010.

Le Quéré, C. L., Harrison, S., P., C., Buitenhuis, E., Aumont, O., Bopp, L., Claustre, H., Cotrim Da Cunha, L., Geider, R., Giraud, X., et al.: Ecosystem dynamics based on plankton functional types for global ocean biogeochemistry models, Global Change Biology, 11, 2016–2040, 2005.

Leblanc, K., Quéguiner, B., Garcia, N., Rimmelin, P., and Raimbault, P.: Silicon cycle in the NW Mediterranean Sea: seasonal study of a coastal oligotrophic site, Oceanologica Acta, 26, 339–355, 2003.

Lefèvre, D., Denis, M., Lambert, C., and Miquel, J.: Is DOC the main source of organic matter remineraliztion in the ocean water column ?, Journal of Marine Systems, 7, 281–291, 1996.

Lévy, M., Mémery, L., and André, J.: Simulation of primary production and export fluxes in the Northwestern Mediterranean Sea, Journal of Marine Research, 56, 197–238, 1998.

Lovdal, T., Skjoldal, E. F., Heldal, M., Norland, S., and Thingstad, T. F.: Changes in morphology and elemental composition of Vibrio splendidus along a gradient from carbon-limited to phosphate-limited growth, Microb. Ecol., 55, 152–161, 2008.

Ludwig, W.: Continental erosion and river transport of organic carbon to the world's Oceans, Ph.D. thesis, Université Louis Pasteur de Strasbourg, 1996.

Ludwig, W., Dumont, E., Meybeck, M., and Heussner, S.: River discharges of water and nutrients to the Mediterranean and Black Sea: Major drivers for ecosystem changes during past and future decades?, Progress in Oceanography, 80, 199–217, 2009.

Macías, D., Stips, A., and Garcia-Gorriz, E.: The relevance of deep chlorophyll maximum in the open Mediterranean Sea evaluated through 3D hydrodynamic-biogeochemical coupled simulations, Ecological Modelling, 281, 26–37, 2014.

Madec, G. and The-NEMO-Team: NEMO ocean engine, Note du pole de modélisation de l'IPSL, 27, 1228–1619, 2008.

Maier-Reimer, E., Mikolajewicz, U., and Winguth, A.: Future ocean uptake of CO2: interaction between ocean circulation and biology, Climate Dynamics, 12, 711–722, 1996.

Marshall, J. and Schott, F.: Open-ocean convection: Observations, theory, and models, Reviews of Geophysics, 37, 1–64, 1999.

Marty, J. and Chiavérini, J.: Hydrological changes in the Ligurian Sea (NW Mediterranean, DYFAMED site) during 1995–2007 and biogeochemical consequences, Biogeosciences, 7, 2117–2128, 2010.

Marty, J., Chiavérini, J., Pizay, M., and Avril, B.: Seasonal and interannual dynamics of nutrients and phytoplankton pigments in the western Mediterranean Sea at the DYFAMED time-series station (1991–1999), Deep Sea Research Part II: Topical Studies in Oceanography, 49, 1965–1985, 2002.

Marty, J.-C., Garcia, N., and Raimbault, P.: Phytoplankton dynamics and primary production under late summer conditions in the NW Mediterranean Sea, Deep Sea Research Part I, 55, 1131–1149, 2008.

Mattia, G., Zavatarelli, M., Vichi, M., and Oddo, P.: The Eastern Mediterranean Sea biogeochemical dynamics in the 1990s: A numerical study, Journal of Geophysical Research: Oceans, 118, 2231–2248, 2013.

Mauriac, R., Moutin, T., and Baklouti, M.: Accumulation of DOC in Low Phosphate Low Chlorophyll (LPLC) area: is it related to higher production under high N: P ratio?, Biogeosciences, 8, 933–950, 2011.

Meador, T., Gogou, A., Spyres, G., Herndl, G., Krasakopoulou, E., Psarra, S., Yokokawa, T., De Corte, D., Zervakis, V., and Repeta, D.: Biogeochemical relationships between ultrafiltered dissolved organic matter and picoplankton activity in the Eastern Mediterranean Sea, Deep Sea Research Part II: Topical Studies in Oceanography, 57, 1460–1477, 2010.

MERMEX-group: Marine ecosystems' responses to climatic and anthropogenic forcings in the Mediterranean, Progress in Oceanography, 91, 97–166, 2011.

Millot, C. and Taupier-Letage, I.: Circulation in the Mediterranean sea, in: The Mediterranean Sea, pp. 29–66, Springer, 2005.

Miquel, J., Martín, J., Gasser, B., Rodriguez-y Baena, A., Toubal, T., and Fowler, S.: Dynamics of particle flux and carbon export in the northwestern Mediterranean Sea: a two decade time-series study at the DYFAMED site, Progress in Oceanography, 91, 461–481, 2011.

Miquel, J. C., Fowler, S. W., La Rosa, J., and Buat-Menard, P.: Dynamics of the downward flux of particles and carbon in the open northwestern Mediterranean Sea, Deep-Sea Research I, 41, 243–261, 1994.

Moore, J. K., Doney, S. C., Kleypas, J. A., Glover, D. M., and Fung, I. Y.: An intermediate complexity marine ecosystem model for the global domain, Deep-Sea Research II, 49, 403–462, 2002.

Morel, A.: Optical modeling of the upper ocean in relation to its biogenous matter content (case I waters), Journal of Geophysical Research: Oceans (1978–2012), 93, 10 749–10 768, 1988.

Moutin, T. and Prieur, L.: Influence of anticyclonic eddies on the Biogeochemistry from the Oligotrophic to the Ultraoligotrophic Mediterranean (BOUM cruise), Biogeosciences, 9, 3827–3855, 2012b.

Moutin, T. and Raimbault, P.: Primary production, carbon export and nutrients availability in Western and Eastern Mediterranean Sea in early summer 1996 (MINOS cruise), Journal of Marine Systems, 33, 273–288, 2002.

Moutin, T., Raimbault, P., and Poggiale, J.: Production primaire dans les eaux de surface de la Mediterranee occidentale. Calcul de la production journaliere, Comptes Rendus de l'Académie des Sciences-Series III-Sciences de la Vie, 322, 651–655, 1999.

Moutin, T., Thingstad, T. F., Van Wambeke, F., Marie, D., Slawyk, G., and Raimbault, P.: Does competition for nanomolar phosphate supply explain the predominance of the cyanobacterium Synechococcus?, Limnology and Oceanography, 47, 1562–1567, 2002.

Moutin, T., Karl, D. M., Duhamel, S., Rimmelin, P., Raimbault, P.and Van Mooy, B. A. S., and Claustre, H.: Phosphate availability and the ultimate control of new nitrogen input by nitrogen fixation in the tropical Pacific Ocean, Biogeosciences, 5, 95–109, 2008.

Moutin, T., Van Wambeke, F., and Prieur, L.: Introduction to the Biogeochemistry from the Oligotrophic to the Ultraoligotrophic Mediterranean (BOUM) experiment, Biogeosciences, 9, 3817–3825, 2012a.

Palmiéri, J.: Modélisation biogéochimique de la mer Méditerranée avec le modèle régional couplé NEMO-MED12/PISCES., Ph.D. thesis, Université de Versailles Saint-Quentin, France, 2014.

Palmiéri, J., Le Vu, B., Dutay, J., Bopp, L., Béranger, K., Beuvier, J., Somot, S., and Éthé, C.: Biogeochemical modelling of the Mediterranean Sea with PISCES MED-12 model., GMD, in prep.

Pasqueron de Fommervault, O., Migon, C., D'Ortenzio, F., Ribera d'Alcalà, M., and Coppola, L.: Temporal variability of nutrient concentrations in the northwestern Mediterranean sea (DYFAMED time-series station), Deep Sea Research Part I, 100, 1–12, 2015.

Paulmier, A., Kriest, I., and Oschlies, A.: Stoichiometries of remineralisation and denitrification in global biogeochemical ocean models, Biogeosciences (BG), 6, 923–935, 2009.

Prowe, A., Pahlow, M., Dutkiewicz, S., Follows, M., and Oschlies, A.: Top-down control of marine phytoplankton diversity in a global ecosystem model, Progress in Oceanography, 101, 1–13, 2012.

Pujo-Pay, M., Conan, P., Oriol, L., Cornet-Barthaux, V., Falco, C., Ghiglione, J., Goyet, C., Moutin, T., and Prieur, L.: Integrated survey of elemental stoichiometry (C, N, P) from the western to eastern Mediterranean Sea, Biogeosciences, 8, 883–899, 2011.

Redfield, A. C.: The biological control of chemical factors in the environment, Am Sci, 46, 205–221, 1958.

Santinelli, C., Nannicini, L., and Seritti, A.: DOC dynamics in the meso and bathypelagic layers of the Mediterranean Sea, Deep Sea Research Part II: Topical Studies in Oceanography, 57, 1446–1459, 2010.

Santinelli, C., D.A., H., and d'Alcala M., R.: Influence of stratification on marine dissolved organic carbon (DOC) dynamics : The Mediterranean Sea case, Progress in Oceanography, 119, 68–77, 2013.

Sarmiento, J. and Gruber, N.: Ocean biogeochemical dynamics, vol. 1015, Princeton University Press Princeton, 2006.

Sarmiento, J., Hughes, T., Stouffer, R., and Manabe, S.: Simulated response of the ocean carbon cycle to anthropogenic climate warming, Nature, 393, 245–249, 1998.

Schaap, D. and Lowry, R.: SeaDataNet–Pan-European infrastructure for marine and ocean data management: unified access to distributed data sets, International Journal of Digital Earth, 3, 50–69, 2010.

Sempéré, R., Yoro, S. C., Van Wambeke, F., and Charrière, B.: Microbial decomposition of large organic particles in the Northwestern Mediterranean Sea: an experimental approach, Mar Ecol Prog Ser, 198, 61–72, 2000.

Siegenthaler, U. and Sarmiento, J.: Atmospheric carbon dioxide and the ocean, Nature, 365, 119–125, 1993.

Siokou-Frangou, I., Christaki, U., Mazzocchi, M., Montresor, M., Ribera d'Alcalà, M., Vaqué, D., and Zingone, A.: Plankton in the open Mediterranean Sea: a review, Biogeosciences, 7, 1543–1586, 2010.

Somot, S., Sevault, F., and Déqué, M.: Transient climate change scenario simulation of the Mediterranean Sea for the twenty-first century using a high-resolution ocean circulation model, Climate Dynamics, 27, 851–879, 2006.

Soto-Navarro, J., Somot, S., Sevault, F., Beuvier, J., Criado-Aldeanueva, F., García-Lafuente, J., and Béranger, K.: Evaluation of regional ocean circulation models for the Mediterranean Sea at the Strait of Gibraltar: volume transport and thermohaline properties of the outflow, Climate Dynamics, 44, 1277–1292, doi:10.1007/S00382-014-2179-4, 2014.

Sournia, A.: La production primaire planctonique en Méditerranée; essai de mise à jour, Cooperative Investigations in the Mediterranean, International Coordinator and Operational Unit; Étude en commun de la Méditerranée, Coordonnateur international et Unité opérationnelle, 1973.

Talarmin, A., Van Wambeke, F., Duhamel, Catala, P., Moutin, T., and Lebaron, P.: Improved methodology to measure taxon-specific phosphate uptake in live and unfiltered samples, Limnol. Oceanogr. Methods, 9, 443–453, doi:10.4319/lom.2011.9.443., 2011.

Thingstad, T., , Hagström, A., and Rassoulzadegan, F.: Accumulation of degradable DOC in surface waters: Is it caused by a malfunctioning microbial loop?, Limnology and Oceanography, 42, 398–404, 1997.

Thingstad, T., Krom, M., Mantoura, R., Flaten, G., Groom, S., Herut, B., Kress, N., Law, C., Pasternak, A., Pitta, P., Psarra, S., Rassoulzadegan, F., Tanaka, T., Tselepides, A., Wassman, P., Woodward, E., Wexels, R., Zodiatis, G., and Zohary, T.: Nature of phosphorus limitation in the ultraoligotrophic eastern Mediterranean, Science, 309, 1068–1071, 2005.

Toggweiler, J., Gnanadesikan, A., Carson, S., Murnane, R., and Sarmiento, J.: Representation of the carbon cycle in box models and GCMs: 1. Solubility pump, Global biogeochemical cycles, 17, 2003.

Tugrul, S. and Besiktepe, S.: Nutrient exchange fluxes between the black sea and the Mediterranean through the turkish strait system (marmara sea, bosphorus and dardanelles), CIESM, 2007.

Uitz, J., Stramski, D., Gentili, B., D'Ortenzio, F., and Claustre, H.: Estimates of phytoplankton class-specific and total primary production in the Mediterranean Sea from satellite ocean color observations, Global Biogeochemical Cycles, 26, doi:10.1029/2011GB004055, 2012.

Vallina, S., Ward, B., Dutkiewicz, S., and Follows, M.: Maximal feeding with active prey-switching: A kill-the-winner functional response and its effect on global diversity and biogeography, Progress in Oceanography, 120, 93–109, 2014.

Van Den Broeck, N., Moutin, T., Rodier, M., and Le Bouteiller, A.: Seasonal variations of phosphate availability in the SW Pacific Ocean near New Caledonia, Mar. Ecol. Progress Ser., 268, 1–12, 2004.

Van Wambeke, F., Christaki, U., Giannakourou, A., Moutin, T., and Souvemerzoglou, K.: Longitudinal and vertical trends of bacterial limitation by phosphorus and carbon in the Mediterranean Sea, Microbial ecology, 43, 119–133, 2002.

Vichi, M., Pinardi, N., and Masina, S.: A generalized model of pelagic biogeochemistry for the global ocean ecosystem. Part I: Theory, Journal of Marine Systems, 64, 89–109, 2007.

Volpe, G., Santoleri, R., Vellucci, V., Ribera d'Alcala, M., Marullo, S., and d'Ortenzio, F.: The colour of the Mediterranean Sea: Global versus regional bio-optical algorithms evaluation and implication for satellite chlorophyll estimates, Remote Sensing of Environment, 107, 625–638, 2007.

Vörösmarty, C., Fekete, B., and Tucker, B.: Global river discharge database, RivDis, Tech. rep., 1996.

Wilhelm, S. W., King, A. L., Twining, B. S., LeCleir, G. R., DeBruyn, J. M., Strzepek, R. F., Breene, C. L., Pickmere, S., Ellwood, M. J., Boyd, P. W., and Hutchins, D. A.: Elemental quotas and physiology of a south-western Pacific Ocean plankton community as a function of iron availability, Aquatic Microbial Ecology, 68, 185–194, 2013.

Wu, J., SUNDA, W., BOYLE, E., and Karl, D.: Phosphate depletion in the western North Atlantic Ocean, Sciences, 289, 759–762, 2000.

Zúñiga, D., Calafat, A., Sanchez-Vidal, A., Canals, M., Price, B., Heussner, S., and Miserocchi, S.: Particulate organic carbon budget in the open Algero-Balearic Basin (Western Mediterranean): Assessment from a one-year sediment trap experiment, Deep Sea Research Part I: Oceanographic Research Papers, 54, 1530–1548, 2007.

Appendix A: Model Skill Assessment

Due to the high complexity of the biogeochemical model and the scarcity of data, the assessment of the model's representativeness at the scale of the Mediterranean Sea is a complex task. This work, however, aims to achieve comparisons on several modeled variables, at different time and space scales when in situ measurements were available. For reasons of brevity, model outputs hereafter have the prefix "m" while corresponding in situ or satellite observations have the prefix "o".

A1 Nutrients

A1.1 Basin scale spatial variability

Data collected during the BOUM cruise offer a basis for assessing the quality of the simulation during the stratified summer period. The comparison between mNO_3 and mPO_4 with the corresponding measured concentrations (i.e. oNO3 and oPO4) along the BOUM transect is shown in Fig. 15 and Table 1.

When compared to in situ data, /blmean mNO_3 [mPO_4 in brackets] in the deep layers (> 1500 m) is underestimated by 1.2 [0.04] μmol l^{-1} in the western basin, and 0.4 [0.01] μmol l^{-1} in the eastern basin. This can be attributed to an underestimation of initial nutrient stocks at depth. There are indeed significant differences between the nutrient concentrations in deep waters provided by the Medatlas climatology data and by the BOUM measurements. As a consequence, and due to the stability of nutrient concentrations in deep water during the simulation, the same disparities can be observed between the model outputs and the BOUM cruise data.

In the surface layer (0-30 m), mNO_3 is less than 1 μmol l^{-1}, with a mean value of around 0.5 μmol l^{-1} for the whole basin, while mPO_4 is almost nil everywhere (< 0.01 μmol l^{-1}). These values are consistent with measured nutrient concentrations, which are low and close to their quantification limits of 0.05 μmol l^{-1} for both NO_3 and PO_4 (Fig. 15, Table 1) though the model tends to overestimate surface nitrate concentrations during periods of intense stratification. This may be related to an

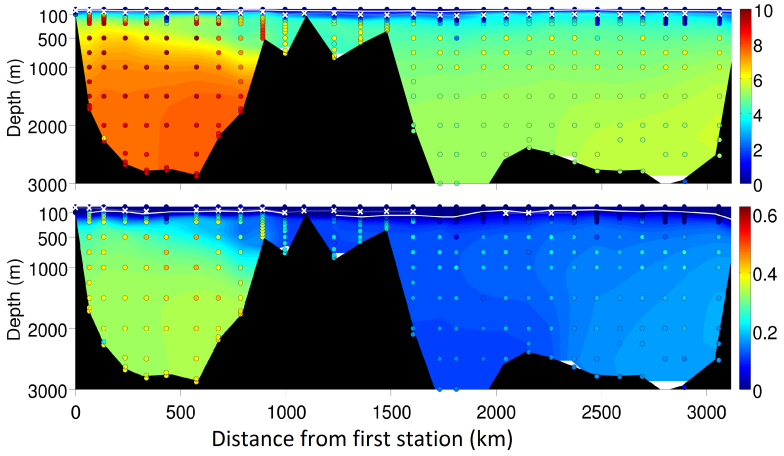

Figure 15. BOUM (top) NO_3 and (bottom) PO_4 (Pujo-Pay et al., 2011). Model outputs are in shaded colors; in situ data are colored circles. Model outputs correspond to the daily outputs averaged over the BOUM cruise period. White crosses represent the data-derived depth of the top nitracline as defined in (Moutin and Prieur, 2012b). The white line indicates the top nitracline from model outputs.

overestimation of nitrification processes, and/or an underestimation of detrital organic matter sinking. Nitrification is, indeed, a linear function with a fixed parameter and does not take into account the potential dependence of the process (e.g. Paulmier et al., 2009). In the western basin, the top of the modeled nitracline is almost 25 m above the top nitracline derived from in situ data, and the gap increases eastward as the top nitracline derived from data gets deeper (Moutin and Prieur, 2012b). The modeled top phosphacline is slightly below the data-derived top phosphacline along most of the BOUM transect. The difference between model outputs and data can also be found in the slope of the nitracline at depths between 150 m and 1000 m: this slope decreases with depth for the model, while it is quite constant for data. As a consequence, significant differences in nitrate concentration can be observed in the "intermediate" waters (between 250 and 1000 m) : mNO3 is underestimated by almost 3 μmol l^{-1} at 500 m in the western basin, and respectively 1.5 and 1.2 μmol l^{-1} in the Ionian and Levantine basins. In the western basin, the same differences between model and data were found in the phosphate vertical profiles (Fig. 15, Table 1), resulting in a maximum difference of 0.15 μmol l^{-1} in phosphate concentrations. However, in the eastern basin, modeled and in situ phosphate gradients are in better agreement than nitrate gradients, except that the phosphacline is less thick than in the data. Finally, some discrepancies between model and observations are attributable to the mislocation of the anti-cyclonic eddies, but this failure of the hydrodynamic model has only a local impact on modeled nutrients.

Table 1. Mean over the BOUM cruise period of modeled (mNO_3, mPO_4) and measured (oNO_3, oPO_4) nutrients concentrations for different layers of the western and eastern basins. Root Mean Squared Difference (RMSD) between model outputs and observations have been calculated. Values in brackets are standard deviations, and BQL stands for Below the Quantification Limit (0.05 μmol l^{-1}).

		Model		Observations		RMSD	
		West	East	West	East	West	East
0-30 m	NO_3	0.4 [0.2]	0.6 [0.1]	BQL	BQL	0.44	0.67
	PO_4	0.02 [0]	0.002 [0]	BQL	BQL	0.020	0.0047
250-1500 m	NO_3	6.3 [1]	4.7 [0.4]	8.7 [1.1]	5.3 [1.4]	2.3	1.90
	PO_4	0.27 [0.1]	0.14 [0]	0.37 [0.1]	0.18 [0.1]	0.12	0.047
$>$ 1500 m	NO_3	7.7 [0.1]	5.4 [0.2]	8.9 [0.5]	5.0 [0.5]	1.2	0.33
	PO_4	0.34 [0]	0.15 [0]	0.38 [0]	0.16 [0]	0.049	0.032
Range	NO_3	[0 ; 7.8]	[0.36 ; 5.7]	[BQL ; 9.8]	[BQL ; 6.3]	2.1	1.7
	PO_4	[0 ; 0.34]	[0 ; 0.18]	[BQL ; 0.44]	[BQL ; 0.28]	0.11	0.042

A1.2 Seasonal and vertical variation

The surface patterns of change in mNO_3 and mPO_4 at the DyFaMed station are plotted in Fig. 16. mNO_3 and mPO_4 exhibit a seasonal pattern, with values regularly lower than 0.5 μmol l^{-1} from May (March for mPO_4) to October, increasing thereafter to reach a maximum in January ranging from 3.2 to 4.2 (0.03 to 0.07 for mPO_4) μmol l^{-1} depending on the year. This is very similar to the change in observed NO_3 which is also below 0.5 μmol l^{-1} from May to October and reaches a maximum ranging from 2 to 6.4 μmol l^{-1} in January-February. In summer, however, oNO_3 is often almost below the quantification limit while mNO_3 is never below 0.2 μmol l^{-1}. oPO_4 is below the quantification limit in almost every observation made above 30 m depth, except between January and March where oPO_4 can reach 0.15 μmol l^{-1}. These maxima are underestimated by the model, as mPO_4 never exceeds 0.07 μmol l^{-1} (close to the quantification limit). The differences between mPO_4 and oPO_4 at very low phosphate concentrations can be partly attributable to the lower reliability of measurements near the detection limit. For higher phosphate concentrations however, especially during the winter convection period, there is a clear deficit in the mPO4 which is not only due to the underestimated initial mPO4 concentration in deep waters (this has already been evidenced by the comparison with BOUM data, see section A1.1), but also potentially due to an underestimation of the MLD in winter.

Between 30 and 1000 m depth, observed and modeled NO_3 and PO_4 concentrations are consistent with each other though observations show higher mean values and larger ranges quite systematically (see Fig. 17 and 18 and table 2). The highest absolute differences within the water column are observed between 250 and 500 m depth for nitrate where mNO_3 is underestimated by 1.5 μmol l^{-1}, and between 30 and 100 m for phosphate where the mean mPO_4 is very low ($<$ 0.02 μmol l^{-1}) while oPO_4 equals 0.14 μmol l^{-1}. The same interpretation of this poor representation of the shape

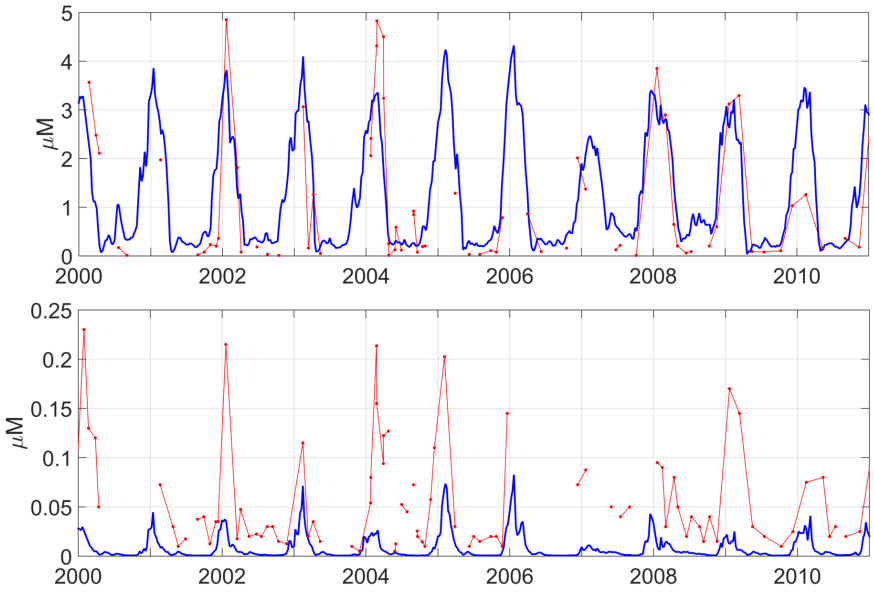

Figure 16. Patterns of change over time of modeled (lines) and observed (dots) surface concentrations in nitrate and phosphate in μmol l^{-1} at the DyFaMed site.

of the nutriclines (well marked in observations and much more diffuse in the model outputs) as the one provided for the comparison with BOUM profiles can be put forward to explain this model failure, namely underestimated deep nutrient concentrations and a lack of detrital particles that would have reached such water depths before being hydrolyzed. It must be borne in mind, however, that DyFaMed observations are compared to a single grid point of the modeled domain which is submitted to variability due to hydrodynamic features. We evaluated the potential impact of variability by calculating the spatial standard deviation using the 8 neighbouring grid points. The impact of spatial variability is weak on temporal means and stays below 0.5 and 0.04 μmol l^{-1} for NO_3 and PO_4 respectively during the whole period, and therefore cannot fully explain the differences observed.

A2 Chlorophyll

A2.1 Basin scale variability

Maps of the annual means of oCHL and mCHL as well as their difference (i.e. oCHL-mCHL) over the 2002-2011 period are plotted in Fig. 19 . mCHL is calculated as the average concentration through the first 10 m of the water column.

At first, year-long high chlorophyll clusters can be seen in both oCHL and mCHL close to the main river mouths (the Nile, Rhone, Po, Ebro or Tiber), but only in oCHL in the Dardanelles Strait, along the western coast of the Adriatic Sea and in the Gulf of Gabes. For the Dardanelles Strait, the difference is likely due to a poor representation of the nutrients inputs at this boundary. For the Adri-

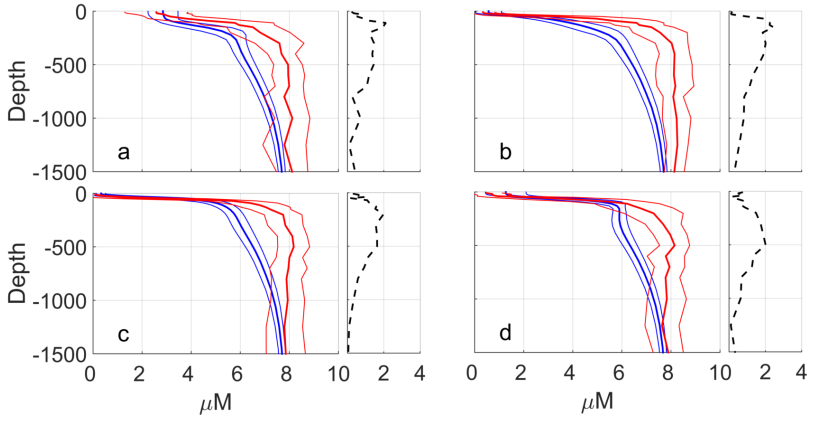

Figure 17. Seasonal climatological data over the 2000-2011 period of modeled (blue lines) and observed (red lines) concentrations in nitrate (μmol l^{-1}) at the DyFaMed site. (a) winter (Dec.-Feb.); (b) spring (Mar.-May); (c) summer (Jun.-Aug.); (d) autumn (Sept.-Nov.). Dotted lines on right panels represent the mean absolute bias between model and data.

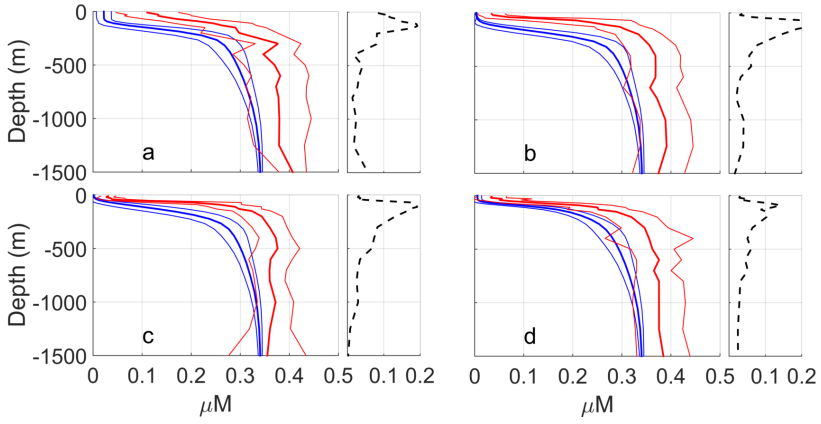

Figure 18. Seasonal climatologies of modeled (blue lines) and observed (red lines) concentrations in phosphate (μmol l^{-1}) at the DyFaMed site. (a) winter (Dec.-Feb.); (b) spring (Mar.-May); (c) summer (Jun.-Aug.); (d) autumn (Sept.-Nov.). Dotted lines on right panels represent the mean absolute bias between model and data.

atic Sea, nutrient inputs from rivers are included in the model, but not the ones inferred by anthropic activities (domestic, industrial, agriculture), which may result in an underestimation of the nutrient inputs in this region, and therefore in an underestimation of the chlorophyll concentrations. Finally,
1105 the differences between mCHL and oCHL in the Gulf of Gabes is likely due to two main features: first, this region is very shallow, which may produce less reliable satellite data. More importantly, the region of Gabes is characterized by an important industrial production of phosphate which effluents induce a strong enrichment in phosphate in this region, and this is not included in the model. Apart from these permanent features, the main differences between the model and satellite data are

Table 2. Mean over the 2000-2011 period of modeled (mNO_3, mPO_4) and measured (oNO_3, oPO_4) nutrients concentrations at the DyFaMed site for different layers. Root Mean Squared Difference (RMSD) between model outputs and observations have been calculated. Std stands for standart deviation. Spatial variability around the DyFaMed grid point is also assessed through the spatial standart deviation calculated using the 8 neighbour points (first column), and the value given in the table (first column) is the highest deviation calculated during the 2000-2011 period.

			NO_3			
	Spatial Std	mNO_3 mean [range]	mNO_3 Std	oNO_3 mean [range]	oNO_3 Std	RMSD
0-30	0.22	1.3 [0.04-4.3]	1.1	1.0 [BQL-5.2]	1.4	1.1
30-100	0.32	3.0 [0.09 6.1]	1.3	3.8 [BQL-8.3]	2.2	1.8
100-250	0.25	5.1 [1.7-6.7]	1.0	7.0 [2.7-9.6]	1.4	1.4
250-500	0.13	6.2 [5.2-7.2]	0.39	8.1 [5.0-9.9]	0.8	2.0
1000-2000	0.03	7.6 [7.0-7.9]	0.21	8.0 [5.9-9.4]	0.75	0.81
			PO_4			
	Spatial Std	mPO_4 mean [range]	mPO_4 Std	oPO_4 mean [range]	oPO_4 Std	RMSD
0-30	0.001	0.008 [0-0.08]	0.12	1.0 [BQL-0.26]	0.06	0.07
30-100	0.02	0.02 [0-0.19]	0.03	0.14 [BQL-0.54]	0.10	0.16
100-250	0.03	0.15 [0.02-0.33]	0.09	0.29 [0.07-0.45]	0.07	0.17
250-500	0.001	0.29 [0.19-0.33]	0.03	0.35 [0.01-0.46]	0.05	0.08
1000-2000	0.001	0.34 [0.32-0.35]	0.01	0.37 [0.21-0.52]	0.05	0.05

observed in the deep convection region of the Liguro-Provencal sub-basin (and extending up to the Ligurian Sea), along the Algerian coast, in the Alboran Sea, and in the south of the eastern basin. The three former are mostly attributable to failures of the hydrodynamic model: first, the fact that the contours of the modeled deep convection region are not the same as the measured ones have already been identified in the hydrodynamical simulation (Beuvier, 2011). Moreover, differences between measured and modeled MLD can also explain differences in the annual surface chlorophyll pattern as for example in the Ligurian Sea where an underestimation of the maximum mNO3 and mPO4 values, likely due to a deficit in the inputs of nutrients from deep waters during winter convection have been evidenced at DyFaMed station (see Fig. 16). The same is true for the Algerian current which is underestimated by the physical model (Soto-Navarro et al., 2014). As a consequence, when the Atlantic waters arrive north of Algeria and Tunisia, they are more nutrient-depleted (and therefore less productive) than what is observed. Furthermore, the Atlantic waters that flow along the coast are less dense and therefore strongly isolated from the rest of the water column and it seems that this property is excessively pronounced in the physical model (Beuvier, 2011). As a result, their nutrients content will be too rapidly consumed leading to underestimated primary production and

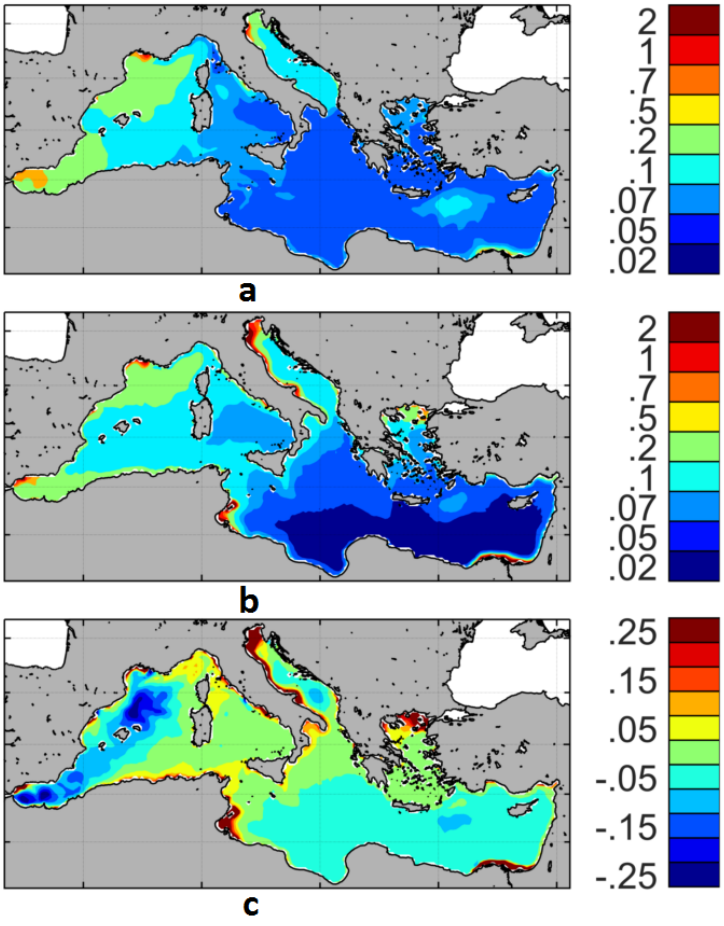

Figure 19. Maps of mean annual surface chlorophyll concentrations (μg l^{-1}) (a) from satellite (i.e. oCHL), (b) from model (i.e. mCHL), and (c) the difference oCHL - mCHL. Model chlorophyll (mCHL) is averaged over the first 10 m of the water column. Period used is 2002-2011 for both model outputs and satellite data.

Chl concentrations in this region. Finally, in the Alboran Sea, the high mesoscale activity is probably not fully captured by the hydrodynamic model. In the eastern basin, mCHL is overestimated nearly everywhere, and mostly in the southern part. This difference is however very weak (less than 0.05 μg l^{-1}) and does not clearly appear in the climatological data presented in Fig. 20. Overall, and apart from the hot spots already discussed, the maximum absolute error does not exceed 0.25 μg l^{-1} in the chlorophyll-rich regions of the western basin (i.e. the deep convection region and the core of the eddies in the Alboran Sea) and 0.15(0.05) μg l^{-1} elsewhere in the western (eastern) basin.

In conclusion, though the aforementioned discrepancies between mCHL and oCHL, the model is able to track the location of: i) most of the major productive areas (except the missing regions for which an explanation has already been put forward, ii) a well-marked Liguro-Provencal bloom, which is, nevertheless, more intensive and more extensive in the model, iii) a clearly visible weakly

productive northern current (NC), and iv) a patch with high chlorophyll concentrations in the Rhodes Gyre.

A2.2 Seasonal surface variability

To further study the seasonal variability of surface chorophyll, we used (for the satellite and model derived chlorophyll concentrations) the metric ΔChl defined as follows :

$$\Delta Chl = \frac{\max(Chl_{\text{year}})}{\text{median}(Chl_{\text{year}})} \tag{A1}$$

Since chlorophyll time distribution does not follow a normal law, this indicator is probably more relevant than the mean and the standard deviation. Moreover, since it is applied to climatological data of chlorophyll outputs, extreme values have already been smoothed. High values of ΔChl can therefore be related to a strong seasonal variability, while low values, typically < 2, can be associated with a constant signal (Fig. 20).

For both model and satellite, the seasonal signal is particularily strong in the Liguro-Provencal sub-basin ($\Delta Chl > 10$) and the Algerian Coast (ΔChl_{sat} about 8, ΔChl_{mod} above 10). ΔChl is broadly above 6 for the model and 4 for satellite data in the western basin west of 9°W. In the Tyrrhenian Sea, ΔChl is close to zero for the model, except for the area along the Italian Coast, while ΔChl for satellite data, it is above 3, with a maximum value around 6.

In the eastern basin, model ΔChl is almost nil everywhere except in the Rhodes Gyre (> 10) and in the Adriatic Sea where two patches of values above 10 can be seen. oCHL values are also low, except in the south Ionian basin (where $\Delta Chl \approx 2$), the Rhodes Gyre and the Gulf of Gabes ($\Delta Chl > 6$). In the Adriatic sea, a patch of values of ΔChl above 3 is visible in the south.

Using SeaWiFS and MODIS surface chlorophyll data from 1998 to 2010 and statistical work from D'Ortenzio and Ribera d'Alcalà (2009), Lavigne et al. (2013) identified 9 different regions on the basis of the seasonality of the chlorophyll signal. These regions are consistent with those emerging from the present study. The north-west bloom region is associated with the region of the highest values of ΔChl_{mod} and ΔChl_{sat}. The Algerian region is characterized by relatively high ΔChl values, while the intermittent Rhodes Gyre region is identified as highly variable in the present study according to satellite data and model outputs. The distinction between the southern and northern Ionian basins in the bioregionalization, also visible satellite ΔChl is however absent in the model ΔChl.

The comparison of modeled and observed time series (climatological data over the 2000-2011 period) provides additional information on the modeli's ability to reproduce surface chlorophyll seasonal variations. Though the model values of the central eastern basin are within the range of observations in the open sea (see Fig. 19), the highest discrepancy in the seasonal signal is observed in the oligotrophic region of the Levantine basin: the mCHL seasonal signal is in phase opposition with that of oCHL, and the maximum mCHL is obtained in summer-autumn against winter for oCHL.

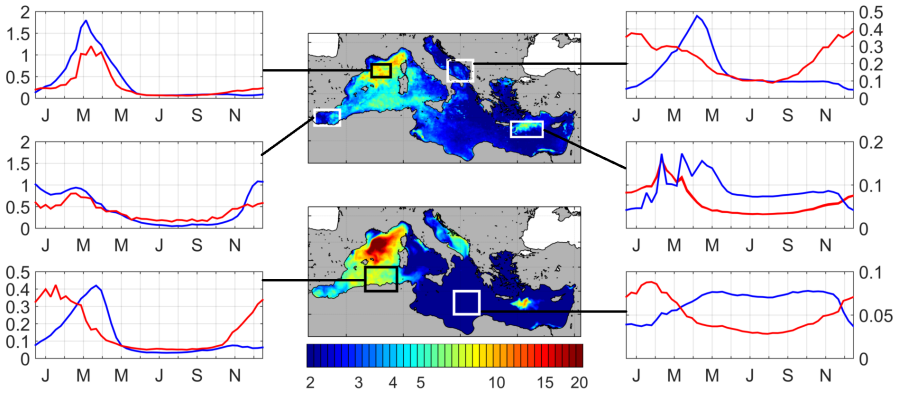

Figure 20. Maps of the ratio ΔChl (Eq. A1) between annual maximum and annual median for satellite (top) and model (bottom) chlorophyll surface concentrations over the 2002-2011 period. A climatology of oCHL (red lines) and mCHL (blue lines) over the same period is also plotted for the most representative regions.

Comparison between models is beyond the scope of this paper, however comparisons with former simulations (Lazzari et al., 2012; Mattia et al., 2013) can offer some information. It is noteworthy that results from Mattia et al. (2013) showed a greater bias in the eastern basin than in the western basin, with higher annual concentrations compared to satellite measurements. However, the maximum of surface chlorophyll in the eastern basin was simulated in winter (as for satellite chlorophyll) in Mattia et al. (2013). This is also the case in the simulation run by Lazzari et al. (2012), however summer concentrations seemed to be underestimated in that case. This shortcoming can however be largely relativized by the fact that the mean surface chlorophyll in summer-autumn does not differ significantly from the satellite measurement. Furthermore, surface chlorophyll in the model is estimated as the mean over the first 10 m of the water column, and therefore includes part of the chlorophyll gradient towards the Deep Chlorophyll Maximum (DCM) which is shallower than that observed in the eastern basin during the stratification period (results not shown though the same bias is observed at the DyFaMed site, see Appendix A2.3). Finally, the summer functioning of the surface layer is well reproduced by the model : small phytoplankton are largely dominant and maintain their activity because of the microbial loop (Siokou-Frangou et al., 2010).

A shift in chlorophyll maximum can also be seen in the south of the western basin, with an earlier and longer bloom in oCHL than in mCHL. This could be partly due to the aforementioned tendency of the model to exagerate the isolation of the surface Atlantic waters from the rest of the water column, thus delaying the input of nutrients from deep water through winter convection. Finally, in the Adriatic Sea, a delayed input of nutrients from deep waters combined with the presence of two eddies with high core mCHL values in winter and mostly in spring that are not observed on oCHL (the position of the two eddies can be seen on the primary production map in Fig. 22), probably explains the shift between oCHL and mCHL. Conversely, in regions associated with high nutrient

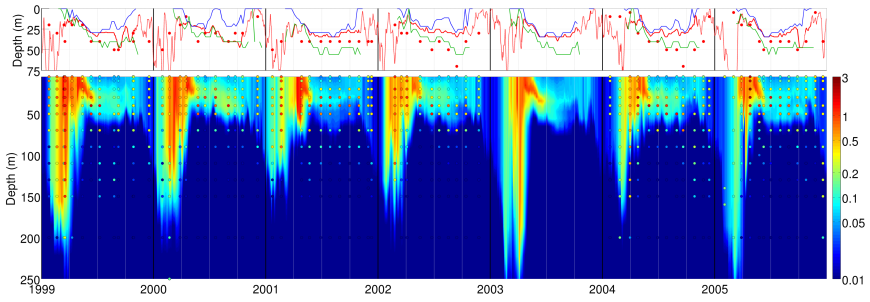

Figure 21. Patterns of change over time of vertical concentrations of chlorophyll (μg l^{-1}) at the DyFaMed site, with model outputs in shaded colors and in situ data (Marty et al., 2008) in colored dots. Top, the depth of chlorophyll maximum is represented with red dots for in situ data and the red line for the model. Depths of maximum chlorophyll for small phytoplankton (blue) and large plankton (green) are also plotted.

inputs (Ligurian Sea, Alboran Sea) the temporal pattern of change of surface chlorophyll is reproduced by the model but concentrations are overestimated during the bloom in the deep convection region, probaly due to too intensive winter mixing (Beuvier, 2011).

A2.3 Vertical variability

At the DyFaMed station, strong seasonal variability in chlorophyll concentrations can be observed in both model outputs and in situ data (Marty et al., 2002; Marty and Chiavérini, 2010). Chlorophyll data (oCHL) and modeled data (mCHL) are mutually consistent as shown in Fig. 21: they both show a bloom occurring in late February early March after the period of maximum mixing (mid February in this area), and characterized by high chlorophyll concentrations within the mixing layer (down to 150 m depth). A second less intense and shallower bloom often follows in April, characterized by chlorophyll concentrations above 1.5 μg l^{-1} in both model outputs and observations. During summer, surface concentrations are at their lowest level with values of mChl and oChl often below 0.1 μg l^{-1}, while their maximum values are observed in early spring.

Following April, a DCM is visible in both observations and model, though it is shallower in the model and its intensity decreases more rapidly than in observations (see Fig. 21-top).

However, when looking at the two chlorophyll contributors of the model, it appears that the position of the DCM associated with large phytoplankton is close to that observed. This means that the difference in the DCM depth is probably due to the underestimation of large phytoplankton concentrations at depth by the model during summer, that may be inferred by the already identified underestimation by the model of nutrient stocks in the intermediate layer (see section A1.1).

A3 Primary production

In the following section, mIPP refers to the modeled integrated Gross Primary Production, i.e. to the total amount of inorganic carbon fixed by the two phytoplankton groups integrated over the water column. The equivalent for observations will be referred to as oIPP.

A3.1 Spatial variability

The mean annual mIPP for the whole basin over the 2000-2012 period equals 82 gC m^{-2} y^{-1}, which is within the range of published values (see Table 3). In this table, the studies by Bosc et al. (2004) and Uitz et al. (2012) both show quite similar oIPP spatial distributions despite the two analyses having been conducted during different periods (1997-2001 for Bosc et al. (2004) and 1998-2007 for Uitz et al. (2012)). IPP calculated by Bosc et al. (2004) tend to overestimate observations, particularily in ultra-oligotrophic regions while IPP from Uitz et al. (2012) does not show a trend of error. In the different geographical regions defined in Bosc et al. (2004) and reported in Tab. 3, mIPP is mostly within the range defined by the two aforementioned studies. More importantly, the hierarchy in terms of IPP values between the different regions is the same for the model and the satellite products.

mIPP values in the Mediterranean Sea range between 35.4 and 270 gC m^{-2} y^{-1}, showing a strong spatial heterogeneity (see Fig. 22a). A gradient in mIPP is observed from west to east : the western basin production is almost twice that of the eastern basin, which is coherent with the dissimilarity in chlorophyll and nutrients already mentioned. This ratio is also coherent with the oIPP values derived from in situ measurements (Moutin and Raimbault, 2002), but higher than that found using satellite data (Uitz et al., 2012; Bosc et al., 2004) or another model (Lazzari et al., 2012).

Figure 22b shows that, except in the regions that benefit from permanent or episodic nutrient inputs from the deep sea (i.e. the deep convection region in the Liguro-Provencal sub-basin, eddies in the Alboran, Adriatic Seas and the Rhodes Gyre region), mIPP is mostly due to small phytoplankton throughout the Mediterranean Basin. In the eastern basin, the proportion of IPP due to small phytoplankton is close to 100% everywhere, except in the Levantine basin in the region of the Rhodes Gyre. These results are consistent with in situ studies (Siokou-Frangou et al., 2010; MERMEX-group, 2011).

A3.2 Seasonal variability

In addition to satellite data, in situ oIPP measured at the DyFaMed station between 2002 and 2006 (Marty et al., 2008) were used for comparison with mIPP (Fig. 23). The model and observations show very similar patterns, with a maximum in March-April, and a slight decrease from July to December. The correlation between mIPP and oIPP is significant as suggested by the right panel in Fig. 23, and does not show any bias though the model fails to reproduce the highest oIPP values.

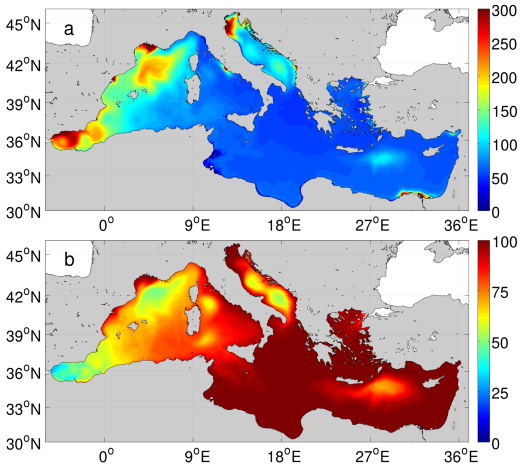

Figure 22. (a) Annual gross primary production calculated over the 2000-2012 period and integrated through the whole water column, in gC m^{-2} y^{-1}, (b) proportion of production due to small phytoplankton group, in %
.

Table 3. Integrated gross primary production (IPP in gC m^{-2} y^{-1}) for the different regions defined by Bosc et al. (2004) and for the whole Mediterranean Basin. mIPP values calculated by the model are compared to IPP values derived from the following references: (a) Bosc et al. (2004), (b) Uitz et al. (2012) (c) Antoine et al. (1995), (d) Lazzari et al. (2012), and (e) Sournia (1973). References (a) to (c) refer to satellite data, (d) to another modeling study, and (e) to a climatology of ^{14}C measurements

Region	Model (mIPP)	(a)	(b)	(c)	(d)	(e)
Alboran Sea	222	150	230			
Gulf of Lion	182	97	194			
Balearic Sea	145	80	167			
Algero-Provencal basin	123	78	153			
Ligurian Sea	109	80	165			
Algerian basin	107	78	163			
Adriatic Sea	102	71	182			
Tyrrhenian Sea	66	67	137			
South Levantine basin	65	59	105			
North Levantine basin	63	60	106			
South Ionian Sea	60	61	115			
North Ionian Sea	55	63	126			
Mediterranean Basin	82	68	136	156	98	80-90

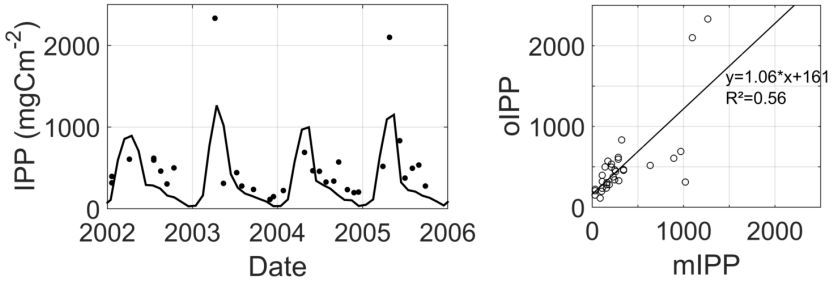

Figure 23. Patterns of change over time of monthly integrated gross primary production (IPP) in mg C^{-2} d^{-1}. oIPP correspond to 0-100 m in situ measurements extracted from the DyFaMed database (dots) and mIPP correspond to the 0-100 m IPP provided by the model during the same period (black line). oIPP were converted to daily gross primary production according to the Moutin et al. (1999) method.

A4 Dissolved organic carbon

Regular measurements of total DOC (i.e. including refractory (RDOC) and semi-refractory (SR-
1250 DOC) pools) performed at the DyFaMed site (Avril, 2002), were used for comparison. Since the model only provides the labile and semi-labile DOC pools, the in situ DOC concentration measured in deep water ($>$ 1000 m), which can be considered as refractory DOC, has been added to the model DOC output. Moreover, since our run does not cover the period of the in situ data, we decided to work on a climatological survey of DOC vertical profiles: bi-monthly mean, maximum and minimum
1255 DOC values were calculated and compared (Fig. 24).

At the DyFaMed grid point, mDOC stock is underestimated throughout the whole water column during winter. Then, mDOC and oDOC increase during spring (April-May), but only near the surface for mDOC. In summer, the mDOC and oDOC values remain high in the upper layers, and finally decrease in autumn. If these seasonal variations are well reproduced by the model, high differences
1260 can however be seen between mDOC and oDOC. If we first focus on the 0-100 m layer, DOC concentrations and seasonal variations of both the model and observations are at a maximum at the surface, but from spring to autumn, mDOC is higher than oDOC near the surface (roughly in the 0-50 m layer), and lower between 50 and 100 m depth, resulting in higher vertical DOC gradients in the model. The same discrepancy can also be evidenced (mostly in the western basin) from the
1265 comparison between mDOC and oDOC during the BOUM cruise that took place in summer (Fig. 25). The overestimated near-surface DOC concentrations may be attributable to an excessive P-limitation in the model, probably due to too low phosphate deep concentrations (see also section 4.3 for the description of the DOC accumulation process under P depletion). The shallower and underestimated DCM as compared to that measured (see section A2.3) may also partly explain the
1270 discrepancy since photosynthesis rates are underestimated. As a consequence, the excess of newly synthetized carbon through photosynthesis which fuels the DOC pool is probably underestimated in the region of the modeled DCM and even below. Too easy access for bacteria to SLDOC, resulting in overcomsuption of DOC by nutrient-replete bacteria, is another possible explanation of this bias.

mDOC concentrations are systematically lower than those of oDOC beyond 100 m depth. The
1275 latter argument relative to SLDOC access by bacteria could also partly explain the systematically underestimated mDOC concentrations below 100 m depth. Again, this model failure is also observed during the BOUM cruise (Fig. 25).

The comparison between oDOC and mDOC requires the addition of an unknown DOC component, namely the semi-refractory and the refractory pools, to the mDOC value. It is indeed generally
1280 assumed that both these pools are constant across the water column and that they correspond to the deep DOC concentration (i.e. 40 μM at DyFaMed station), but this is a clear source of bias, especially below 100 m depth where the SRDOC concentrations are significant and may vary, as suggested in Santinelli et al. (2010).

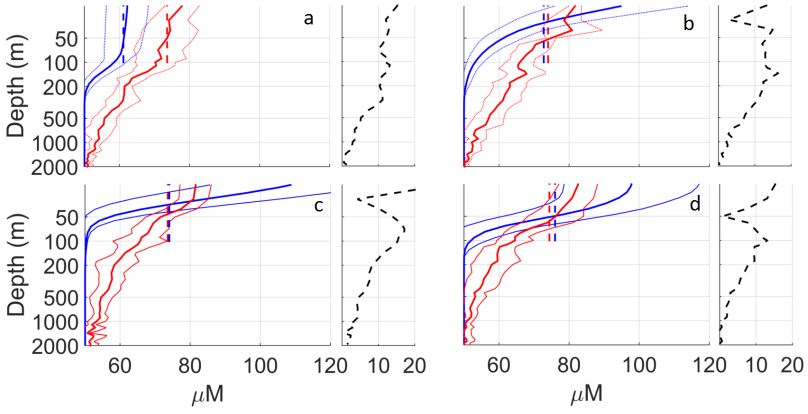

Figure 24. Vertical profiles of total DOC (μmol l^{-1}) at DyFaMed site (a) in winter, (b) spring, (c) summer and (d) autumn. mDOC are weekly averaged outputs. Blue and red lines respectively refer to modeled (mDOC) and measured (oDOC) DOC. Thick lines represent the mean of DOC over the period, while thin lines represent the standard deviation for each depth. oDOC and mDOC respectively cover the 1991-1993 (Avril, 2002) and the 2000-2012 simulation period. The dotted lines in the right panels represent the mean absolute bias between oDOC and mDOC.

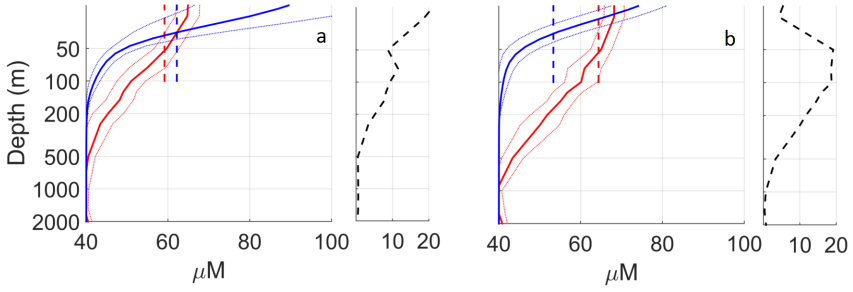

Figure 25. Vertical profiles of total DOC (μmol l^{-1}) during the BOUM cruise. mDOC are weekly averaged outputs over the whole BOUM section. Blue and red lines respectively refer to modeled (mDOC) and measured (oDOC) DOC. Thick lines represent the mean of DOC over the period, while thin lines represent the standard deviation for each depth. The dotted lines in the right panels represent the mean absolute bias between oDOC and mDOC.

The fact that the modeled 0-100 m integrated stocks are quite similar to the measured ones (though
1285 the slight underestimation in the eastern basin during the BOUM cruise since DOC accumulation has not yet reached its maximum value in summer) is however an essential point as regards the DOC export at 100 m.

Finally, the Taylor diagram presented in Fig. 26 summarizes the numerous comparisons between model outputs and the DyFaMed station observations undertaken in the present study.

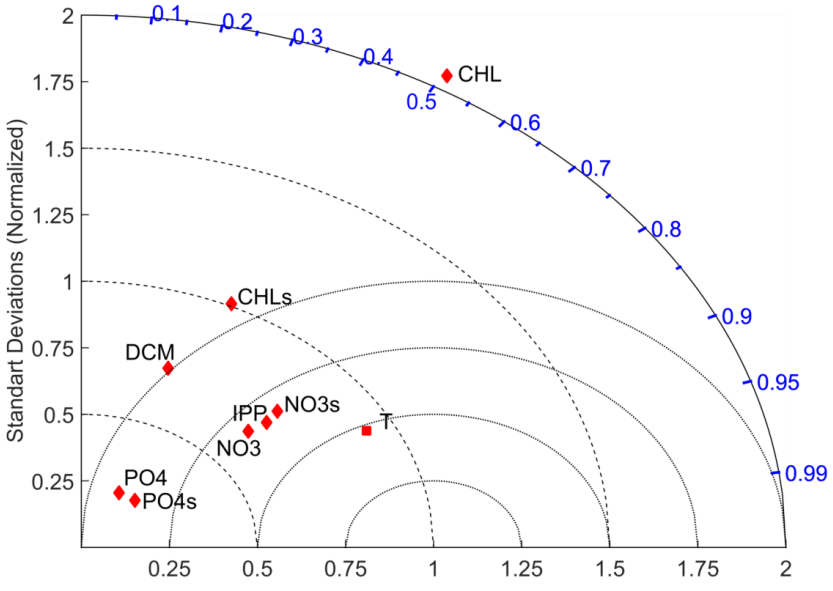

Figure 26. Taylor diagram of simulated and observed variables in the 0-100 m layer. Model outputs and in situ data are taken at the same depth and time. PO4s, NO3s and CHLs are surface concentrations of phosphate, nitrate and chlorophyll respectively. T refers to temperature. Chlorophyll concentrations are log-transformed.

Manuscript prepared for Biogeosciences
with version 2014/09/16 7.15 Copernicus papers of the LaTeX class copernicus.cls.
Date: 7 September 2015

New insights into the organic carbon export in the Mediterranean Sea from 3D modeling

A. Guyennon[1], M. Baklouti[1], F. Diaz[1], J. Palmieri[2], J. Beuvier[3,4], C. Lebaupin-Brossier[4], T. Arsouze[5,6], K. Béranger[5], J.-C. Dutay[7], and T. Moutin[1]

[1]Aix Marseille Université, CNRS/INSU, Université de Toulon, IRD, Mediterranean Institute of Oceanography (MIO) UM110, 13288, Marseille, France
[2]Southampton University – National Oceanography Center (NOC), Waterfront Campus, European Way, Southampton SO14 3ZH, UK
[3]Mercator Ocean, Ramonville Saint-Agne, France
[4]CNRM-GAME, Météo-France/CNRS, Toulouse, France
[5]UME, ENSTA-ParisTech, Palaiseau, France
[6]Laboratoire de Météorologie Dynamique, École Polytechnique, Palaiseau, France
[7]LSCE/IPSL, Laboratoire des Sciences du Climat et de l'Environnement, CEA-CNRS-UVSQ, Gif-sur-Yvette, France

Correspondence to: melika.baklouti@mio.osupytheas.fr

COLOR CODE:

~~RED~~ = DELETED TEXT

BLUE = NEW TEXT

BLACK = OLD TEXT

Abstract. The Mediterranean Sea is one of the most oligotrophic regions of the oceans, and nutrients have been shown to limit both phytoplankton and bacterial activities, resulting in a potential major role of dissolved organic carbon (DOC) export in the biological pump. ~~This has direct implications on the stock of dissolved organic carbon (DOC), whose~~ ~~High variability~~ Strong DOC accumulation in surface waters ~~has~~ is already ~~been~~ well-documented, though ~~even if~~ measurements of DOC stocks and export flux are still sparse and ~~are~~ associated with ~~important~~ major uncertainties. ~~We here propose a Mediterranean basin-scale view of the export of organic carbon, under its dissolved and particulate forms.~~ This study provides the first basin-scale oveview and analysis of organic carbon stocks and export fluxes in the Mediterranean Sea through a modeling approach based on ~~For this purpose, we have used~~ a coupled model combining a mechanistic biogeochemical model (Eco3M-MED) and a high-resolution (eddy-resolving) hydrodynamic simulation (NEMO-MED12). ~~This is the first basin-scale application of t~~ The ~~biogeochemical~~ model ~~Eco3M-MED~~ ~~and~~ is shown to reproduce the main spatial and seasonal biogeochemical characteristics of the Mediterranean Sea. Model estimations of carbon export are also of the same order of magnitude as estimations from

in situ observations, and their respective spatial patterns are mutually consistent. ~~with each other.~~ ~~As for surface chlorophyll, nutrient concentrations, and productivity~~ Strong differences between the western and eastern basins are evidenced by the model for organic carbon export. Though less oligotrophic than the eastern basin, the western basin only supports ~~, with only~~ 39 % of organic carbon (particulate and dissolved) export. ~~taking place in the western basin.~~ Another ~~The~~ major result is that except for the Alboran Sea, ~~dissolved organic carbon~~ the DOC contribution to organic carbon export is higher than that of particulate organic carbon (POC) throughout ~~in~~ the ~~whole~~ Mediterranean Sea, ~~basin~~ especially in the eastern basin. This paper also investigates the seasonality of DOC and POC exports as well as the differences in the processes involved in DOC and POC exports in the light of intracellular quotas. Finally, according to the model, strong phosphate limitation of both bacteria and phytoplankton growth is one of the main drivers of DOC accumulation and therefore of export.

1 Introduction

The biological pump is recognized as a major component of carbon export ~~by~~ in the ocean and plays a significant role in the carbon cycle as a whole (Siegenthaler and Sarmiento, 1993). The sinking of organic particles has long been identified as the main process involved in the biological pump, thereby sustaining the vertical carbon and nutrient gradients in the ocean (Eppley and Peterson, 1979; Sarmiento and Gruber, 2006). ~~Major~~ Considerable attention has therefore been paid to the export of organic carbon ~~under~~ in its particulate form.

~~The improvement of~~ Advances in the characterization of dissolved organic pools have led to ~~investigation into~~ a better knowledge of the role of the dissolved organic carbon (DOC) compartment in the ocean carbon cycle. As a non-sinking tracer, the fate of DOC ~~fate~~ is strongly linked to physical processes and its export occurs via vertical mixing and/or downwelling when it ~~reaches~~ lies in intermediate waters, and via oceanic overturning circulation ~~when it reaches the~~ in deep ~~est layers~~ water (Hansell et al., 2002, 2009). If the early works of Copin-Montégut and Avril (1993) in the Mediterranean Sea and Carlson et al. (1994) in the Sargasso Sea were the first attempts to ~~evaluate~~ quantify ~~the~~ DOC export flux ~~of DOC~~ below the euphotic zone, ~~the~~ estimation of detrital particulate organic carbon (POC) export ~~calculation had begun~~ began years before with the deployment of sediment traps and isotopics ~~following~~ measurements (Buesseler, 1991).

The seasonal variability of DOC in the euphotic zone has been widely recorded in the sub-tropical and temperate areas of the ocean (Carlson et al., 1994; Avril, 2002; Hansell and Carlson, 2001; Santinelli et al., 2013). The results of these studies indicate a time lag between DOC production and consumption, ~~sources and sinks,~~ causing summer accumulation in the upper layers due to both biotic and abiotic processes, which either alter DOC bioavailability or reduce bacterial activity. ~~Indeed, t~~ The inefficiency of the microbial loop in organic carbon mineralization - the so-called malfunctioning microbial loop (Thingstad et al., 1997) - induces an accumulation of bioavailable DOC. This

inefficiency is directly related to low phosphate availability in the upper waters of the Mediterranean Sea (Moutin et al., 2002; Van Wambeke et al., 2002; Thingstad et al., 2005; Santinelli et al., 2013).

~~The pathway of organic carbon not only allows to estimate the total amount of fixed carbon, but it is also crucial to determine the biological pump efficiency.~~ In this paper, our aim is to investigate the pathways of organic carbon (OC) at the scale of the Mediterranean Sea, and more specifically to characterize OC export fluxes since this is crucial to determine the efficiency of the biological pump. High resolution 3D modeling using the biogeochemical mechanistic model Eco3M-MED (Alekseenko et al., 2014) forced by the physical model NEMO-MED12 (Beuvier et al., 2012b) was chosen to address this question. ~~, taking into account the high heterogeneity of situations encountered in the Mediterranean Sea. In line with these considerations, the biogeochemical model was designed to be relevant in every region (see Sect. 2).~~ Major modeling work has already been done to estimate organic carbon export using box models (e.g. Toggweiler et al., 2003), ocean carbon-cycle models (e.g. Bopp et al., 2001; Sarmiento et al., 1998; Maier-Reimer et al., 1996; Sarmiento and Gruber, 2006) and ecosystem models coupled with hydrodynamic models (e.g. Le Quéré et al., 2010). ~~The objective of this paper is to fit within this framework, but at a the scale of the Mediterranean Basin and at high spatial and temporal resolution, with detailed description of biological processes.~~ Several coupled models have also been developed to study the whole of the Mediterranean Sea, starting with the early simulation by Crispi et al. (1998) and Crise et al. (1998). The number of models designed for this purpose is increasing (Lazzari et al., 2013; Mattia et al., 2013; Macías et al., 2014), but to our knowledge, no modeling work has yet focused on organic carbon fluxes for the entire Mediterranean Sea. Here, our aim is to focus on OC export in the Mediterranean Sea by characterizing and quantifying the associated fluxes, studying their temporal and spatial variability, and providing the first estimations at this scale of the respective contributions of DOC and POC (which refers to the detrital particulate organic carbon only in the present paper) to carbon export. We also aim to analyze the processes involved in DOC and POC production export ~~Moreover, the biogeochemical model Eco3M-MED is able to analyze biogeochemical fluxes and stocks~~ in the light of the intracellular quotas of planktonic organisms calculated by Eco3M-MED. ~~In this paper, we aim to further investigate organic carbon export in the Mediterranean Sea in order to quantify the associated fluxes, to study their temporal and spatial variabilities, and to provide the first estimations at this scale of the respective contributions of DOC and POC (i.e. the detrital particulate organic carbon) to carbon export. To achieve this objective, we undertook 3D biogeochemical modeling of the Mediterranean Sea using the biogeochemical model Eco3M-MED (Alekseenko et al., 2014), forced by physical simulations made with NEMO-MED12 (Beuvier et al., 2012b).~~ The paper is organized as follows: After the introduction (Sec. 1), a succinct overview (Sect. 2) of ~~both models~~ the hydrodynamical model NEMO-MED12 (Sec. 2.1) and the biogeochemical model Eco3M-MED (Sec. 2.2) is ~~given~~ provided, given that they are ~~fully detailed~~ described in detail in the aforementioned papers. Simulation set-up and datasets used for model comparison are also presented. Sect. 3 first focuses on the

results related to organic carbon inventory and export at the scale of the Mediterranean Basin, and for the purpose of discussion, ~~needs~~ results on intracellular quotas in phytoplankton and bacteria as well as on exudation fluxes are also presented. In Sect. 4 results on export are discussed in the context of previous POC and DOC export evaluations in the Mediterranean Sea, and in the light of processes and intracellular quotas in phytoplankton and bacteria. Finally, an appendix ~~a supplementary material~~ is associated with this paper ~~for~~ containing the assessment of the biogeochemical model outputs (nutrients, chlorophyll, primary production and DOC) through comparison with available data and analysis of the main discrepancies.

2 Material and methods

2.1 The hydrodynamic model

The physical run used in this work is described in Beuvier et al. (2012b). It has been simulated by the regional circulation model NEMO-MED12 Beuvier et al. (2012a) which is part of a suite of Mediterranean regional versions of OPA and NEMO (Madec and The-NEMO-Team, 2008) as OPAMED16 (Béranger et al., 2005), OPAMED8 (Somot et al., 2006) and NEMO-MED8 (Beuvier et al., 2010).

Model resolution is 1/12 ° ($\approx$ 8 km) which means that most of the mesoscale features are explicitely resolved, and the domain includes the whole of the Mediterranean Sea as well as the Atlantic Ocean West of 11°W (Fig. 2). More details of the model and its parametrization are given in Beuvier et al. (2012a).

The simulation ~~is~~ was initiated in October 1958 with temperature and salinity data representative of the 1955–1965 period using the MEDATLAS dataset (MEDAR/MEDATLAS-Group 2002, Rixen et al., 2005). Atmosphere forcings are applied daily and come from the ARPERA dataset (Herrmann and Somot, 2008), a 55-year simulation at 50 km and daily resolutions. SST-relaxation and water-flux correction terms, as well as fresh water input from rivers and the Black Sea and Atlantic exchanges are the same as described in Beuvier et al. (2010, 2012a).

2.2 The biogeochemical model

The biogeochemical model Eco3M-MED is embedded in the Eco3M modular numerical tool (Baklouti et al., 2006b), and its structure is similar to the model presented in Alekseenko et al. (2014). Fig. 1 summarizes the interactions between the state variables through the biogeochemical processes. We chose to represent three different element cycles C, N and P in order ~~allowing~~ to reproduce the different limitations and co-limitations observed in the Mediterranean Sea. Silicium, potentially limiting in some regions (Leblanc et al., 2003) is not represented in the model, as P and N limitations are the most common ones in the Mediterranean Sea. Six different planktonic functional types (P.F.T., see Le Quéré et al. (2005) for a proper definition) are represented : 2 primary producers (phytoplankton),

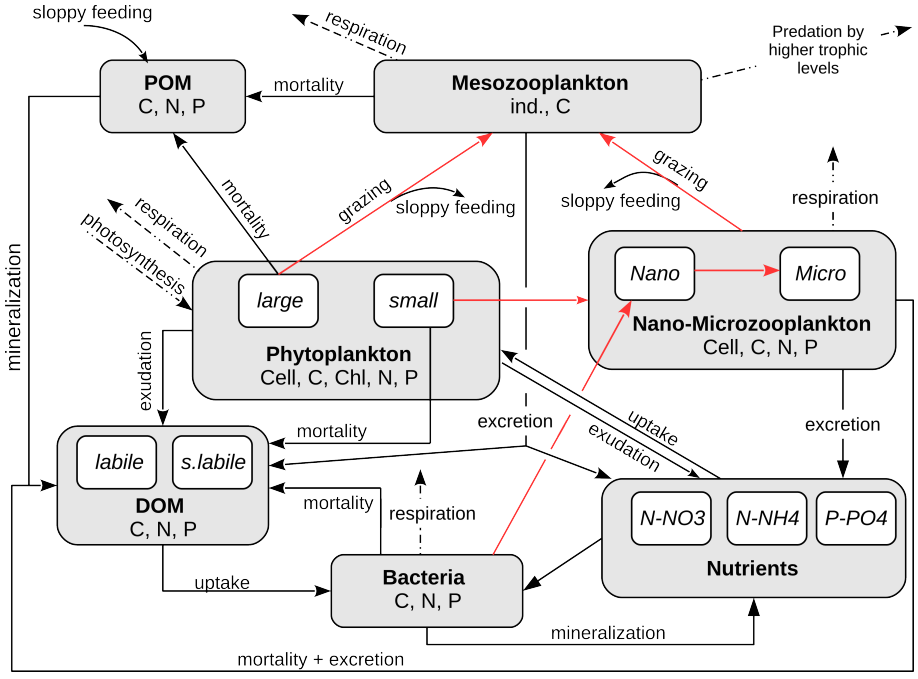

Figure 1. Conceptual diagram of the biogeochemical model Eco3M-MED. Grey boxes represent major compartments and white boxes sub-compartments. State variables for each sub-compartment are listed at the bottom of compartment boxes. Red arrows indicate grazing processes from the prey to the predator.

1 decomposer (heterotrophic bacteria) and 3 consumers (nano-, micro- and meso-zooplanktons). The structure of the trophic web thereby includes the main P.F.T.s of the Mediterranean Sea (Siokou-Frangou et al., 2010).

Each P.F.T. of the model is represented through several state variables, namely C, N, P (and Chl for producers) concentrations and a cell number (i.e. an abundance), ~~Every P.F.T. is represented in terms of several biomasses (C, N, P, and Chlorophyll for producers) and an abundance (cells per unit volume),~~ except for meso-zooplankton which is only represented through its C concentration and its abundance (in individuals per unit volume). Intracellular ratios (i.e. the ratio between two elemental concentrations) as well as intracellular quotas (i.e. the quantity of a given element per cell) can therefore be calculated dynamically by the model. Intracellular ratios are indicators of plankton stoichiometry, i.e. of its C:N:P elemental composition. Early biogeochemical models (NPZD models) have considered a constant C:N:P ratio in plankton given by the canonical Refield ratio of 106:16:1 (Redfield, 1958). Based on Droop's work (e.g. Droop, 1968, 1975), an increasing number of biogeochemical models (e.g. Baretta et al., 1995; Geider et al., 1998) have in recent decades assumed flexible plankton stoichiometry. Though Droop's original quota function relating growth rate to the intracellular quota of the limiting element was based on cell quotas, these biogeochemical models have used intracellular ratios instead of quotas to regulate the rate of biomass synthesis (and other

process rates) with quota functions similar to that of Droop. These flexible stoichiometry models have been widely used in the framework of theoretical batch or chemostat studies (e.g. Geider et al., 1998; Baklouti et al., 2006b) or for large-scale studies with ERSEM (Baretta et al., 1995), BFM (Vichi et al., 2007) or others (e.g. Moore et al., 2002) models. In such models, substrate uptake and biomass synthesis are decoupled, but cell division is not explicitly represented.

Intracellular quotas (or cell quotas) as they are defined in the present paper are indicators of the C, N and P cellular content of plankton. They are an original feature of the Eco3M-MED model in the category of 3D coupled physical-biogeochemical models. This model is based on the assumption that there are a minimum ($Q_X^{\min}$) and a maximum ($Q_X^{\max}$) intracellular content for each element X among (C, N, P). $Q_X^{\min}$ can be interpreted as the amount of element X used in cellular structure and machinery, and the accumulated surplus as storage for future growth (Klausmeier et al., 2008). The variability in cell quotas has indeed been widely evidenced through several experimental and in situ studies (e.g. Brown and Harris, 1978; Fukuda et al., 1998; Lovdal et al., 2008; Heldal et al., 2003; Bertilsson et al., 2003; Wilhelm et al., 2013).

The use of cell numbers as state variables and of the associated intracellular quotas offers several advantages: firstly, it makes it possible to distinguish between cell division, which is described by a specific equation, see Eq. 1), biomass synthesis, and uptake. Second, intracellular quotas are indicative of the actual internal status of cells, i.e. they indicate whether cells are rich or depleted in a given element, while intracellular ratios only provide relative values. In other words, a given value of intracellular ratio Q_{XY} can correspond to several different cell statuses (for example, a given C:N ratio can be obtained with an infinity of pairs of C and N intracellular concentration values). Thus, intracellular ratios can only provide information on the internal relative quantity of X as compared to that of Y, while intracellular quotas inform on intracellular absolute quantities. The latter information is very useful for the analysis of plankton dynamics since it is informative about the nutritional status of each P.F.T. of the trophic web (see the Discussion section). It is also a good proxy of the quality of the prey available for zooplankton (i.e. whether prey are rich or depleted in a given element). Thirdly, the parameters determined at cell level can be used without using conversion factors. For example, uptake rate measured at cell level (Talarmin et al., 2011), or grazing parameters expressed in number of prey per predator per unit time, such as the ones provided in Christaki et al. (2009) for HNF and ciliates can be used directly.

~~If we denote X and Y two molecules among C, N, P and Chl, this allows to dynamically calculate for each P.F.T. not only intracellular ratios Q_{XY} which are the ratio between X and Y biomasses (as this is done in previous variable stoichiometry models such as ERSEM (Baretta et al., 1995) and BFM (Vichi et al., 2007)), but intracellular quotas Q_X which are the X content per cell (expressed in mol X cell^{-1}). These intracellular quotas provide a very important additional information since intracellular ratios are only indicative of the relative quantities of a given biomass compared to another one. But for a given intracellular ratio, cells can be either depleted or repleted. By contrast,~~

~~intracellular quotas give an additional information relative to cell status, that is if cells are rich or depleted in a given element. It also gives an indication of prey quality for predators.~~ Intracellular quotas have already been used in previous modeling studies to study phytoplankton growth (Klausmeier et al., 2004) or the dynamics of the planktonic food web (Thingstad et al., 2005). In the latter study, however, cell quotas of carbon were assumed to be fixed in the protozoa, while fixed C:N-ratios were assumed for bacteria and phytoplankton. Moreover, this model was used without being coupled with a physical model (i.e. for the simulation of microcosm and lagrangian experiments).

~~The~~ In the model, the producers are split into two different P.F.T.s according to their theoretical size, i.e. large phytoplankton (> 10 μm) mainly encompassing diatoms, and small phytoplankton ($<$ 10 μm) which includes picophytoplankton and the remaining nanophytoplankton. The two P.F.T.s have different parameters, distinct predators and ~~they~~ fuel different detritic pools (Fig. 1). Decomposers are represented by heterotrophic bacteria and are responsible for the organic matter mineralization, including hydrolysis of particles. Zooplankton is divided into three different size groups, heterotrophic nanoflagellate (HNF) which feeds on bacteria and small phytoplankton, ciliate which feeds on small phytoplankton and HNF, and mesozooplankton (copepods) which feeds on ciliate, HNF and large phytoplankton. Copepods are the only metazoans ~~of~~ in the model, and mechanisms such as individual growth, egg production or reproduction are implicitely represented (Alekseenko et al., 2014).

The processes used in the model are extensively described in the aforementioned reference. However, for the ~~needs~~ purposes of the present paper, we ~~remind~~ recall that POC is fueled by the natural mortality of largest organisms (mesozooplankton, diatoms and ciliates) and by the egestion of fecal pellets and sloppy feeding by mesozooplankton, and consumed by POC hydrolysis to DOC. The DOC pool has many inputs (phytoplankton exudation, zooplankton excretion, mortality of small organisms, POC hydrolysis) and a single output (uptake by bacteria). The formulations of most of the biogeochemical processes, for which details are extensively given in Baklouti et al. (2006a, 2011); Mauriac et al. (2011), and Alekseenko et al. (2014), follow cell level mechanistic considerations. Intracellular ratios (Q_{XY}) and intracellular quotas (Q_X) are used to regulate growth via Droop's quota function (Droop, 1968) and net uptake and grazing rates via Geider's limitation formulation (Geider et al., 1998). For example, the specific growth rate (i.e. the division rate) μ of all unicellulars in the model is given by the following equation:

$$\mu = \mu^{\max} \min_{X \in \{\mathrm{C,\,N,\,P}\}} \left(1 - \frac{Q_X^{min}}{Q_X}\right) \tag{1}$$

where $\mu^{\max}$ is the maximum division rate and $Q_X^{\min}$ the minimum intracellular X quota.

Grazing, primary production and uptake rates are controlled firstly by the organism's environment (either prey ~~preys~~ or nutrient concentration, or light availibility). Secondly, the internal cell status represented by intracellular quotas and ratios drives a feedback regulation of the net incorporated

biomass through quota functions. Hence, the uptaken ~~extra~~ surplus (which becomes more and more significant as the intracellular quota approaches Q^{max}) is either released in its initial form or exuded in the form of DOM. In the same way, ~~The same assumptions are applied to estimate~~ excretion ~~(ammonium, phosphate)~~ and fecal pellet production fluxes are proportional to the grazing flux and to a quota function the value of which increases as the quota approaches Q^{max}. Furthermore, 10 % of the material grazed by mesozooplankton directly fuels the particulate organic matter stock, to represent sloppy feeding. Respiration rates are estimated via energy costs for every plankton activity (Alekseenko et al., 2014). Nitrification is represented through first order kinetics while particulate hydrolysis function depends on bacteria intracellular quotas (POC hydrolysis increases with bacterial C-limitation). Grazing by higher trophic levels is implicitely taken into account via ~~a~~ quadratic mortality affecting only mesozooplankton. Grazing function is a Holling II type (Holling, 1959; Kooijman, 2000) for multiple prey. The only difference with the configuration of Alekseenko et al. (2014) ~~configuration~~ lies in the formulation used to represent predator preferences for multiple prey. We here used the "Kill The Winner" (KTW) formulation depicted in Vallina et al. (2014), which combines active-switching (i.e. the preference of a predator for a given prey depends on prey density) and an ingestion rate always increasing with the total biomass of prey. This active-switching formulation was used to preserve foodweb diversity (e.g Prowe et al., 2012) and to prevent unrealistic predator-prey oscillations.

Since the model relies on a mechanistic basis, parameters are mainly physiological (and measurable) and they were either taken from literature or derived from other parameters on the basis of physiological considerations and in the interests of greater consistency between parameters. For example, maximum intracellular quotas are inferred from minimum ones as done in Thingstad et al. (2005). Another example lies in the relationship between the maximum uptake rate of a given element, which is the product of the maximum specific growth rate and the maximum intracellular quota in that element. Other examples as well as the whole set of parameters are given in Alekseenko et al. (2014).

2.3 Model coupling

The models NEMO and Eco3M-MED have been associated for the first time. The coupling between the hydrodynamic and biogeochemical models is offline, i.e. biological retroaction on the physics is not taken into account. Daily-averaged water velocities were used for the advection of biogeochemical tracers, using a MUSCL scheme (horizontal and vertical diffusion fluxes are calculated according to a centered scheme). The time-step used for the numerical integration of the tracer conservation equations equals 1200 s. A sinking velocity of 2 m d^{-1} is applied only on the particulate organic pool (i.e. the detrital compartment). ~~This compartment aims at representating~~ The aim of this compartment is to represent particles with different sizes and sinking velocities and the value of

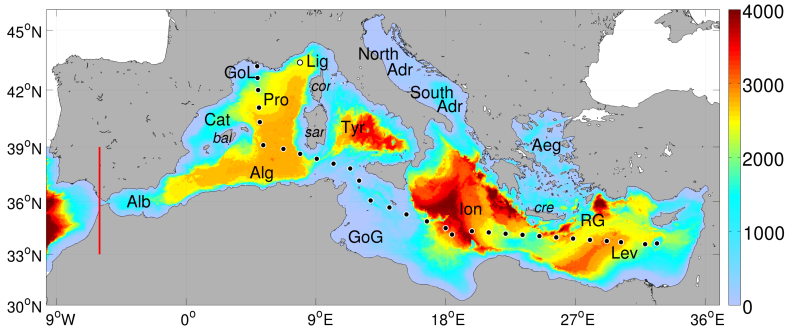

Figure 2. Bathymetry of the grid in meters, black dots represent the BOUM cruise stations (Moutin et al., 2012a) while white dot is DyFaMed position (Marty and Chiavérini, 2010). The area west of the red line constitutes the buffer-zone. Acronyms indicate ~~Acronymes indicates~~ different sub-basin names and islands (in italic). Terminology is taken from Millot and Taupier-Letage (2005). From west to east, **Alb** stands for Alboran Sea, **Cat** ~~the~~ for Catalan Sea, **GoL** for ~~the~~ Gulf of Lions, **Pro** ~~the~~ for Provencal sub-basin, **Alg** ~~the~~ for Algerian basin, **Lig** for ~~the~~ Ligurian Sea, **Tyr** for ~~the~~ Tyrrhenian Sea, **GoG** for ~~the~~ Gulf of Gabes, **North Adr** and **South Adr** for ~~the~~ north and south Adriatic Sea respectively, **Ion** for ~~the~~ Ionian sub-basin, **Aeg** for ~~the~~ Aegean Sea, **Lev** for ~~the~~ Levantine sub-basin and **RG** ~~the~~ for Rhodes Gyre. Major islands names are also plotted, *bal* stands for the Balearic islands, *sar* for Sardinia, *Cor* for corsica, *cre* for Crete.

2 m d^{-1} is within the usual range found in the litterature (Vichi et al., 2007; Fasham et al., 2006). Light attenuation in the water column is modeled via the formulation of Morel (1988).

2.4 Initial and boundary biogeochemical conditions

Initial nutrient and chlorophyll fields are derived from annual means of ~~the~~ Mediterranean Sea climatological data (Schaap and Lowry, 2010). The remaining biogeochemical variables are derived from chlorophyll using conversion factors derived from published works (see Alekseenko et al. (2014) for details).

A "buffer-zone" has been defined between the domain western boundary and the Gibraltar Strait (from 11°W to 6°W), in which a damping procedure towards ~~the~~ Atlantic conditions has been applied. The restoring time is 2 days west of 7.5°W, linearly increasing to 90 days from 7.5°W to 6°W (Fig. 2). Atlantic nutrient concentrations come from the World Ocean Atlas monthly climatology (Garcia et al., 2006), so that the nutrients damping in the "buffer-zone" takes into account the nutrients' monthly variability. Given the ~~imprecisions~~ inaccuracies in phosphate measurements, we decided to compute phosphate profiles from that of nitrate by imposing a redfield ratio of 16 in order to be more consistent ~~coherent~~ with observed NO_3:PO_4 ratios in this region (Gómez, 2003).

Chlorophyll concentrations were not provided in this database. We therefore used in situ data from the SeaDataNet database to create a mean vertical chlorophyll profile for the Atlantic, and then used a climatology of surface chlorophyll from the GlobColour product in this region to represent an annual cycle of the chlorophyll vertical profile. The remaining Atlantic biogeochemical variables were derived from chlorophyll using the same procedure as for initial conditions.

Nutrient (NO_3 and PO_4) inputs from riverine influx and coastal runoffs are derived from Ludwig et al. (2009), following the same procedure as for the riverine freshwater inputs in the circulation model (Beuvier et al., 2010, 2012b). The nutrient influx of the 29 rivers included in the RivDis database (Vörösmarty et al., 1996) are taken into account in the simulation, while the nutrients of the remaining rivers from the Ludwig et al. (2009) database are averaged for every sub-basin and distributed along their respective sub-basin's coast as coastal runoffs. Dissolved organic carbon inputs in the Mediterranean Sea are distributed in every sub-basin according to the riverine DOC estimates of Ludwig (1996) (a total of $\sim$ 1.8 Tg C y^{-1} in the whole of the Mediterranean Sea). Sub-basin DOC inputs were then distributed among fluvial estuarine and coastal runoffs to match circulation model freshwater geographical distribution (Palmiéri, 2014; Palmiéri et al., in prep).

Mass exchanges with the Black Sea ~~at~~ in the Dardanelles Strait are treated as river inputs, with nutrients and DOC input concentrations provided by the SESAME project (Tugrul and Besiktepe, 2007; Meador et al., 2010). But, since NO_3 budget indicates a negative net flux of NO_3 the Dardanelles Strait (i.e. exiting from the Mediterranean), NO_3 flux at Dardanelles is set to zero and the outcome is transferred on the Aegean sub-basin's runoffs. These runoffs are artificially reduced in order to keep the riverine budget of NO_3 in the Aegean sub-basin realistic.

2.5 Simulation set-up

Using the biogeochemical initial conditions defined in Sect. 2.4, we have conducted a 5 years simulation using physical forcings from the years 1973-1977. This first simulation was considered as a 'spin-up', in order to reduce the impact of state variables adjustment in the simulations. It has deliberately been done long enough before the Eastern Mediterranean Transient period (starting around 1991) which is not stable enough to be chosen as a spin-up period. Moreover, due to high computational costs, it was not possible to run this first simulation until the year 1996. We therefore used the final biogeochemical state of this spin-up as initial conditions for a second simulation running from 1996 to 2012. In this second simulation, only the years following 1998 are considered, since the first 3 years were treated as an additional spin-up beyond which the stability of the run was ensured (i.e. no drift could be observed).

2.6 Data description

The aim of the present work is ~~intends~~ to study and to quantify organic carbon export fluxes ~~with~~ using a 3D physical-biogeochemical model. For this purpose, our first aim ~~objective~~ was to assess

the reliability of our model by examining the agreement between different model outputs and corresponding available data : chlorophyll, nutrients, DOC concentrations and primary production rates.

Three type of comparisons were undertaken : (i) at basin scale, using surface chlorophyll fields provided by satellite for comparisons (ii) at basin scale, using BOUM cruise transect as a "snapshot" to compare nutrients and DOC vertical profiles during the stratified period (iii) at a local scale using the time series data collected at DyFaMed station

2.6.1 Chlorophyll data derived from satellite

Among the specificities of the Mediterranean Sea, its strong oligotrophy and the major influence of colored dissolved organic matter, make the use of classical satellite chlorophyll products difficult (e.g. Claustre et al., 2002). Several algorithms have already been developed (Bosc et al., 2004; D'Ortenzio et al., 2002; Volpe et al., 2007), using different satellite reflectances and datasets. Here, we used a daily surface chlorophyll product delivered by the Myocean project (http://www.myocean.eu). In this product, chorophyll concentrations have been derived using the MEDOC4 algorithm developped by Volpe et al. (2007). This algorithm ~~has been~~ was built using a large dataset of ~~in situ~~ chlorophyll concentrations collected in situ and reflectance measurements from 3 satellites (Seawifs, MERIS and MODIS), constituting ~~an~~ a homogeneous series from September 1997 to March 2012.

2.6.2 The BOUM cruise data

The BOUM cruise took place during summer 2008 (from June 16 to July 20) and ~~crossed~~ traversed both the western and eastern basins of the Mediterranean Sea (Moutin et al., 2012a). The data acquired during this cruise ~~give~~ provide a unique picture of the biogeochemical status of the Mediterranean Sea since many biogeochemical variables ~~have been~~ were observed. Measurements of nutrients and DOC concentrations were used to perform a basin-scale comparison during the summer stratified period with the model outputs obtained at the same dates as the cruise, and averaged over this period.

2.6.3 The DyFaMed station data

The DyFaMed station is located in the Ligurian Sea at 7.9°E and 43.4°N (Fig. 2) and is isolated from coastal inputs by the Mediterranean Northern Current. A strong winter mixing is observed in this area, although it is less ~~intense~~ intensive than the deep convection occuring in the Provencal subbasin (Marshall and Schott, 1999). Nutrients (Pasqueron de Fommervault et al., 2015), chlorophyll (Marty et al., 2008), dissolved organic carbon (Avril, 2002) and primary production rates (Marty et al., 2008) time series were used for comparison. The comparison of the model outputs with DyFaMed time series can be done through different methods. The simplest ~~one~~ consists in using a single grid point which is the nearest ~~from~~ to the DyFaMed station location. This implies that the model

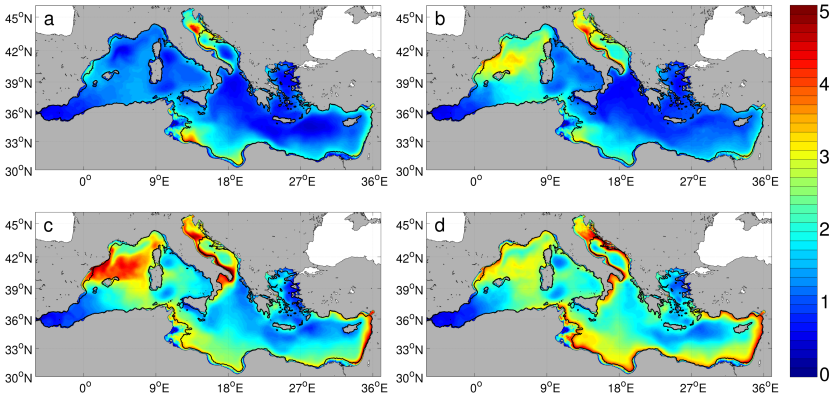

Figure 3. Modeled dissolved organic carbon inventory (mol m^{-2}) integrated over the first 100 m. Maps are averaged over the 2000-2012 period in (a) winter (Dec.-Feb.), (b) spring (Mar.-May), (c) summer (Jun.-Aug.), (d) autumn (Sept.-Nov.).

perfectly reproduces spatial patterns in this region, which is obviously never the case. On the other hand, the use of model outputs averaged on several grid points around the DyFaMed station amounts to dampening signal variability. We finally chose to use the nearest gridpoint to the DyFaMed station, while assessing spatial variability in the 8 neighbouring grid points (Table 2).

3 Results

3.1 Organic carbon inventory and export

3.1.1 Dissolved organic carbon inventory

In ~~what follows~~ the following section, mDOC refers to the modeled dissolved organic carbon integrated over the first 100 m of the water column. Seasonal variations of mDOC are given in Fig. 3. Low mDOC values (< 1 mol m^{-2}) are observed throughout the year in the Alboran Sea (and up to the Balearic Islands), the North Levantine basin, and in some well marked structures in the Tyrrhenian Sea. ~~On the opposite,~~ In contrast, very high mDOC values (up to 5 mol m^{-2}) can be found ~~all along the year~~ throughout in the North Adriatic Sea and along the Lybian Coast. Apart from these regions, mDOC is low everywhere (below 2 mol m^{-2}) in winter (Fig. 3 a), and this is also true in spring except in the region of the spring bloom in the Provencal sub-basin. In the western basin, highest DOC concentrations are generally observed in summer, with values reaching 4 mol m^{-2} in the bloom region of the Liguro-Provencal sub-basin. In the eastern basin, they are reached in autumn and mostly concern the Adriatic Sea, and the regions along the southern and eastern coasts.

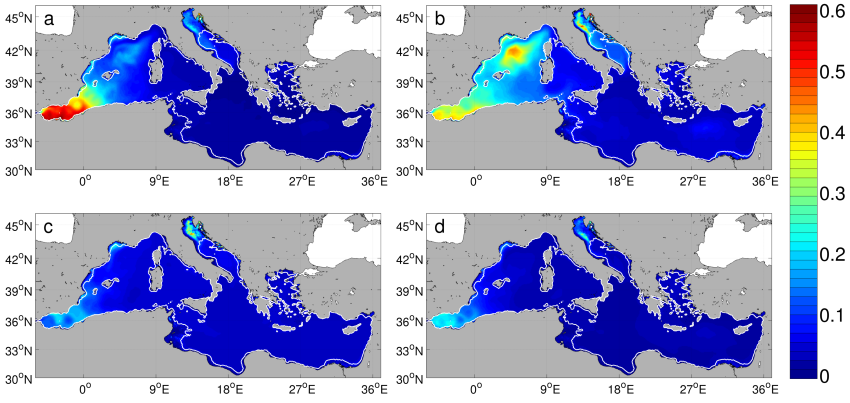

Figure 4. Modeled particulate organic carbon inventory (mol m^{-2}) integrated over the first 100 m. Maps are averaged over the 2000-2012 period in (a) winter (Dec.-Feb.), (b) spring (Mar.-May), (c) summer (Jun.-Aug.), (d) autumn (Sept.-Nov.). White lines are the 0 m and 100 m isolines.

3.1.2 Particulate organic carbon inventory

In what follows, mPOC refers to the modeled particulate organic carbon integrated over the first 100 m of the water column. Seasonal variations of mPOC are given in Fig. 4. Unlike mDOC, mPOC highest values are observed in winter and spring. This is mostly true for the western basin since, in the eastern basin, mPOC remains low (< 0.05 mol m^{-2}) all over the year, except for the Adriatic Sea and a local maximum in the Rhodes Gyre distinguishable in spring. During winter (Fig. 4 a), the highest values of mPOC (> 0.5 mol m^{-2}) are found in the region of the Alboran Sea and the surrounding Balearic Islands and also in the Liguro-Provencal sub-basin though with much lower concentrations. In the Adriatic Sea, mPOC is in the range [0.1;0.2] mol m^{-2}. Elsewhere, mPOC is low (< 0.2 mol m^{-2}). During spring (Fig. 4 b), the maximum mPOC is observed in the region of the bloom in the Provencal sub-basin (≈ 0.4 mol m^{-2}) and the North Adriatic Sea. During summer and autumn (Fig. 4 c and d), overall values are low (< 0.05 mol m^{-2}), except in the Alboran Sea (where values reach 0.3 mol m^{-2}) and in the North Adriatic Sea.

3.1.3 Dissolved and particulate organic carbon export

Organic carbon fluxes are computed by adding the contribution of advection (vertical velocity and settling velocity for POC) and vertical diffusion (~~implicitely~~ implicitly representing turbulent and ~~convection~~ convective mixing) ~~processes.~~ fluxes across an horizontal section of the grid. Negative fluxes account for downward fluxes. For clarity, modeled fluxes will be referred to as F_{DOC} , F_{POC} and F_{OC} as the sum of the latter two. F_{DOC} and F_{POC} have been computed at 100 m and 200 m so as to include most of the productive layer and to allow the comparison in space and time between

regions. These depths are also used in several other modeling studies (Lévy et al., 1998; Bopp et al., 2001).

The yearly amount of mOC export at 100 m is equal to 48.4 MtC y^{-1}. The eastern basin is the main contributor to this export with a total export of 28.7 against 19.7 MtC y^{-1} for the western basin. mDOC export is equal to 38.8 MtC y^{-1}, and comparatively, river inputs of mDOC ~~is~~ are equal to 1.8 MtC y^{-1}, thereby representing ~~only~~ less than 5% of the exported mDOC. mDOC contribution to the total organic carbon flux is dominant. In the western basin, the ~~global~~ total amounts of exported mPOC and mDOC below 100 m are respectively 7.0 MtC y^{-1} and 12.7 MtC y^{-1}, meaning that 64 % of this export is due to DOC. In the eastern basin, DOC is responsible ~~of~~ for 90 % of the organic carbon export below 100 m, with an annual flux of 26.1 (against 2.6 for POC) MtC y^{-1}.

3.1.4 Spatial variability of export fluxes

Mean F_{OC} over the whole basin equals -22.8 gC m^{-2} y^{-1}, but a ~~large~~ wide spatial variability can be observed in Fig. 5. Hence, the main regions of mOC export are the Liguro-Provencal sub-basin, the Alboran Sea, the southern continental slopes and the Adriatic Sea.

In the western basin, high positive values (i.e. upward) of F_{DOC} are simulated along the French and Spanish coasts, the entrance ~~of~~ to the Sicilian Strait and north-eastern ~~of~~ Corsica. Excluding these areas, the highest downward fluxes of DOC are calculated in the Provencal sub-basin (especially in the region of deep convection), the north of the Balearic Islands and along the Algerian slope, where downward F_{DOC} can be higher than 60 gC m^{-2} y^{-1}.

In the eastern basin, the complexity of topography and hydrodynamic regimes in the Aegean Sea may explain the high heterogeneity of the fluxes calculated in this region that are difficult to interpret. Highest downward F_{DOC} values are located along the continental slope from the ~~Lybian~~ Libyan to the Turkish coasts and in the Adriatic Sea. Elsewhere (i.e. in the open sea), F_{DOC} distribution is more homogeneous, ~~in the open sea,~~ with a median of -17 gC m^{-2} y^{-1}.

A strong difference exists between the western and eastern basins regarding F_{POC} at 100 m. The mean value of downward F_{POC} ~~over~~ throughout the western basin is -9.8 gC.m^{-2}.y^{-1} ~~and~~ against -2.4 gC m^{-2} y^{-1} in the eastern basin (Fig. 5 bottom).

In the western basin, F_{POC} is the highest in the Alboran Sea, particularly in the south east of the easily identifiable anticyclonic eddies. Following the pathway of the Atlantic waters, downward F_{POC} values decrease to reach absolute values lower than 5 gC m^{-2} y^{-1} in the Tyrrhenian Sea. In the Provencal basin high POC fluxes linked to the deep convection, with values ranging from -15 to -30 gC m^{-2} y^{-1} ~~are~~ have been modeled. ~~All over~~ Throughout the eastern basin, F_{POC} is low except in the Adriatic Sea.

Finally, as suggested ~~by~~ in Fig. 5, the spatial correlation between POC and DOC fluxes is weak almost everywhere. Regions of high POC or DOC export generally do not match. The only areas

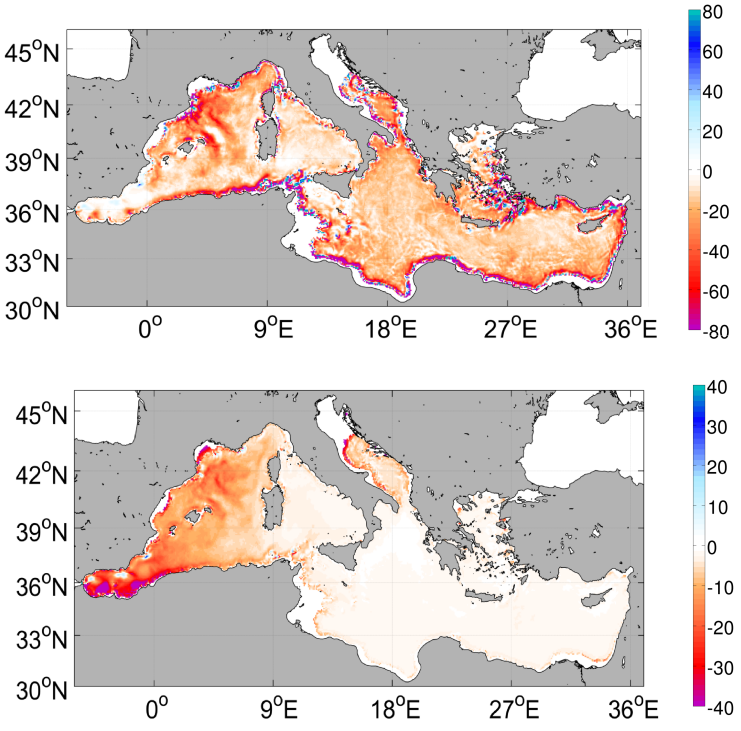

Figure 5. Maps of modeled annual DOC fluxes (top) and POC fluxes (bottom) below the 100 m layer in gC m^{-2} y^{-1}. Note the colorscale differences. Negative (red) means a downward flux.

associated with both high POC and DOC exports are the Algerian coast, the Adriatic coast, the regions of deep convection and a band east of the Balearic Islands.

3.1.5 Seasonal variability

The seasonal variability and the spatial distribution of F_{DOC} and F_{POC} differ significantly (Fig. 6 and 7). In winter (Fig. 6a), F_{DOC} values are high in almost all of the Mediterranean Basin except the Alboran Sea, with maximum values that can be observed in the Provencal sub-basin and along the continental slopes, especially along the southern and eastern coasts of the eastern basin. F_{DOC} distribution is quite similar in autumn, though with values that are significantly lower everywhere. During the rest of the year, F_{DOC} values are very low in spring nearly everywhere, and almost null in summer. ~~Maximum values of F_{DOC} are reached in early winter in the Provencal sub-basin and along the continental slopes from autumn to early spring.~~ In several areas (Tyrrhenian and Adriatic Seas, Levantine and Ionian basins), high downward F_{DOC} values are observed in winter while they are almost null during the rest of the year.

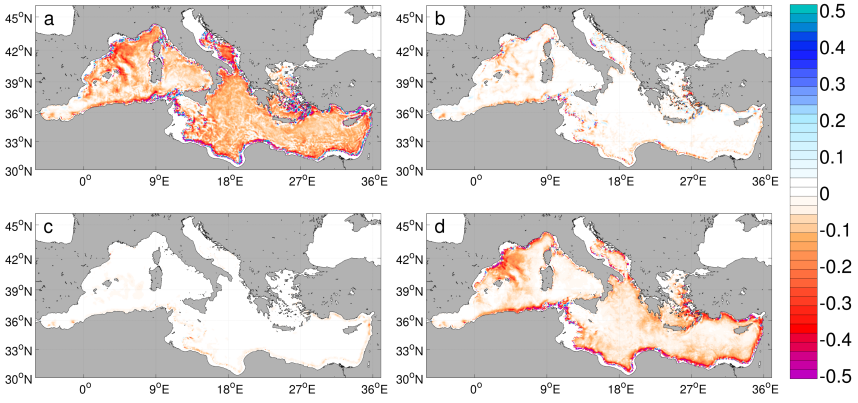

Figure 6. Maps of modeled DOC fluxes across the 100 m layer (F_{DOC}) in gC m^{-2} d^{-1} in (a) winter (Dec.-Feb.), (b) spring (Mar.-May), (c) summer (Jun.-Aug.), (d) autumn (Sept.-Nov.). Negative (red) means a downward flux.

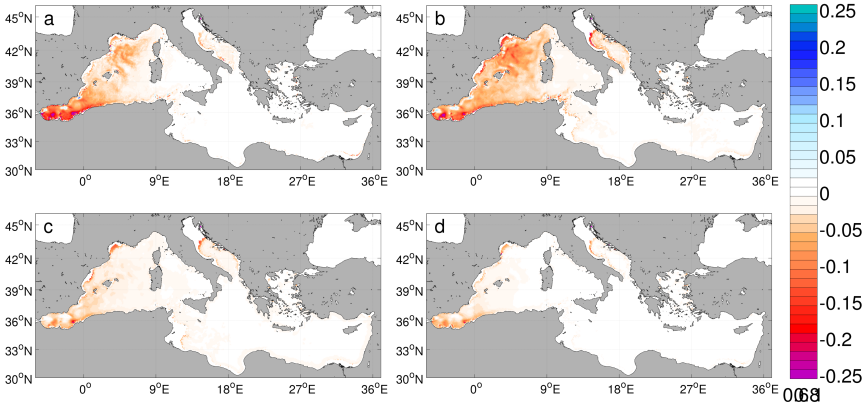

Figure 7. Maps of modeled POC fluxes across the 100 m layer F_{POC} in gC m^{-2} d^{-1} in (a) winter (Dec.-Feb.), (b) spring (Mar.-May), (c) summer (Jun.-Aug.), (d) autumn (Sept.-Nov.). Negative (red) means a downward flux.

High ~~absolute values of F_{POC}~~ downward POC fluxes at 100 m ~~are~~ were calculated from winter to spring west of 7°E, namely in the Alboran Sea and the Provencal sub-basin (Fig. 7). In these regions, ~~associated with the highest downward F_{POC} values (West of 7°E, see Fig. 5 bottom), the~~ maximum values are reached ~~occurs~~ in late winter (February-March) in the Alboran Sea, and in spring (March-April) in the Algerian Sea and the Provencal sub-basin. POC export in the eastern basin (excluding the Adriatic Sea) is very weak (even in the Rhodes Gyre) all year long. ~~Elsewhere, the m~~ Maximum values can however be identified in spring in the Tyrrhenian Sea, the Levantine basins (except for the Rhodes Gyre where the maximum is earlier in winter) and in the Adriatic Sea.

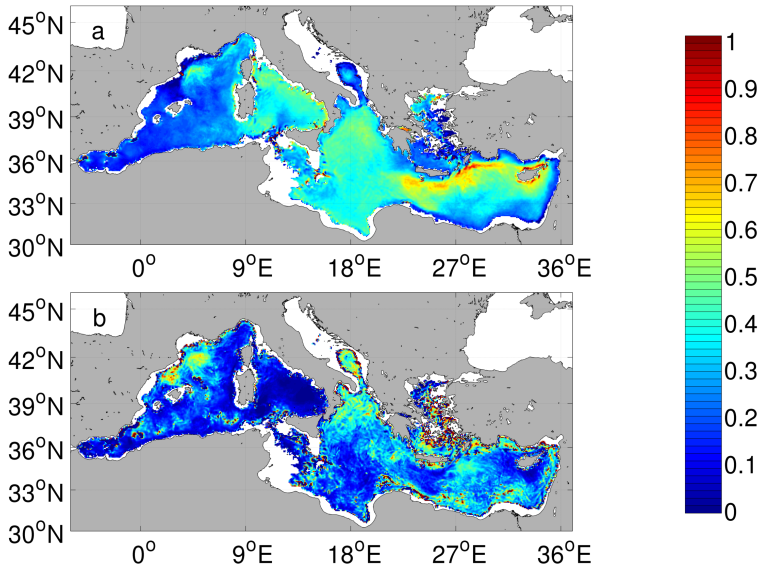

Figure 8. Ratio between export fluxes at 200 m and at 100 m (a) for POC, (b) for DOC.

3.1.6 Export below 200 m

Below 100 m, organic carbon is progressively consumed via the bacterial activity and respiration. At 200 m, the calculated mean export fluxes of total organic carbon are reduced by almost 87 % and 64 % compared to those at 100 m, respectively in the western and eastern basins. However, the ratio between export at these two depths is highly variable, depending on the region (see Fig. 8).

For POC (Fig. 8 a), if we consider first the regions where the annual F_{POC} values are significant, i.e. west of 7°E, (see Fig. 5 bottom), the 200 m to 100 m ratio is lower than 0.25 (i.e. only 25 % of the carbon exported at 100 m goes below 200 m) in a region including the Alboran Sea, the western Algerian Sea and the Balearic Sea. ~~where POC export at 100 m is high (see Fig. 5 bottom).~~ This ratio is slighly higher but still below 0.3 for the central Algerian Sea and the Adriatic Sea. The Provencal sub-basin is the only region of high export below 200 m with a ratio about 0.4. In regions of low annual POC export (i.e. east of 7°E), the ~~In the Tyrrhenian Sea, the Ionian and Levantine basins,~~ ratio ranges between 0.4 and 0.8 in the Tyrrhenian Sea, the Ionian and Levantine basins. ~~but are associated with low downward POC fluxes below 100 m.~~

For DOC (Fig. 8 b), the ratio is more spatially variable, and in some regions the ratio is higher than 0.4, namely in the Provencal sub-basin, along the coasts of ~~continental slopes in~~ the Levantine basin, in the North Ionian basin, the Rhodes Gyre and the Adriatic Sea. Some patches of high ratios are also visible close to the Algerian Coast. Elsewhere the ratio ranges from almost zero (Tyrrhenian Sea, the Alboran Sea) to 0.2 in the eastern basin.

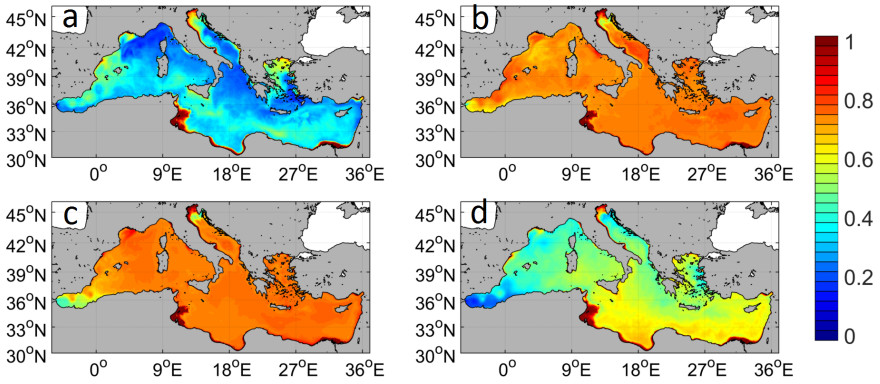

Figure 9. Seasonal variations of mean 0-50 m carbon relative quotas in small phytoplankton: (a) winter (Dec.-Feb.), (b) spring (Mar.-May), (c) summer (Jun.-Aug.), (d) autumn (Sept.-Nov.). Relative quotas are equal to 0 when the quota is mimimum (i.e. when $Q_C = Q_C^{min}$) and equal to 1 when the quota is maximum (i.e. when $Q_C = Q_C^{max}$)

3.2 Intracellular quotas in bacteria and phytoplankton

Intracellular quotas in phytoplankton and bacteria are required for a further analysis of POC and DOC export fluxes and are presented in ~~what follows~~ the following section. Carbon quota (Q_C) in small phytoplankton is maximum (> 0.7) ~~the highest~~ in spring and summer in almost all of the Mediterranean Sea, though Q_C values are slightly lower in spring than in summer in the western basin, ~~than in the eastern one,~~ especially in the bloom region (Fig. 9). In autumn, though Q_C has decreased in nearly all of the Mediterranean Sea, Q_C values along the southern and eastern coasts of the eastern basin are significantly higher than in the rest of the open sea. In winter, Q_C values are even lower, with local maximum located in the Balearic Sea and in the south of the eastern basin.

The seasonal signal of the P quota (Q_P) in small phytoplankton is nearly the opposite of that of Q_C ~~one~~, with the highest Q_P values in autumn and mostly in winter in nearly the whole of the Mediterranean Basin, and the lowest ones in spring and summer (Fig. 10). All year long, Q_P values are lower along the southern and eastern coasts than in the rest of the eastern basin.

Bacteria Q_C generally increases from winter to summer in most of the Mediterranean Basin (Fig. 11). In autumn, the decrease in Q_C is observed everywhere except ~~along~~ throughout the same already identified region (namely along the southern and eastern coasts of the eastern basin). All year round, Q_C values are higher in this region than in the rest of the basin and even reach the $Q_C^{\max}$ value in summer and autumn thus indicating that carbon needs for bacteria growth are fully satisfied. In the deep convection regions (Liguro-Provencal sub-basin, Adriatic, Rhodes Gyre region), and in some eddies well identified in the Alboran and Tyrrhennian seas, the carbon quota is generally lower than in the surrounding waters, especially in autumn.

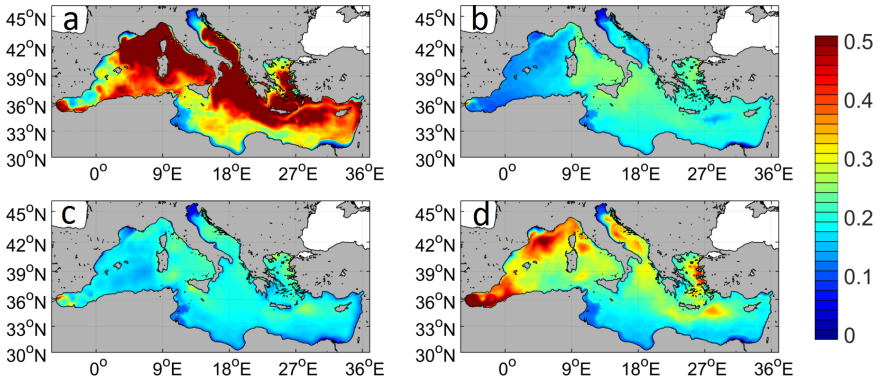

Figure 10. Seasonal variations of mean 0-50 m phosphorous relative quotas in small phytoplankton: (a) winter (Dec.-Feb.), (b) spring (Mar.-May), (c) summer (Jun.-Aug.), (d) autumn (Sept.-Nov.). Relative quotas are equal to 0 when the quota is mimimum (i.e. when $Q_P = Q_P^{min}$) and equal to 1 when the quota is maximum (i.e. when $Q_P = Q_P^{max}$)

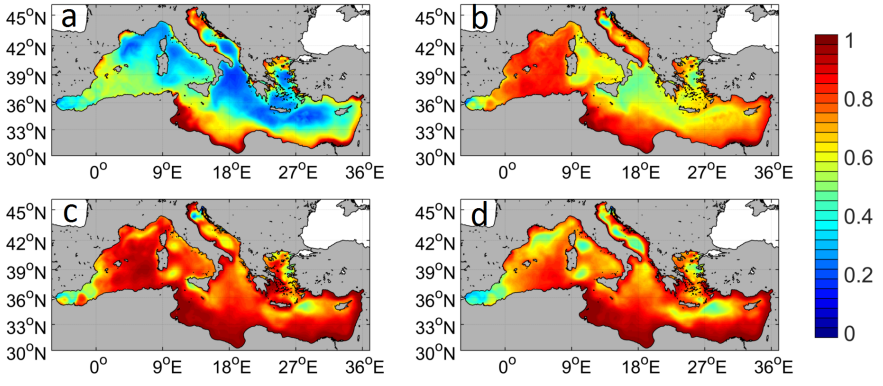

Figure 11. Seasonal variations of mean 0-50 m carbon relative quotas in bacteria: (a) winter (Dec.-Feb.), (b) spring (Mar.-May), (c) summer (Jun.-Aug.), (d) autumn (Sept.-Nov.). Relative quotas are equal to 0 when the quota is mimimum (i.e. when $Q_C = Q_C^{min}$) and equal to 1 when the quota is maximum (i.e. when $Q_C = Q_C^{max}$)

Bacteria Q_P values are very low everywhere in spring and summer except in the latter regions. The minimum Q_P values (i.e. the highest bacterial P-limitation) are observed in spring in the western basin, while they are reached in summer in the eastern basin. As for phytoplankton, Q_P values are lower all year round along the southern and eastern coasts than in the rest of the eastern basin.

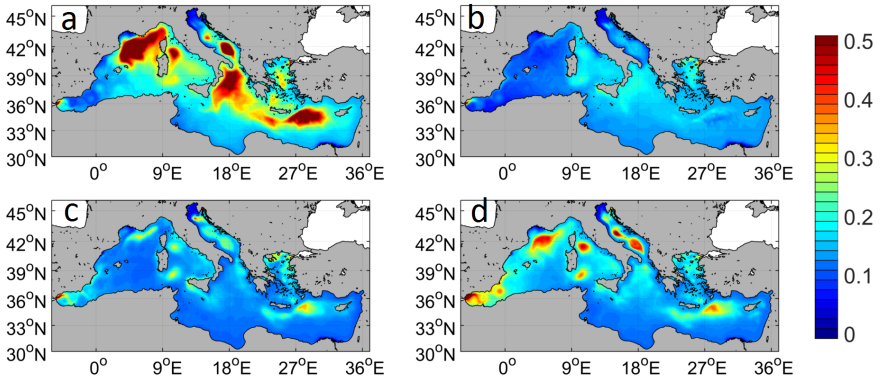

Figure 12. Seasonal variations of mean 0-50 m phosphorous relative quotas in bacteria: (a) winter (Dec.-Feb.), (b) spring (Mar.-May), (c) summer (Jun.-Aug.), (d) autumn (Sept.-Nov.). Relative quotas are equal to 0 when the quota is mimimum (i.e. when $Q_P = Q_P^{min}$) and equal to 1 when the quota is maximum (i.e. when $Q_P = Q_P^{max}$)

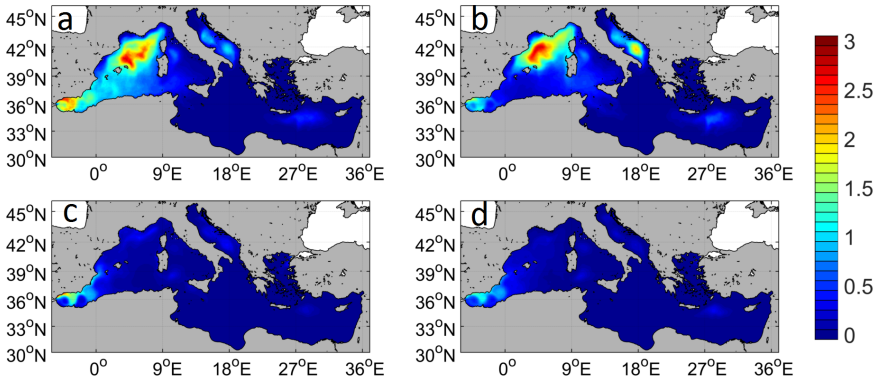

Figure 13. Seasonal variations of DOC mean 0-100 m exudation ~~cumulated~~ accumulated flux by large phytoplankton (in mol C.m^{-2}).

3.3 DOC exudation by phytoplankton

DOC exudation by large phytoplankton mainly occurs in the bloom region of the western basin (especially in the deep convection zone), in (late) winter and spring where ~~cumulated~~ accumulated fluxes are up to 2.8 mol C.m^{-2} (Fig. 13). Elsewhere, exudation fluxes are very low ~~all along~~ throughout the year, except in the Alboran Sea, two eddies of the Adriatic Sea and in the Rhodes gyre region.

The seasonality and the spatial patterns of DOC exudation flux by small phytoplankton are rather different. The highest mDOC exudation fluxes are modeled in spring in the western basin, especially in the Gulf of Lions and the deep convection zone where ~~cumulated~~ accumulated fluxes up to 3 mol C.m^{-2} are calculated. In the eastern basin, the highest fluxes are observed in spring and summer. During these seasons, apart from ~~the~~ the Adriatic Sea (especially in the north and along the eastern coast where ~~cumulated~~ accumulated fluxes also reach 3 mol C.m^{-2}) and some hot spots (Rhodes gyre, Nile plume), mDOC exudation seems homogeneous though a north-south gradient is present. Hot spots of mDOC exudation are also present nearly all year long in the plumes of the main rivers.

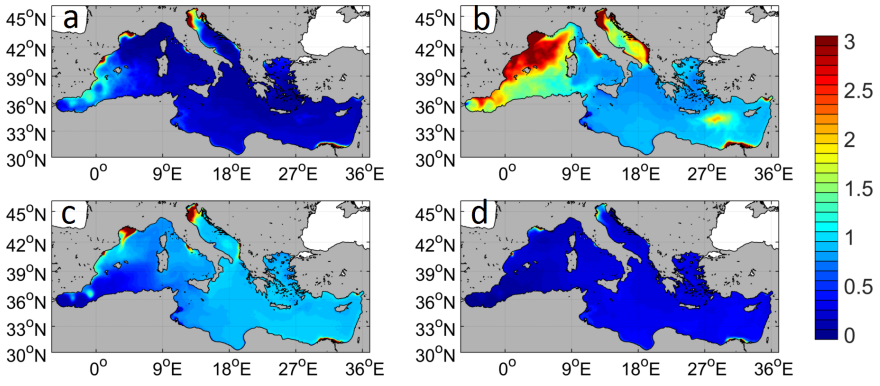

Figure 14. Seasonal variations of mDOC mean 0-100 m exudation ~~cumulated~~ accumulated flux by small phytoplankton (in mol C.m^{-2}).

4 Discussion

485 4.1 The dissolved fraction in the organic carbon export is predominant at the scale of the Mediterranean Sea

One of the main results of this study is that mDOC export exceeds mPOC export in the whole of the Mediterranean Basin, with the exception of the Alboran Sea (west of 3°W). This is consistent with the comparisons between POC and DOC exports performed in the Tyrrhennian, North Ionian 490 and Ligurian seas by Copin-Montégut and Avril (1993); Santinelli et al. (2013) or by Lefèvre et al. (1996) who estimated that DOC was the main source of remineralization processes in the aphotic layer. In the western basin, the ratio of mDOC over mPOC export fluxes ranges between 2 and 5, and is approximately equal to 4 at the DyFaMed grid point. Observations at the DyFaMed station led to a oDOC export estimation of about 11.9 gC $m^{-2}.y^{-1}$, markedly higher than oPOC export estimations 495 at 200 m (Avril, 2002, and references herein). Moreover, oPOC fluxes calculated by Miquel et al. (2011) during the 2001-2005 period ranged from 1.6 to 2.6 gC $m^{-2}.y^{-1}$. ~~between 2001 and 2005~~ For ~~(by~~ comparison, mPOC export flux was in the range [1.5;3.1] gC $m^{-2}.y^{-1}$ during the same period. In the northwestern basin, the modeled ratio is about 2 at 100 m and 200 m, while in the same area a modeling study (Herrmann et al., 2014) led to a ratio at 200 m which ranged from 0.9 500 to 1.8, even though the corresponding export fluxes were higher than in the present study.

The ratio between modeled DOC and POC exports at 100 m ranges from 2 to 8 in the Adriatic Sea. In the same region, a oDOC flux of 15.4 (against 23 for mDOC) gC $m^{-2}.y^{-1}$ was estimated from observations by Santinelli et al. (2013). This is nearly 5 times higher than the measured oPOC export flux estimated by Boldrin et al. (2002) under the euphotic zone of 3.3 (against 4.5 for mPOC 505 export at 100 m) gC $m^{-2}.y^{-1}$. These oDOC and oPOC fluxes were ~~which was,~~ however ~~sampled~~ estimated ~~during a~~ at different periods. ~~(Boldrin et al., 2002).~~

In the eastern basin, mDOC export is regularily more than 10 times that of mPOC, due to the very weak mPOC export and to the high mDOC export along the coasts and in the open sea. Few observations and estimations are available for this region. In the northern Ionian Sea, Boldrin et al. 510 (2002) reported annual oPOC fluxes at 150 m of 2.4 gC $m^{-2}.y^{-1}$, which are in the same order of magnitude as the annual mPOC fluxes calculated in the same area but for a different period (1.2 gC $m^{-2}.y^{-1}$ and 0.6 gC $m^{-2}.y^{-1}$ at 100 m and 200 m, respectively).

DOC predominance in the OC export flux is first due to the higher DOC gross production fluxes as compared to those of POC, ~~ones,~~ and this still holds if the POC to DOC hydrolysis flux is ~~cancelled~~ 515 ruled out (i.e. if the DOC inputs due to POC hydrolysis are not taken into account). At the scale of the Mediterranean Basin as a whole, mDOC and mPOC gross production fluxes are indeed respectively equal to 20 10^{12} and 2.7 10^{12} molC.y^{-1}. In the western basin, mDOC predominance in the export of OC ~~is still observed al~~ still holds though to a lesser extent, with mDOC and mPOC gross production fluxes respectively equal to 8.7 10^{12} and 1.9 10^{12} molC.y^{-1}. In ~~what follows,~~ the following section,

the reasons ~~of~~ for these differences will be further analyzed in the light of the processes associated with DOC and POC production.

4.2 POC and DOC exports are characterized by different processes and timing

Strong disparities can be identified between the spatial patterns of the annual DOC and POC export fluxes (figure 5), with rather homogeneous DOC export fluxes across the Mediterranean Sea (though with well identified regions of maximum export that will be analyzed later), contrasting with the high east-west gradient in POC export. This is consistent with in situ measurements of daily POC export across the Mediterranean Sea at 200 m that showed much lower POC export in the eastern basin than in the western basin (Moutin and Raimbault, 2002).

~~Strong~~ There are also considerable differences ~~also exist~~ in the seasonality of DOC and POC export fluxes (Fig. 6 and 7). ~~Hence, o~~ Over the whole of the Mediterranean Sea, 88 % of DOC export occurs between November and February, which is consistent ~~coherent~~ with observations at the DyFaMed station where 90% of annual DOC export was linked to winter mixing (Avril, 2002). By contrast, POC export is more even throughout the year, and during the same period only 23 % of POC is exported.

In the model, only the detrital compartment (POC) is allowed to sink. The sinking process is therefore the only source of explicit distinction between POC and DOC exports, but it is ~~likely~~ probably not sufficient to explain the strong aforementioned differences. The main source of difference lies in the biogeochemical processes that fuel or consume POC and DOC pools (see section 2.2). In the model, POC is fueled by the natural mortality of the largest organisms (mesozooplankton, diatoms and ciliates) and by the egestion of fecal pellets and sloppy feeding by mesozooplankton. Thus, higher concentrations of large organisms in the western basin, primarily due to the spring bloom in the Liguro-Provencal sub-basin associated with high primary production rates is the main reason for the higher POC production and export in this basin. Hence, POC export is at a maximum in spring (i.e. from March to May in figure 7) since it is the period including the maximum and the end of the bloom during which detrital concentrations of large organisms are ~~the~~ highest. Moreover, according to the model, mortality is the main process that fuels the POC pool, far ahead of the egestion and sloppy feeding processes. More generally, a strong correlation between annual primary production and POC export has been evidenced at basin scale (Spearman's rank correlation coefficient is 0.84), while this is not the case for DOC export (correlation below 0.01).

As shown in the Results section, the regions of high POC or DOC export are generally not the same, except for the regions characterized by high primary production rates during the spring bloom, namely the Alboran Sea, the bloom region in the NW Mediterranean Sea and the south of the Adriatic Sea (see also ~~later in the discussion~~ section 4.3). Apart from these regions, the annual DOC export at 100 m is relatively high in almost all of the Mediterranean Basin, particularily in autumn and winter, and is the consequence of DOC accumulation in the 0-100 m layer during summer and autumn (Fig.

3). ~~since~~ DOC export does indeed take place when DOC rich surface waters plunge or are mixed with poorer deeper waters.

This accumulation of DOC is primarily due to water stratification that results in nutrient ~~exhaustion~~ depletion in the 0-100 m layer. As a result, the pool of DOC in phytoplankton is saturated with newly synthesized organic compounds since photosynthesis (i.e. carbon production), which is not controlled by P-availability, takes place more rapidly than is required to supply the needs of growth (~~growth~~ cell division being limited by the intracellular quota of P). This results in high DOC exudation by phytoplankton, which is the main source of DOC in the model. The contribution of zooplankton excretion is at a maximum in spring in the bloom region of the NW Mediterranean, but remains always much lower than that of exudation (results not shown). Similarly, the annual contribution of POC hydrolysis to the DOC production flux is weak (around 10 %). Bacteria are the first consumers of DOC, and the second ingredient for DOC accumulation is therefore a strong nutrient limitation that will highly restrict the bacteria growth rate (see Eq. 1). In this ~~such a~~ situation, DOC availability may exceed bacteria needs and result in DOC accumulation when DOC production by phytoplankton exceeds DOC uptake by bacteria. ~~, and t~~ This process is enhanced in hydrodynamic situations where the surface layers are isolated from the deep waters (i.e. stratification period). Such a mechanism of DOC accumulation due to a malfunctioning microbial loop has already been described in Thingstad et al. (1997) and is also the main driver of DOC accumulation in the model. Destratification in autumn leads to a net export as well as an increase of DOC consumption through bacterial activity, driven by nutrient supply from deep water.

4.3 DOC accumulation in the light of intracellular quotas

The regions of highest DOC export fluxes correspond to the regions where the highest DOC accumulation occurs. It is therefore informative to analyze the occurrence of DOC accumulation in the light of intracellular quotas. Geographical and hydrological considerations are indeed not sufficient for a ~~thorough comprehension~~ full understanding of the DOC accumulation pattern at the scale of the Mediterranean Sea.

It has already been said that, according to the model, phytoplankton exudation is the primary source of DOC. High DOC exudation by phytoplankton occurs in nutrient-depleted waters. In such a situation N and/or P phytoplankton nutrient quotas are low and limit growth rate (i.e. the cell division rate). In the model, phytoplankton (and bacteria) ~~specific growth rate (i.e. their~~ cell division rate is indeed controlled by the most strongly limiting element among C, N and P (see Eq. 1). In other words, the intracellular quota which is the closest to its minimum value controls the division rate. When P (and/or N) are the most strongly limiting, growth will proceed at low rate and the carbon input due to photosynthesis will rapidly meet phytoplankton needs, thus resulting in an increase in the carbon quota Q_C. Since DOC exudation flux per cell increases with Q_C through a Geider et al. (1998) non-linear quota function, DOC exudation flux will highly increase as the quota approaches

its maximum value Q_C^{max}. Phytoplankton carbon quota is therefore a good indicator ~~for~~ of DOC exudation.

In the oligotrophic Mediterranean Sea, nutrient (and mostly P in the model) depletion is at a maximum at the end or just after the spring bloom, or under well established conditions of water stratification, thus leading to maximum exudation fluxes (see Fig. 13 and 14). In the rest of the Mediterranean, DOC exudation is at a maximum in (late) spring and summer, and mainly due to small phytoplankton. The latter is indeed characterized by low phosphorous quotas (see Fig. 10) and high carbon quotas (see Fig. 10).

The driving processes of DOC accumulation are not the same in the western and the eastern Mediterranean. In the western Mediterranean, and especially in the enlarged bloom region, large phytoplankton blooms first and is rapidly P-limited (as early as February) and the same occurs for small phytoplankton though later (i.e. only in spring, see Fig. 10). This is consistent with observations performed in the NW Mediterranean Sea (Gulf of Lions) (Diaz et al., 2001). In this ~~this~~ situation, the high phytoplankton exudation fluxes are not only due to phytoplankton carbon quotas that are relatively high (around 50-60%, see the small phytoplankton carbon quota in Fig. 9), resulting in relatively high exudation flux per cell, but to the high phytoplankton abundance. Though exudation fluxes are high in (late) winter due to large phytoplankton (Fig. 13a), the high bacteria P-quotas (Fig. 12a) combined with winter mixing prevents DOC accumulation (Fig. 3a). In spring, and mostly in late spring, bacteria are strongly P-limited (Fig. 12b) since the bloom has rapidly consumed the available nutrients and vertical mixing has stopped. As a result, DOC accumulation starts in this region (Fig. 3b) and reaches its maximum in summer (Fig. 3c) during the stratification period since DOC exudation by phytoplankton still proceeds (though at a lower rate) and bacteria are still strongly P-limited (Fig. 12c). Finally, the end of the stratification in autumn will not only dilute the DOC-rich surface concentrations with DOC-poor deep waters, but allow the P-enrichment of surface waters (see the increase in bacteria Q_P in Fig. 12d).

In the eastern Mediterranean, DOC accumulation is mainly visible along the southern and eastern coasts. Moreover, it starts later than in the western Mediterranean (i.e. in summer against spring for the west), and is at a maximum in autumn. In the model, the Atlantic waters that flow along the coast are less dense (with densities slightly underestimated as compared to in situ measurements (Beuvier, 2011)) and therefore strongly isolated from the rest of the water column. As a result, their nutrient content will be progressively consumed and these waters become more and more oligotrophic as they flow along the southern coast of the basin, and always remain more oligotrophic than the rest of the eastern basin. In summer and autumn, they can even be considered as ultra-oligotrophic (see the phytoplankton Q_P in Fig. 10c and d). Moreover, they extend over a layer of around 100 m in thickness in which concentrations are roughly homogeneous. During summer and autumn, bacteria are also strongly P-limited but more and more carbon-rich (see Fig. 11) since phytoplankton exudation still proceeds (though at extremely low rates in autumn). Moreover, the vertical mixing that

starts in autumn is not sufficiently deep to reach the nutrient-rich waters since the MLD is shallower than the bottom of these Atlantic waters. In addition, since DOC concentration is high over the whole layer, DOC surface concentrations are not diluted by the mixing. As a result, accumulation still proceeds until winter ~~where~~ during which higher MLD will allow the P-enrichment in surface waters and dilute surface DOC concentrations as well.

Furthermore, DOC concentrations (as well as DOC annual export flux though this is more difficult to see in Fig.5) are negligeable throughout the year in some well-identified regions, namely the two cyclonic structures in the Tyrrhenian Sea, the south of the Adriatic Sea (excluding the coastal zones), and the region of the Rhodes Gyre in the Levantine basin. All these structures are characterized by regular input of nutrients from deep waters, resulting in an absence of strong P-limitation in bacteria. ~~In~~ Under such conditions, the bacteria carbon quota is rather low and DOC accumulation and export cannot occur.

Finally, the strong link between low phosphate availability in the upper surface water of the Mediterranean Sea and DOC accumulation due to nutrient limitation of bacterial production that is evidenced in this modeling study is consistent with previous in situ (Moutin et al., 2002; Van Wambeke et al., 2002) and modeling (Thingstad et al., 1997) studies and is shown to apply at the scale of the whole of the Mediterranean Sea, with the exception of the aforementioned specific regions.

4.4 Robustness of results

Though difficult to achieve in a rigorous way, the robustness of our main results will be discussed in the following section. ~~what follows~~ As shown in section (2.2), the model includes many DOC and POC production and consumption processes. A sensitivity study on all the parameters they involve is obviously impossible to achieve, though some ~~attempts~~ steps towards this goal have already been ~~done~~ made in Baklouti et al. (2006b). Moreover, accounting for the fact that most of the parameters used have a physiological ~~meaning~~ significance (including cell size considerations), and constitute a coherent set that remains unchanged for the different studies undertaken with Eco3M-MED (even outside the Mediterranean), we consider that their values are reasonably ~~rather~~ reliable. However, the POC to DOC degradation (i.e. hydrolysis) rate and the sinking velocity are not physiological parameters and their impact on the results will be discussed later.

The comparison of DOC stocks with the few available results (see section A4 in Appendix) showed that, though the shape of the modeled DOC vertical profiles were quite different (but the values were in the same order of magnitude) ~~than the~~ from those measured, ~~ones,~~ modeled and measured integrated DOC stocks over the 0-100 m layer showed much better agreement. Furthermore, when compared to in situ estimations of DOC export from the DyFaMed station (Avril, 2002) and the Adriatic and ~~the~~ Tyrrhenian seas (Santinelli et al., 2013), the model always provides higher DOC export values. These differences in DOC export may be partly attributable to the model failures discussed in section (A4) but, as already mentioned, ~~high uncertainties are also associated with~~ in

situ estimations also involve considerable uncertainties. Hence, according to Santinelli et al. (2013), DOC export computations from stock differences below the euphotic layer probably underestimate the real flux. This is also the conclusion we came to by using model outputs to compute export fluxes with our method and with the in situ method. If we assume, however, that the different in situ estimations ~~evaluations~~ are consistent with each other, it appears that the highest DOC export occurs in the Adriatic Sea, followed by the DyFaMed station (Ligurian Sea) and then by the Tyrrhenian Sea, and the same order can be inferred from the model outputs.

Two parameters are essential in POC export, namely POC to DOC ~~hydrolysis~~ degradation rate and the sinking velocity.

Since our model includes a single detrital compartment, an intermediate value of 2 m d^{-1} has been used for the sinking velocity. This value is intended to be representative of the high sinking rates (> 100 m/day) of very large particles as well as the very low sinking rates of small particles. It may however reflect an underestimation of the actual mean value though this is difficult to verify. In several other models (e.g. Lévy et al., 1998; Lacroix and Gregoire, 2002; Herrmann and Somot, 2008), two detrital compartments are used, thus making it possible to differentiate ~~allowing to differenciate~~ between low and high sinking rates of detrital particules. However, in these models, the large detrital compartment (to which high sinking rates are affected) is only fueled by ~~meso~~ zooplankton fecal pellets (Lévy et al., 1998; Herrmann and Somot, 2008) ~~, by micro and mesozooplankton fecal pellets (Herrmann and Somot, 2008)~~ and by ~~or by the~~ mesozooplankton mortality ~~and fecal pellets~~ in Lacroix and Gregoire (2002). These fluxes, except the latter, ~~mesozooplankton mortality~~ are probably ~~likely~~ weak compared to the other POC sources in our model (which is dominated by the mortality of the largest organisms). Finally, in these models, the remaining sources of POC fuel the small detrital compartment for which the sinking velocities are lower than that used in our model. ~~Moreover, our model includes more POC sources since ciliates mortality and sloppy feeding by mesozooplankton also fuel the POC pool.~~

More importantly, it can be considered that the likely underestimated sinking velocity used in the present model is compensated by the very low POC degradation rate. In our model, its maximum value is set at 0.03 d^{-1} but it ~~. In the model, the hydrolysis rate of POC to DOC~~ is modulated by the bacteria carbon quota. In substance, the higher the carbon quota, the more the ~~hydrolysis~~ degradation rate decreases and eventually becomes 0 when the bacteria carbon quota is maximum. As a result, the effective POC degradation rate is always less than 0.03 d^{-1} in the model, and it is lower in the surface layers since bacteria are more rich in carbon than in deep waters. It is also lower than all the values used in the aforementioned models. Concerning in situ data for the degradation rate, Sempéré et al. (2000) have determined values at 50 and 200 m for labile and less labile POC in three regions of the Mediterranean Sea, showing that, for the labile POC (which represent a significant part in the latter study), the degradation rate can be up to 100 times higher than that used in the present study. ~~Moreover, the influence of the hydrolysis rate is all the more important that~~

~~the sinking velocity is low. When sinking velocity is high, POC will indeed be quickly exported before being hydrolyzed. In the present model, there is a single detrital compartment which includes small and large particles. The sinking velocity has been fixed to an intermediate value of 2 m d^{-1} which may reflect an underestimation of the actual mean value though this is difficult to verify. In several other models (e.g. Lévy et al., 1998; , 2002; , 2008), two detrital compartments are used, thus allowing to differenciate between low and high sinking rates of detrital particules. However, in these models, the large detrital compartment is only fueled by mesozooplankton fecal pellets (Lévy et al., 1998), by micro and mesozooplankton fecal pellets (Herrmann and Somot, 2008), or by the mesozooplankton mortality and fecal pellets (Lacroix and Gregoire, 2002), and these fluxes, except the mesozooplankton mortality, are likely weak compared to the other POC sources in our model (which is dominated by the mortality of the largest organisms). Moreover, our model includes more POC sources since ciliates mortality and sloppy feeding by mesozooplankton also fuel the POC pool.~~

~~Finally, the hydrolyzis rate that has been used (i.e. 0.03 d^{-1}) is rather low compared to the aforementioned modeling papers, and may partly compensate the likely underestimated sinking rate.~~ Apart from these two parameters, it has been seen that the model underestimates Chl concentrations at the DCM (mainly due to a lack of large phytoplankton) and this may also lead to an underestimation of POC export. However, the 0-100 m mIPP values are consistent with oIPP thereby suggesting that this DCM underestimation has only a limited impact on carbon production. Overall, the annual POC export flux at 100 m provided by the model is around 8% of the annual primary production, a value that is consistent ~~coherent~~ with in situ estimations (Miquel et al., 1994).

Between 100 m and 200 m, however, the mean bacteria carbon quota is lower since POC hydrolysis and bacteria and heterotrophic nanoflagellate mortalities are the only sources of DOC, resulting in higher hydrolysis rates and in lower POC export at 200 m. Looking at the vertical attenuation of POC fluxes, it is common to use a power law expressed as $F(z) = F(z = z_0) * (\frac{z}{z_0})^{-b}$, where F(z) is the depth-dependent POC flux and b a positive coefficient whose values may vary according to the location or the period. In regions of significant export, b values inferred from the model outputs fluctuate between 0.9 in the Provencal sub-basin and 2.3 for the Algerian basin. Values of b derived from observations tend to be lower, i.e. respectively equal to 0.92 and 1.0 for the western and eastern moorings ~~, respectively~~ (Gogou et al., 2014), or 0.75 in the Alboran Sea (Zúñiga et al., 2007). This again suggests that the attenuation of POC export flux between 100 m and 200 m is too great in the model. Furthermore, when compared to the few available data for ~~of~~ POC export fluxes, the model always underestimates the export flux in the eastern basin. However, all the in situ estimations we could find in the literature were done at 150 m or 200 m depth, which ~~that~~ means in the 100-200 m layer where the modeled POC export is more likely to be underestimated. In summary, all this suggests that the underestimation of POC export fluxes is more to be the case ~~likely effective~~ at 200 m than at 100 m depth though the comparison at the DyFaMed station shows that the mean mPOC

export rate (5.6 gC.m^{-2}.y^{-1} and 2.2 gC.m^{-2}.y^{-1} at 100 m and 200 m respectively) is within the range of the measured ~~one~~ rate at 200 m (i.e. [1.6;2.6] gC.m^{-2}.y^{-1} (Copin-Montégut and Avril, 1993; Miquel et al., 2011)). Finally, it is very unlikely that these ~~aforementioned~~ uncertainties could shed doubt on ~~put in question~~ the predominance of DOC in the OC export in the eastern basin. This conclusion also applies in the western basin (though ~~will~~ with less certainty), all the more so in that in situ measurements allow ~~to draw~~ the same conclusion to be drawn in the sampled stations of the NW Mediterranean (Copin-Montégut and Avril, 1993; Avril, 2002; Miquel et al., 2011).

5 Conclusions

A 14-year simulation combining a high resolution physical model (NEMO-MED12) and a mechanistic biogeochemical model (Eco3M-MED) has been ~~built~~ developed to study carbon organic production and fate at the scale of the Mediterranean Sea.

A preliminary work presented in the Appendix focused on the Model Skill Assessment through an extensive comparison of different model outputs (i.e. chlorophyll, nutrients, primary production and DOC profiles) with available data at various time and space scales. This work allowed to verify the model's ability to represent ~~in representing~~ the main features of the biogeochemical functioning of the Mediterranean Sea. In the Results section, carbon export fluxes are investigated. Previous estimations of DOC export in the Mediterranean Sea were restricted to specific regions of the Mediterranean ~~Sea~~ (e.g. the Ligurian, Adriatic, Tyrrhenian Seas). We here propose the first Mediterranean-scale view of annual DOC and POC export fluxes, as well as an analysis of their spatial and seasonal variations in the light of plankton intracellular quotas.

The two major results of this modeling study ~~lye~~ lie in (i) the predominance of the eastern basin in OC export (with nearly 60 % of the OC export occuring in the eastern basin), and (ii) in the crucial role of the dissolved fraction in the total organic carbon export. At ~~the~~ Mediterranean scale, DOC export represents about four fifths of total organic carbon fluxes, thereby attesting to its major role in the carbon cycle and the biological pump in the Mediterranean Sea. The concept of a malfunctioning microbial loop (Thingstad et al., 1997), due to high P-limitation of both phytoplankton and bacteria ~~, and~~ leading to high DOC exudation fluxes beyond bacterial needs, also applies in the present study though it is generalized to the whole of the Mediterranean Basin, except for some specific P-rich regions (see Results and Discussion). Export in the eastern basin is markedly high despite its lower productivity compared to the western basin. By contrast, POC export is closely associated with regions characterized by high productivity. As a consequence, total carbon export in the eastern basin is considerably higher than expected as regards its low primary productivity. Results also show high spatial variability in organic carbon fluxes and a temporal uncoupling between POC and DOC exports. This is attributable to the differences in the processes involved in the production and export of POC and DOC.

Further comparisons with observations are clearly necessary to confirm these results, which emphasizes the need for in situ temporal monitoring to properly quantify organic carbon export. This study also highlights ~~identifies~~ the need to examine the microbial food web in detail in order to further investigate the carbon cycle in the Mediterranean Sea. Furthermore, the implementation of an explicit inorganic carbon compartment in the biogeochemical model would close the carbon budget and help in the full characterization of the biological pump.

In conclusion, the strong link between low phosphate availability in the upper surface water of the Mediterranean Sea and DOC accumulation due to nutrient limitation of bacterial production already identified by previous modeling (Thingstad et al., 1997) and in situ (Moutin et al., 2002; Van Wambeke et al., 2002) studies, is ~~strenghtened~~ confirmed by this modeling study, which may therefore be of interest for other oceanic regions. ~~Upper waters~~ The low phosphate availability ~~availabilities~~ of the upper waters ~~have~~ has ~~indeed~~ been identified in other oceanic regions such as ~~like~~ the Sargasso Sea (Wu et al., 2000), the North Pacific ~~or~~ and the South West Pacific (Van Den Broeck et al., 2004), and high DOC accumulation ~~were~~ has also been reported in some of these areas (Carlson et al., 1994). This work may therefore be of interest for these oceanic regions. Finally, in the context of climate change, the enhanced stratification and the ~~likely~~ probable geographical extension of low phosphate availability in upper waters (Karl et al., 1997; Moutin et al., 2008) is expected to result in an increase in DOC production (Santinelli et al., 2013; Lazzari et al., 2013), and thereby further increase the importance of DOC in the biological carbon pump.

Acknowledgements. The authors are grateful to the ~~different supports~~ various organisations that funded this work. This includes the French PACA Region (~~who~~ which funded the PhD thesis of A. Guyennon), the Mercator Ocean group (which ~~who~~ funded the SiMED project that provided an efficient framework for this work), the MED-ICCBIO project (funded by the *Groupement d' Intérêt Scientifique* "Climat, Environnement et Société"), and the OT-MED Labex. This work is a contribution to the MerMEx and the OT-MED programs and it was granted access to the HPC resources of IDRIS (Institut du Développement et des Ressources en Informatique Scientifique) of the Centre National de la Recherche Scientifique (CNRS). The DYFAMED time series ~~have been~~ was provided by the Oceanological Observatory (CNRS-UPMC) of Villefranche-sur-Mer (L.Coppola). This project is funded by CNRS-INSU and ALLENVI through the MOOSE ~~observing~~ observation network. The satellite data used in this is study are MyOcean Products. Authors are also grateful to Jean-Michel André for his help and valuable ~~relevant~~ advice, and to L. Coppola for his very efficient assistance ~~to obtain~~ in obtaining in situ data from the DyFaMed station.

References

Alekseenko, E., Raybaud, V., Espinasse, B., Carlotti, F., Queguiner, B., Thouvenin, B., Garreau, P., and Baklouti, M.: Seasonal dynamics and stoichiometry of the planktonic community in the NW Mediterranean Sea: a 3D modeling approach, Ocean Dynamics, 64, 179–207, 2014.

Antoine, D., Morel, A., and André, J.: Algal pigment distribution and primary production in the eastern Mediterranean as derived from coastal zone color scanner observations, Journal of Geophysical Research, 100, 16 193–16, 1995.

Avril, B.: DOC dynamics in the northwestern Mediterranean Sea (DYFAMED site), Deep Sea Research Part II: Topical Studies in Oceanography, 49, 2163–2182, 2002.

Baklouti, M., Diaz, F., Pinazo, C., Faure, V., and Quéguiner, B.: Investigation of mechanistic formulations depicting phytoplancton dynamics for models of marine pelagic ecosystems and description of a new model, Progress in Oceanography, 71, 1–33, 2006a.

Baklouti, M., Faure, V., Pawlowski, L., and Sciandra, A.: Investigation and sensitivity analysis of a mechanistic phytoplankton model implemented in a new modular numerical tool (Eco3M) dedicated to biogeochemical modelling, Progress in Oceanography, 71(1), 34–58, 2006b.

Baklouti, M., Chevalier, C., Bouvy, M., Corbin, D., Pagano, M., Troussellier, M., and Arfi, R.: A study of plankton dynamics under osmotic stress in the Senegal River Estuary, West Africa, using a 3D mechanistic model, Ecological Modelling, 222, 2704–2721, 2011.

Baretta, J., Ebenhoh, W., and Ruardij, P.: The European Regional Seas Ecosystem Model, a complex marine ecosystem model, J. Sea Res., 33, 233–246, 1995.

Béranger, K., Mortier, L., and Crépon, M.: Seasonal variability of water transport through the Straits of Gibraltar, Sicily and Corsica, derived from a high-resolution model of the Mediterranean circulation, Progress in Oceanography, 66, 341–364, 2005.

Bertilsson, S., Berglund, O., Karl, D. M., and Chisholm, S. W.: Elemental composition of marine Prochlorococcus and Synechococcus: Implications for the ecological stoichiometry of the sea, Limnol. Oceanogr., 48, 1721–1731, 2003.

Beuvier, J.: Modélisation de la variabilité climatique de la circulation et des masses d'eau en mer Méditerranée: impact des échanges océan-atmosphére, Ph.D. thesis, Ecole Polytechnique, 2011.

Beuvier, J., Sevault, F., Herrmann, M., Kontoyiannis, H., Ludwig, W., Rixen, M., Stanev, E., Béranger, K., and Somot, S.: Modeling the Mediterranean Sea interannual variability during 1961–2000: focus on the Eastern Mediterranean Transient, Journal of Geophysical Research: Oceans (1978–2012), 115, doi:10.1029/2009JC005950, 2010.

Beuvier, J., Béranger, K., Brossier, C., Somot, S., Sevault, F., Drillet, Y., Bourdallé-Badief, R., Ferry, N., Lyard, F., et al.: Spreading of the Western Mediterranean Deep Water after winter 2005: Time scales and deep cyclone transport., Journal of Geophysical Research, 117, doi:10.1029/2011JC007679, 2012a.

Beuvier, J., Lebeaupin Brossier, C., Béranger, K., Arsouze, T., Bourdallé-Badie, R., C., D., Drillet, Y., Drobinski, P., Lyard, F., Ferry, N., Sevault, F., and Somot, S.: Oceanic component for the modeling of the regional Mediterranean Eart System., Mercator Ocean Quarterly Newsletter, 46, 60–66, 2012b.

Boldrin, A., Miserocchi, S., Rabitti, S., Turchetto, M., Balboni, V., and Socal, G.: Particulate matter in the southern Adriatic and Ionian Sea: characterisation and downward fluxes, Journal of Marine Systems, 33, 389–410, 2002.

Bopp, L., Monfray, P., Aumont, O., Dufresne, J., Le Treut, H., Madec, G., Terray, L., and Orr, J.: Potential climate change on marine export production, Global Biogeochemical Cycles, 15, 81–99, 2001.

Bosc, E., Bricaud, A., and Antoine, D.: Seasonal and interannual variability in algal biomass and primary production in the Mediterranean Sea, as derived from 4 years of SeaWiFS observations, Global Biogeochemical Cycles, 18, GB1005, doi:10.1029/2003GB002034, 2004.

Brown, E. J. and Harris, R. F.: Kinetics of algal transient phosphate uptake and the cell quota concept, Limnol. Oceanogr., 23, 35–40, 1978.

Buesseler, K.: Do upper-ocean sediment traps provide an accurate record of particle flux ?, Nature, 353, 420–423, 1991.

Carlson, C., Ducklow, H., and Michaels, A.: Annual flux of dissolved organic carbon from the euphotic zone in the northwestern Sargasso Sea, Nature, 371, 405–408, 1994.

Christaki, U., Courties, C., Joux, F., Jeffrey, W. H., Neveux, J., and Naudin, J.: Community structure and trophic role of ciliates and heterotrophic nanoflagellates in Rhone River diluted mesoscale structures (NW Mediterranean Sea), Aquat Microb Ecol, 57, 263–277, 2009.

Claustre, H., Morel, A., Hooker, S., Babin, M., Antoine, D., Oubelkheir, K., Bricaud, A., Leblanc, K., Queguiner, B., and Maritorena, S.: Is desert dust making oligotrophic waters greener ?, Geophysical Research Letters, 29, 107–1–107–4, 2002.

Copin-Montégut, G. and Avril, B.: Vertical distribution and temporal variation of dissolved organic carbon in the North-Western Mediterranean Sea, Deep Sea Research Part I: Oceanographic Research Papers, 40, 1963–1972, 1993.

Crise, A., Crispi, G., and Mauri, E.: A seasonal three-dimensional study of the nitrogen cycle in the Mediterranean Sea: Part I. Model implementation and numerical results, Journal of Marine Systems, 18, 287–312, 1998.

Crispi, G., Crise, A., and Solidoro, C.: Three-dimensional oligotrophic ecosystem models driven by physical forcing: the Mediterranean Sea case, Environmental Modelling Software, 13, 483–490, 1998.

Diaz, F., Raimbault, P., Boudjellal, B., Garcia, N., and Moutin, T.: Early spring phosphorus limitation of primary productivity in a NW Mediterranean coastal zone (Gulf of Lions), Marine Ecology Progress Series, 211, 51–62, 2001.

D'Ortenzio, F. and Ribera d'Alcalà, M.: On the trophic regimes of the Mediterranean Sea: a satellite analysis, Biogeosciences, 6, 139–148, 2009.

D'Ortenzio, F., Marullo, S., Ragni, M., Ribera d'Alcalà, M., and Santoleri, R.: Validation of empirical SeaWiFS algorithms for chlorophyll-a retrieval in the Mediterranean Sea: A case study for oligotrophic seas, Remote Sensing of Environment, 82, 79–94, 2002.

Droop, M.: Vitamin B12 and marine ecology. IV. The kinetics of uptake, growth and inhibition in Monochrysis lutheri, J. Mar. Biol. Assoc. UK, 48, 689–733, 1968.

Droop, M.: The nutrient status of algal cells in batch culture, J. Mar. Biol. Assoc. UK, 55, 541–555, 1975.

Eppley, R. and Peterson, B.: Particulate organic matter flux and planktonic new production in the deep ocean, Nature, 282, 677–680, 1979.

Fasham, M., Flynn, K., Pondaven, P., Anderson, T., and Boyd, P.: Development of a robust marine ecosystem model to predict the role of iron in biogeochemical cycles: A comparison of results for iron-replete and iron-limited areas, and the SOIREE iron-enrichment experiment, Deep Sea Research Part I: Oceanographic Research Papers, 53, 333–366, 2006.

Fukuda, R., Ogawa, H., Nagata, T., and Koike, I.: Direct Determination of Carbon and Nitrogen Contents of Natural Bacterial Assemblages in Marine Environments, Appl Environ Microbiol, 64, 3352–3358, 1998.

Garcia, H. E., Locarnini, R., Boyer, T., and Antonov, J.: World Ocean Atlas 2005. Vol. 4, Nutrients (phosphate, nitrate, silicate), 2006.

Geider, R., MacIntyre, H., and Kana, T.: A dynamic regulatory model of phytoplankton acclimation to light, nutrients, and temperature, Limnology and Oceanography, 43, 679–694, 1998.

Gogou, A., Sanchez-Vidal, A., Durrieu de Madron, X., Stavrakakis, S., Calafat, A. M., Stabholz, M., Psarra, S., Canals, M., Heussner, S., Stavrakaki, I., et al.: Carbon flux to the deep in three open sites of the Southern European Seas (SES), Journal of Marine Systems, 129, 224–233, 2014.

Gómez, F.: The role of the exchanges through the Strait of Gibraltar on the budget of elements in the Western Mediterranean Sea: consequences of human-induced modifications, Marine Pollution Bulletin, 46, 685–694, 2003.

Hansell, D. and Carlson, C.: Marine Dissolved Organic Matter and the Carbon Cycle, Oceanography, 14, 685–716, 2001.

Hansell, D., Carlson, C., and Suzuki, Y.: Dissolved organic carbon export with North Pacific Intermediate Water formation, Global Biogeochemical Cycles, 16, 7–1–7–8, 2002.

Hansell, D., Repeta, D., Carlson, C., and Schlitzer, R.: Dissolved organic matter in the ocean: A controversy stimulates new insights, Oceanography, 22, 202–211, 2009.

Heldal, M., Scanlan, D. J., Norland, S., Thingstad, F., and Mann, N. H.: Elemental composition of single cells of various strains of marine Prochlorococcus and Synechococcus using X-ray microanalysis, Limnol. Oceanogr., 48, 1732–1743, 2003.

Herrmann, M. and Somot, S.: Relevance of ERA40 dynamical downscaling for modeling deep convection in the Mediterranean Sea, Geophysical Research Letters, 35, doi:10.1029/2007GL032442, 2008.

Herrmann, M., Diaz, F., Estournel, C., Marsaleix, P., and Ulses, C.: Impact of atmospheric and oceanic interannual variability on the Northwestern Mediterranean Sea pelagic planktonic ecosystem and associated carbon cycle, Journal of Geophysical Research: Oceans, 118, 1–22, 2014.

Holling, C.: Some characteristics of simple types of predation and parsitism, The Candian Entomologist, 91, 385–398, 1959.

Karl, D. M., Letelier, R. M., Tupas, L., Dore, J., Christian, J., and Hebel, D.: The role of nitrogen fixation in biogeochemical cycling in the subtropical North Pacific Ocean, Nature, 387, 533–538, 1997.

Klausmeier, C., Litchman, E., and Levin, S.: Phytoplankton growth and stoichiometry under multiple nutrient limitation, Limnology and Oceanography, 49, 1463–1470, 2004.

Klausmeier, C., Litchman, E., Daufresne, T., and Levin, S.: Phytoplankton stoichiometry, Ecol. Res., 23, 479–485, 2008.

Kooijman, S. A. L. M.: Dynamic Energy and Mass Budgets in Biological Systems, Cambridge University Press, Cambridge, UK, 2000.

Lacroix, G. and Gregoire, M.: Revisited ecosystem model (MODECOGeL) of the Ligurian Sea: seasonal and interannual variability due to atmospheric forcing, Journal of Marine Systems, 37, 229–258, 2002.

Lavigne, H., D'Ortenzio, F., Migon, C., Claustre, H., Testor, P., d'Alcalà, M., Lavezza, R., Houpert, L., and Prieur, L.: Enhancing the comprehension of mixed layer depth control on the Mediterranean phytoplankton phenology, Journal of Geophysical Research: Oceans, 118, 3416–3430, 2013.

Lazzari, P., Solidoro, C., Ibello, V., Salon, S., Teruzzi, A., Béranger, K., Colella, S., and Crise, A.: Seasonal and inter-annual variability of plankton chlorophyll and primary production in the Mediterranean Sea: a modelling approach, Biogeosciences, 8, 5379–5422, 2012.

Lazzari, P., Mattia, G., Solidoro, C., Salon, S., Crise, A., Zavatarelli, M., Oddo, P., and Vichi, M.: The impacts of climate change and environmental management policies on the trophic regimes in the Mediterranean Sea: Scenario analyses, Journal of Marine Systems, 2013.

Le Quéré, C., Takahashi, T., Buitenhuis, E., Rödenbeck, C., and Sutherland, S.: Impact of climate change and variability on the global oceanic sink of CO2, Global Biogeochemical Cycles, 24, 2016–2040, 2010.

Le Quéré, C. L., Harrison, S., P., C., Buitenhuis, E., Aumont, O., Bopp, L., Claustre, H., Cotrim Da Cunha, L., Geider, R., Giraud, X., et al.: Ecosystem dynamics based on plankton functional types for global ocean biogeochemistry models, Global Change Biology, 11, 2016–2040, 2005.

Leblanc, K., Quéguiner, B., Garcia, N., Rimmelin, P., and Raimbault, P.: Silicon cycle in the NW Mediterranean Sea: seasonal study of a coastal oligotrophic site, Oceanologica Acta, 26, 339–355, 2003.

Lefèvre, D., Denis, M., Lambert, C., and Miquel, J.: Is DOC the main source of organic matter remineraliztion in the ocean water column ?, Journal of Marine Systems, 7, 281–291, 1996.

Lévy, M., Mémery, L., and André, J.: Simulation of primary production and export fluxes in the Northwestern Mediterranean Sea, Journal of Marine Research, 56, 197–238, 1998.

Lovdal, T., Skjoldal, E. F., Heldal, M., Norland, S., and Thingstad, T. F.: Changes in morphology and elemental composition of Vibrio splendidus along a gradient from carbon-limited to phosphate-limited growth, Microb. Ecol., 55, 152–161, 2008.

Ludwig, W.: Continental erosion and river transport of organic carbon to the world's Oceans, Ph.D. thesis, Université Louis Pasteur de Strasbourg, 1996.

Ludwig, W., Dumont, E., Meybeck, M., and Heussner, S.: River discharges of water and nutrients to the Mediterranean and Black Sea: Major drivers for ecosystem changes during past and future decades?, Progress in Oceanography, 80, 199–217, 2009.

Macías, D., Stips, A., and Garcia-Gorriz, E.: The relevance of deep chlorophyll maximum in the open Mediterranean Sea evaluated through 3D hydrodynamic-biogeochemical coupled simulations, Ecological Modelling, 281, 26–37, 2014.

Madec, G. and The-NEMO-Team: NEMO ocean engine, Note du pole de modélisation de l'IPSL, 27, 1228–1619, 2008.

Maier-Reimer, E., Mikolajewicz, U., and Winguth, A.: Future ocean uptake of CO2: interaction between ocean circulation and biology, Climate Dynamics, 12, 711–722, 1996.

Marshall, J. and Schott, F.: Open-ocean convection: Observations, theory, and models, Reviews of Geophysics, 37, 1–64, 1999.

Marty, J. and Chiavérini, J.: Hydrological changes in the Ligurian Sea (NW Mediterranean, DYFAMED site) during 1995–2007 and biogeochemical consequences, Biogeosciences, 7, 2117–2128, 2010.

Marty, J., Chiavérini, J., Pizay, M., and Avril, B.: Seasonal and interannual dynamics of nutrients and phytoplankton pigments in the western Mediterranean Sea at the DYFAMED time-series station (1991–1999), Deep Sea Research Part II: Topical Studies in Oceanography, 49, 1965–1985, 2002.

Marty, J.-C., Garcia, N., and Raimbault, P.: Phytoplankton dynamics and primary production under late summer conditions in the NW Mediterranean Sea, Deep Sea Research Part I, 55, 1131–1149, 2008.

Mattia, G., Zavatarelli, M., Vichi, M., and Oddo, P.: The Eastern Mediterranean Sea biogeochemical dynamics in the 1990s: A numerical study, Journal of Geophysical Research: Oceans, 118, 2231–2248, 2013.

Mauriac, R., Moutin, T., and Baklouti, M.: Accumulation of DOC in Low Phosphate Low Chlorophyll (LPLC) area: is it related to higher production under high N: P ratio?, Biogeosciences, 8, 933–950, 2011.

Meador, T., Gogou, A., Spyres, G., Herndl, G., Krasakopoulou, E., Psarra, S., Yokokawa, T., De Corte, D., Zervakis, V., and Repeta, D.: Biogeochemical relationships between ultrafiltered dissolved organic matter and picoplankton activity in the Eastern Mediterranean Sea, Deep Sea Research Part II: Topical Studies in Oceanography, 57, 1460–1477, 2010.

MERMEX-group: Marine ecosystems' responses to climatic and anthropogenic forcings in the Mediterranean, Progress in Oceanography, 91, 97–166, 2011.

Millot, C. and Taupier-Letage, I.: Circulation in the Mediterranean sea, in: The Mediterranean Sea, pp. 29–66, Springer, 2005.

Miquel, J., Martín, J., Gasser, B., Rodriguez-y Baena, A., Toubal, T., and Fowler, S.: Dynamics of particle flux and carbon export in the northwestern Mediterranean Sea: a two decade time-series study at the DYFAMED site, Progress in Oceanography, 91, 461–481, 2011.

Miquel, J. C., Fowler, S. W., La Rosa, J., and Buat-Menard, P.: Dynamics of the downward flux of particles and carbon in the open northwestern Mediterranean Sea, Deep-Sea Research I, 41, 243–261, 1994.

Moore, J. K., Doney, S. C., Kleypas, J. A., Glover, D. M., and Fung, I. Y.: An intermediate complexity marine ecosystem model for the global domain, Deep-Sea Research II, 49, 403–462, 2002.

Morel, A.: Optical modeling of the upper ocean in relation to its biogenous matter content (case I waters), Journal of Geophysical Research: Oceans (1978–2012), 93, 10 749–10 768, 1988.

Moutin, T. and Prieur, L.: Influence of anticyclonic eddies on the Biogeochemistry from the Oligotrophic to the Ultraoligotrophic Mediterranean (BOUM cruise), Biogeosciences, 9, 3827–3855, 2012b.

Moutin, T. and Raimbault, P.: Primary production, carbon export and nutrients availability in Western and Eastern Mediterranean Sea in early summer 1996 (MINOS cruise), Journal of Marine Systems, 33, 273–288, 2002.

Moutin, T., Raimbault, P., and Poggiale, J.: Production primaire dans les eaux de surface de la Mediterranee occidentale. Calcul de la production journaliere, Comptes Rendus de l'Académie des Sciences-Series III-Sciences de la Vie, 322, 651–655, 1999.

Moutin, T., Thingstad, T. F., Van Wambeke, F., Marie, D., Slawyk, G., and Raimbault, P.: Does competition for nanomolar phosphate supply explain the predominance of the cyanobacterium Synechococcus?, Limnology and Oceanography, 47, 1562–1567, 2002.

Moutin, T., Karl, D. M., Duhamel, S., Rimmelin, P., Raimbault, P.and Van Mooy, B. A. S., and Claustre, H.: Phosphate availability and the ultimate control of new nitrogen input by nitrogen fixation in the tropical Pacific Ocean, Biogeosciences, 5, 95–109, 2008.

Moutin, T., Van Wambeke, F., and Prieur, L.: Introduction to the Biogeochemistry from the Oligotrophic to the Ultraoligotrophic Mediterranean (BOUM) experiment, Biogeosciences, 9, 3817–3825, 2012a.

Palmiéri, J.: Modélisation biogéochimique de la mer Méditerranée avec le modèle régional couplé NEMO-MED12/PISCES., Ph.D. thesis, Université de Versailles Saint-Quentin, France, 2014.

Palmiéri, J., Le Vu, B., Dutay, J., Bopp, L., Béranger, K., Beuvier, J., Somot, S., and Éthé, C.: Biogeochemical modelling of the Mediterranean Sea with PISCES MED-12 model., GMD, in prep.

Pasqueron de Fommervault, O., Migon, C., D'Ortenzio, F., Ribera d'Alcalà, M., and Coppola, L.: Temporal variability of nutrient concentrations in the northwestern Mediterranean sea (DYFAMED time-series station), Deep Sea Research Part I, 100, 1–12, 2015.

Paulmier, A., Kriest, I., and Oschlies, A.: Stoichiometries of remineralisation and denitrification in global biogeochemical ocean models, Biogeosciences (BG), 6, 923–935, 2009.

Prowe, A., Pahlow, M., Dutkiewicz, S., Follows, M., and Oschlies, A.: Top-down control of marine phytoplankton diversity in a global ecosystem model, Progress in Oceanography, 101, 1–13, 2012.

Pujo-Pay, M., Conan, P., Oriol, L., Cornet-Barthaux, V., Falco, C., Ghiglione, J., Goyet, C., Moutin, T., and Prieur, L.: Integrated survey of elemental stoichiometry (C, N, P) from the western to eastern Mediterranean Sea, Biogeosciences, 8, 883–899, 2011.

Redfield, A. C.: The biological control of chemical factors in the environment, Am Sci, 46, 205–221, 1958.

Santinelli, C., Nannicini, L., and Seritti, A.: DOC dynamics in the meso and bathypelagic layers of the Mediterranean Sea, Deep Sea Research Part II: Topical Studies in Oceanography, 57, 1446–1459, 2010.

Santinelli, C., D.A., H., and d'Alcala M., R.: Influence of stratification on marine dissolved organic carbon (DOC) dynamics : The Mediterranean Sea case, Progress in Oceanography, 119, 68–77, 2013.

Sarmiento, J. and Gruber, N.: Ocean biogeochemical dynamics, vol. 1015, Princeton University Press Princeton, 2006.

Sarmiento, J., Hughes, T., Stouffer, R., and Manabe, S.: Simulated response of the ocean carbon cycle to anthropogenic climate warming, Nature, 393, 245–249, 1998.

Schaap, D. and Lowry, R.: SeaDataNet–Pan-European infrastructure for marine and ocean data management: unified access to distributed data sets, International Journal of Digital Earth, 3, 50–69, 2010.

Sempéré, R., Yoro, S. C., Van Wambeke, F., and Charrière, B.: Microbial decomposition of large organic particles in the Northwestern Mediterranean Sea: an experimental approach, Mar Ecol Prog Ser, 198, 61–72, 2000.

Siegenthaler, U. and Sarmiento, J.: Atmospheric carbon dioxide and the ocean, Nature, 365, 119–125, 1993.

Siokou-Frangou, I., Christaki, U., Mazzocchi, M., Montresor, M., Ribera d'Alcalà, M., Vaqué, D., and Zingone, A.: Plankton in the open Mediterranean Sea: a review, Biogeosciences, 7, 1543–1586, 2010.

Somot, S., Sevault, F., and Déqué, M.: Transient climate change scenario simulation of the Mediterranean Sea for the twenty-first century using a high-resolution ocean circulation model, Climate Dynamics, 27, 851–879, 2006.

Soto-Navarro, J., Somot, S., Sevault, F., Beuvier, J., Criado-Aldeanueva, F., García-Lafuente, J., and Béranger, K.: Evaluation of regional ocean circulation models for the Mediterranean Sea at the Strait of Gibraltar: volume transport and thermohaline properties of the outflow, Climate Dynamics, 44, 1277–1292, doi:10.1007/S00382-014-2179-4, 2014.

Sournia, A.: La production primaire planctonique en Méditerranée; essai de mise à jour, Cooperative Investigations in the Mediterranean, International Coordinator and Operational Unit; Étude en commun de la Méditerranée, Coordonnateur international et Unité opérationnelle, 1973.

Talarmin, A., Van Wambeke, F., Duhamel, Catala, P., Moutin, T., and Lebaron, P.: Improved methodology to measure taxon-specific phosphate uptake in live and unfiltered samples, Limnol. Oceanogr. Methods, 9, 443–453, doi:10.4319/lom.2011.9.443., 2011.

Thingstad, T., , Hagström, A., and Rassoulzadegan, F.: Accumulation of degradable DOC in surface waters: Is it caused by a malfunctioning microbial loop?, Limnology and Oceanography, 42, 398–404, 1997.

Thingstad, T., Krom, M., Mantoura, R., Flaten, G., Groom, S., Herut, B., Kress, N., Law, C., Pasternak, A., Pitta, P., Psarra, S., Rassoulzadegan, F., Tanaka, T., Tselepides, A., Wassman, P., Woodward, E., Wexels, R., Zodiatis, G., and Zohary, T.: Nature of phosphorus limitation in the ultraoligotrophic eastern Mediterranean, Science, 309, 1068–1071, 2005.

Toggweiler, J., Gnanadesikan, A., Carson, S., Murnane, R., and Sarmiento, J.: Representation of the carbon cycle in box models and GCMs: 1. Solubility pump, Global biogeochemical cycles, 17, 2003.

Tugrul, S. and Besiktepe, S.: Nutrient exchange fluxes between the black sea and the Mediterranean through the turkish strait system (marmara sea, bosphorus and dardanelles), CIESM, 2007.

Uitz, J., Stramski, D., Gentili, B., D'Ortenzio, F., and Claustre, H.: Estimates of phytoplankton class-specific and total primary production in the Mediterranean Sea from satellite ocean color observations, Global Biogeochemical Cycles, 26, doi:10.1029/2011GB004055, 2012.

Vallina, S., Ward, B., Dutkiewicz, S., and Follows, M.: Maximal feeding with active prey-switching: A kill-the-winner functional response and its effect on global diversity and biogeography, Progress in Oceanography, 120, 93–109, 2014.

Van Den Broeck, N., Moutin, T., Rodier, M., and Le Bouteiller, A.: Seasonal variations of phosphate availability in the SW Pacific Ocean near New Caledonia, Mar. Ecol. Progress Ser., 268, 1–12, 2004.

Van Wambeke, F., Christaki, U., Giannakourou, A., Moutin, T., and Souvemerzoglou, K.: Longitudinal and vertical trends of bacterial limitation by phosphorus and carbon in the Mediterranean Sea, Microbial ecology, 43, 119–133, 2002.

Vichi, M., Pinardi, N., and Masina, S.: A generalized model of pelagic biogeochemistry for the global ocean ecosystem. Part I: Theory, Journal of Marine Systems, 64, 89–109, 2007.

Volpe, G., Santoleri, R., Vellucci, V., Ribera d'Alcala, M., Marullo, S., and d'Ortenzio, F.: The colour of the Mediterranean Sea: Global versus regional bio-optical algorithms evaluation and implication for satellite chlorophyll estimates, Remote Sensing of Environment, 107, 625–638, 2007.

Vörösmarty, C., Fekete, B., and Tucker, B.: Global river discharge database, RivDis, Tech. rep., 1996.

Wilhelm, S. W., King, A. L., Twining, B. S., LeCleir, G. R., DeBruyn, J. M., Strzepek, R. F., Breene, C. L., Pickmere, S., Ellwood, M. J., Boyd, P. W., and Hutchins, D. A.: Elemental quotas and physiology of a south-western Pacific Ocean plankton community as a function of iron availability, Aquatic Microbial Ecology, 68, 185–194, 2013.

Wu, J., SUNDA, W., BOYLE, E., and Karl, D.: Phosphate depletion in the western North Atlantic Ocean, Sciences, 289, 759–762, 2000.

Zúñiga, D., Calafat, A., Sanchez-Vidal, A., Canals, M., Price, B., Heussner, S., and Miserocchi, S.: Particulate organic carbon budget in the open Algero-Balearic Basin (Western Mediterranean): Assessment from a one-year sediment trap experiment, Deep Sea Research Part I: Oceanographic Research Papers, 54, 1530–1548, 2007.

Appendix A: Model Skill Assessment

Due to the high complexity of the biogeochemical model and the scarcity of data, the assessment of the model's representativeness at the scale of the Mediterranean Sea is a complex task. This work, however, aims ~~at performing~~ to achieve comparisons on several modeled variables, at different time and space scales when in situ measurements were available. For reasons of brevity, model outputs hereafter have the prefix "m" while corresponding in situ or satellite observations have the prefix "o".

A1 Nutrients

A1.1 Basin scale spatial variability

Data collected during the BOUM cruise ~~allow to appreciate~~ offer a basis for assessing the quality of the simulation during the stratified summer period. The comparison between mNO_3 and mPO_4 with the corresponding measured concentrations (i.e. oNO3 and oPO4) along the BOUM transect is ~~done~~ shown in Fig. 15 and Table 1.

When compared to in situ data, ~~average~~ /blmean mNO_3 [mPO_4 in brackets] in the deep layers (> 1500 m) is underestimated by 1.2 [0.04] μmol l^{-1} in the western basin, and 0.4 [0.01] μmol l^{-1} in the eastern basin. This can be attributed to an underestimation of initial nutrient stocks at depth. There are indeed significant differences between the nutrient concentrations in deep waters provided by the Medatlas climatology data and by the BOUM measurements. As a consequence, and due to the stability of nutrient concentrations in deep water during the simulation, the same disparities can be observed between the model outputs and the BOUM cruise data.

In the surface layer (0-30 m), mNO_3 is less than 1 μmol l^{-1}, with a mean value of around 0.5 μmol l^{-1} for the whole basin, while mPO_4 is almost nil everywhere (< 0.01 μmol l^{-1}). These values are consistent with measured nutrient concentrations, which are low and close to their quantification limits of 0.05 μmol l^{-1} for both NO_3 and PO_4 (Fig. 15, Table 1) though the model tends

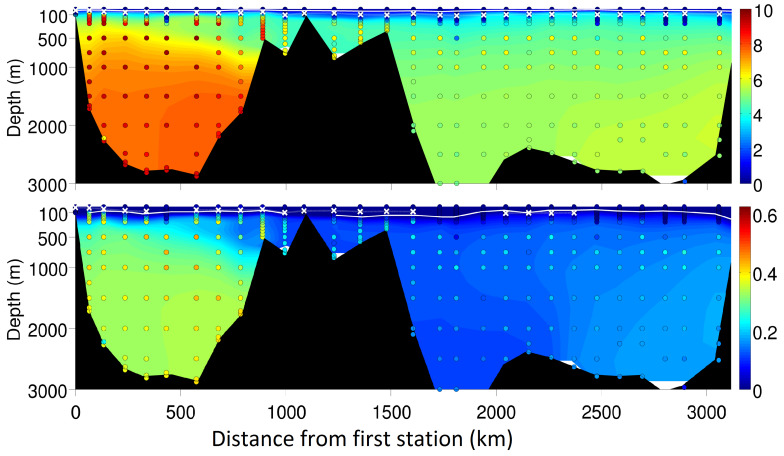

Figure 15. BOUM (top) NO_3 and (bottom) PO_4 (Pujo-Pay et al., 2011). Model outputs are in shaded colors; in situ data are colored circles. Model outputs correspond to the daily outputs averaged over the BOUM cruise period. White crosses represent the data-derived depth of the top nitracline as defined in (Moutin and Prieur, 2012b). The white line indicates the top nitracline from model outputs.

to overestimate surface nitrate concentrations during periods of intense stratification. This may be related to an overestimation of nitrification processes, and/or an underestimation of detrital organic matter sinking. Nitrification is, indeed, a linear function with a fixed parameter and does not take into account the potential dependence ~~dependancies~~ of the process (e.g. Paulmier et al., 2009). In the western basin, the top of the modeled nitracline is almost 25 m ~~over~~ above the top nitracline derived from in situ data, and the gap increases eastward as the top nitracline derived from data gets deeper (Moutin and Prieur, 2012b). The modeled top phosphacline is slightly ~~also~~ below the data-derived top phosphacline along most of the BOUM transect. The difference between model outputs and data can also be found in the slope of the nitracline at depths ~~of~~ between 150 m and 1000 m: this slope decreases with depth for the model, while it is quite constant for data. As a consequence, significant differences in nitrate concentration can be observed in the "intermediate" waters (between 250 and 1000 m) : ~~model mean concentrations are~~ mNO3 is underestimated by almost 3 μmol l^{-1} at 500 m in the western basin, and respectively 1.5 and 1.2 μmol l^{-1} in the Ionian and Levantine basins. In the western basin, the same differences between model and data were found in the phosphate vertical profiles (Fig. 15, Table 1), resulting in a maximum difference of 0.15 μmol l^{-1} in phosphate concentrations. However, in the eastern basin, modeled and in situ phosphate gradients are in better agreement than nitrate gradients, except that the phosphacline is less thick than in the data. Finally, some discrepancies between model and observations are attributable to the mislocation of the anti-cyclonic eddies, but this failure of the ~~hydrodynamical~~ hydrodynamic model has only a local impact on modeled nutrients.

Table 1. Mean over the BOUM cruise period of modeled (mNO_3, mPO_4) and measured (oNO_3, oPO_4) nutrients concentrations for different layers of the western and eastern basins. Root Mean Squared Difference (RMSD) between model outputs and observations have been calculated. Values in brackets are standard deviations, and BQL stands for Below the Quantification Limit (0.05 μmol l^{-1}).

		Model		Observations		RMSD	
		West	East	West	East	West	East
0-30 m	NO_3	0.4 [0.2]	0.6 [0.1]	BQL	BQL	0.44	0.67
	PO_4	0.02 [0]	0.002 [0]	BQL	BQL	0.020	0.0047
250-1500 m	NO_3	6.3 [1]	4.7 [0.4]	8.7 [1.1]	5.3 [1.4]	2.3	1.90
	PO_4	0.27 [0.1]	0.14 [0]	0.37 [0.1]	0.18 [0.1]	0.12	0.047
$>$ 1500 m	NO_3	7.7 [0.1]	5.4 [0.2]	8.9 [0.5]	5.0 [0.5]	1.2	0.33
	PO_4	0.34 [0]	0.15 [0]	0.38 [0]	0.16 [0]	0.049	0.032
Range	NO_3	[0 ; 7.8]	[0.36 ; 5.7]	[BQL ; 9.8]	[BQL ; 6.3]	2.1	1.7
	PO_4	[0 ; 0.34]	[0 ; 0.18]	[BQL ; 0.44]	[BQL ; 0.28]	0.11	0.042

A1.2 Seasonal and vertical ~~variabilities~~ variation

The surface patterns of change ~~evolutions of~~ in mNO_3 and mPO_4 at the DyFaMed station are plotted in Fig. 16. mNO_3 and mPO_4 exhibit a seasonal pattern, with values regularly lower than 0.5 μmol l^{-1} from May (March for mPO_4) to October, increasing thereafter to reach a maximum in January ranging from 3.2 to 4.2 (0.03 to 0.07 for mPO_4) μmol l^{-1} depending on the year. This is very similar to the change in ~~evolution of~~ observed NO_3 which is also below 0.5 μmol l^{-1} from May to October and reaches a maximum ranging from 2 to 6.4 μmol l^{-1} in January-February. In summer, however, oNO_3 is often almost below the quantification limit while mNO_3 is never below 0.2 μmol l^{-1}. oPO_4 is below the quantification limit in almost every observation made above 30 m depth, except between January and March where oPO_4 can reach 0.15 μmol l^{-1}. These maxima are underestimated by the model, as mPO_4 never exceeds 0.07 μmol l^{-1} (close to the quantification limit). The differences between mPO_4 and oPO_4 at very low phosphate concentrations can be partly attributable to the lower reliability of measurements near the detection limit. For higher phosphate concentrations however, especially during the winter convection period, there is a clear deficit in the mPO4 which is not only due to the underestimated initial mPO4 concentration in deep waters (this has already been evidenced by the comparison with BOUM data, see section A1.1), but also potentially due to an underestimation of the MLD in winter.

Between 30 and 1000 m depth, observed and modeled NO_3 and PO_4 concentrations are consistent with each other though observations show higher mean values and larger ranges quite systematically (see Fig. 17 and 18 and table 2). The highest absolute differences ~~along~~ within the water column are observed between 250 and 500 m depth for nitrate where mNO_3 is underestimated by 1.5 μmol l^{-1}, and between 30 and 100 m for phosphate where the mean mPO_4 is very low ($<$ 0.02 μmol l^{-1})

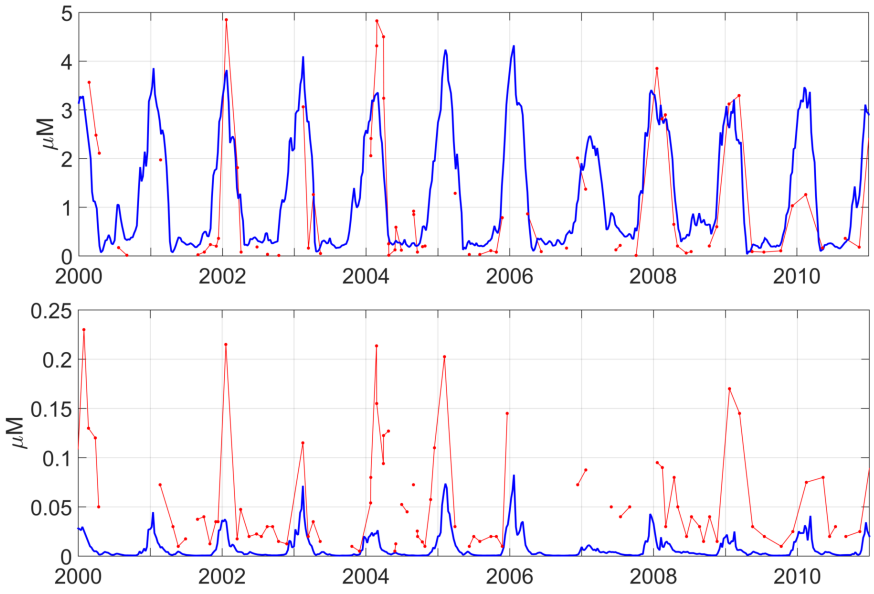

Figure 16. Patterns of change over time ~~Time evolution~~ of modeled (lines) and observed (dots) surface concentrations in nitrate and phosphate in μmol l^{-1} at the DyFaMed site.

while oPO_4 equals 0.14 μmol l^{-1}. The same interpretation ~~for~~ of this poor representation of the shape of the nutriclines (well marked in observations and much more diffuse in the model outputs) as the one provided for the comparison with BOUM profiles can be put forward to explain this model failure, namely underestimated deep nutrient concentrations and a lack of detrital particles that would have reached such water depths before being hydrolyzed. It must be ~~reminded~~ borne in mind, however, that DyFaMed observations are compared to a single grid point of the modeled domain which is submitted to variability due to hydrodynamic features. We evaluated the potential impact of variability by calculating ~~the RMSD between~~ the spatial standard deviation using the 8 neighbouring grid points. ~~and the single grid point chosen.~~ The impact of spatial variability is weak on temporal means and stays below 0.5 and 0.04 μmol l^{-1} for NO_3 and PO_4 respectively during the whole period, and therefore cannot fully explain the differences observed.

A2 Chlorophyll

A2.1 Basin scale variability

Maps of the annual means of oCHL and mCHL as well as their difference (i.e. oCHL-mCHL) over the 2002-2011 period are plotted in Fig. 19 . mCHL is calculated as the average concentration through the first 10 m of the water column.

At first, year-long high chlorophyll clusters can be seen in both oCHL and mCHL close to the main river mouths (the Nile, Rhone, Po, Ebro or Tiber), but only in oCHL in the Dardanelles Strait,

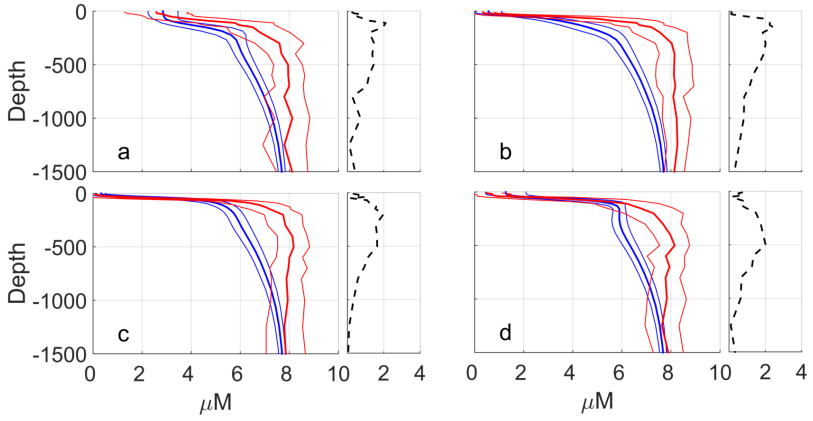

Figure 17. Seasonal ~~climatologies~~ climatological data over the 2000-2011 period of modeled (blue lines) and observed (red lines) concentrations in nitrate (μmol l^{-1}) at the DyFaMed site. (a) winter (Dec.-Feb.); (b) spring (Mar.-May); (c) summer (Jun.-Aug.); (d) autumn (Sept.-Nov.). Dotted lines on right panels represent the mean absolute bias between model and data.

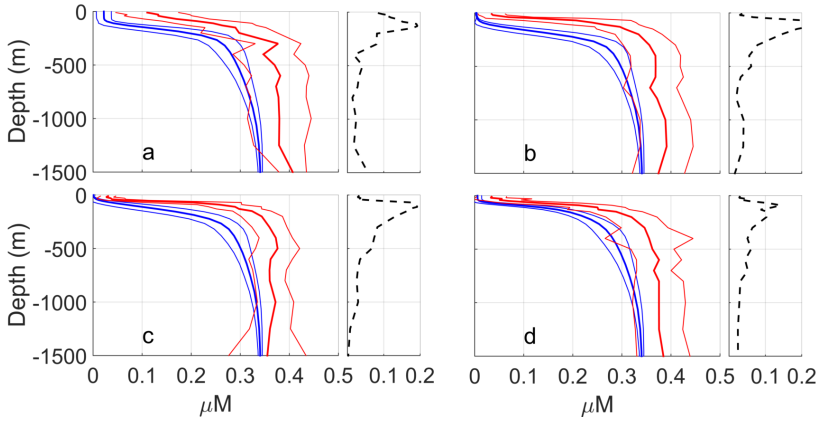

Figure 18. Seasonal climatologies of modeled (blue lines) and observed (red lines) concentrations in phosphate (μmol l^{-1}) at the DyFaMed site. (a) winter (Dec.-Feb.); (b) spring (Mar.-May); (c) summer (Jun.-Aug.); (d) autumn (Sept.-Nov.). Dotted lines on right panels represent the mean absolute bias between model and data.

along the western coast of the Adriatic Sea and in the Gulf of Gabes. For the Dardanelles Strait, the difference is likely due to a poor representation of the nutrients inputs at this boundary. For the Adriatic Sea, nutrient inputs from rivers are included in the model, but not the ones inferred by anthropic activities (domestic, industrial, agriculture), which may result in an underestimation of the nutrient inputs in this region, and therefore in an underestimation of the chlorophyll concentrations. Finally, the differences between mCHL and oCHL in the Gulf of Gabes is likely due to two main features: first, this region is very shallow, which may produce less reliable satellite data. More importantly, the region of Gabes is characterized by an important industrial production of phosphate which efflu-

Table 2. Mean over the 2000-2011 period of modeled (mNO_3, mPO_4) and measured (oNO_3, oPO_4) nutrients concentrations at the DyFaMed site for different layers. Root Mean Squared Difference (RMSD) between model outputs and observations have been calculated. Std stands for standart deviation. Spatial variability around the DyFaMed grid point is also assessed through the spatial standart deviation calculated using the 8 neighbour points (first column), and the value given in the table (first column) is the highest deviation calculated during the 2000-2011 period.

			NO_3			
	Spatial Std	mNO_3 mean [range]	mNO_3 Std	oNO_3 mean [range]	oNO_3 Std	RMSD
0-30	0.22	1.3 [0.04-4.3]	1.1	1.0 [BQL-5.2]	1.4	1.1
30-100	0.32	3.0 [0.09 6.1]	1.3	3.8 [BQL-8.3]	2.2	1.8
100-250	0.25	5.1 [1.7-6.7]	1.0	7.0 [2.7-9.6]	1.4	1.4
250-500	0.13	6.2 [5.2-7.2]	0.39	8.1 [5.0-9.9]	0.8	2.0
1000-2000	0.03	7.6 [7.0-7.9]	0.21	8.0 [5.9-9.4]	0.75	0.81
			PO_4			
	Spatial Std	mPO_4 mean [range]	mPO_4 Std	oPO_4 mean [range]	oPO_4 Std	RMSD
0-30	0.001	0.008 [0-0.08]	0.12	1.0 [BQL-0.26]	0.06	0.07
30-100	0.02	0.02 [0-0.19]	0.03	0.14 [BQL-0.54]	0.10	0.16
100-250	0.03	0.15 [0.02-0.33]	0.09	0.29 [0.07-0.45]	0.07	0.17
250-500	0.001	0.29 [0.19-0.33]	0.03	0.35 [0.01-0.46]	0.05	0.08
1000-2000	0.001	0.34 [0.32-0.35]	0.01	0.37 [0.21-0.52]	0.05	0.05

ents induce a strong enrichment in phosphate in this region, and this is not included in the model. Apart from these permanent features, the main differences between the model and satellite data are observed in the deep convection region of the Liguro-Provencal sub-basin (and extending up to the Ligurian Sea), along the Algerian coast, in the Alboran Sea, and in the south of the eastern basin. The three former are mostly attributable to failures of the hydrodynamic model: first, the fact that the contours of the modeled deep convection region are not the same as the measured ones have already been identified in the hydrodynamical simulation (Beuvier, 2011). Moreover, differences between measured and modeled MLD can also explain differences in the annual surface chlorophyll pattern as for example in the Ligurian Sea where an underestimation of the maximum mNO3 and mPO4 values, likely due to a deficit in the inputs of nutrients from deep waters during winter convection have been evidenced at DyFaMed station (see Fig. 16). The same is true for the Algerian current which is underestimated by the physical model (Soto-Navarro et al., 2014). As a consequence, when the Atlantic waters arrive north of Algeria and Tunisia, they are more nutrient-depleted (and therefore less productive) than what is observed. Furthermore, the Atlantic waters that flow along the coast are less dense and therefore strongly isolated from the rest of the water column and it seems

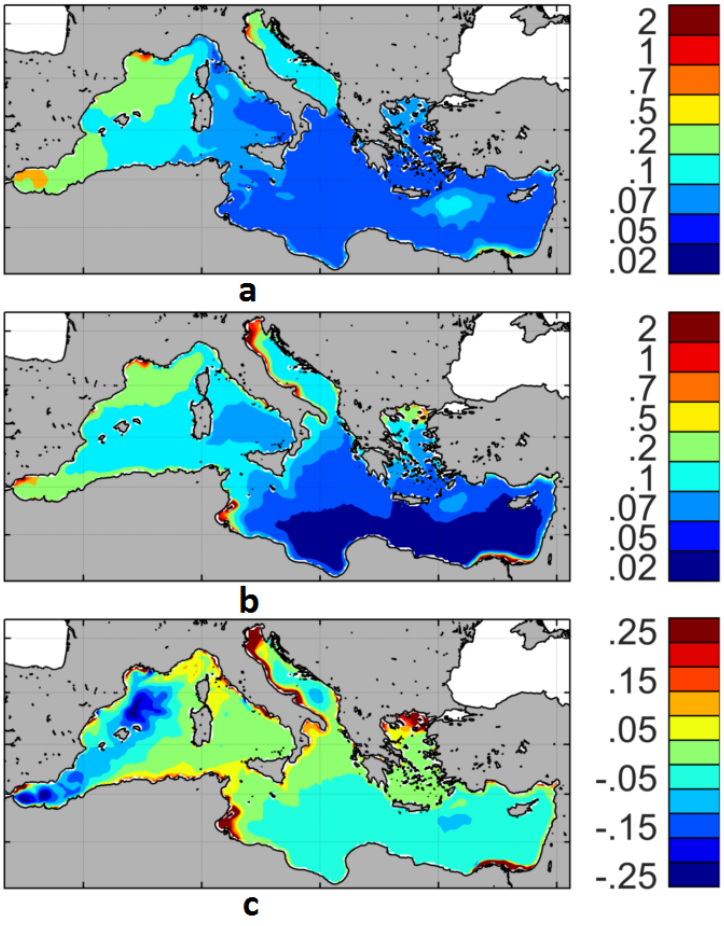

Figure 19. Maps of mean annual surface chlorophyll concentrations (μg l^{-1}) (a) from satellite (i.e. oCHL), (b) from model (i.e. mCHL), and (c) the difference oCHL - mCHL. Model chlorophyll (mCHL) is averaged over the first 10 m of the water column. Period used is 2002-2011 for both model outputs and satellite data.

that this property is excessively pronounced in the physical model (Beuvier, 2011). As a result, their nutrients content will be too rapidly consumed leading to underestimated primary production and Chl concentrations in this region. Finally, in the Alboran Sea, the high mesoscale activity is ~~likely~~ probably not fully captured by the ~~hydrodynamical~~ hydrodynamic model. In the eastern basin, ~~the~~ mCHL is overestimated nearly everywhere, and mostly in the southern part. This difference is however very weak (less than 0.05 μg l^{-1}) and does not clearly appear in the ~~climatology~~ climatological data presented in Fig. 20. Overall, and apart from the hot spots already discussed, the maximum absolute error does not exceed 0.25 μg l^{-1} in the chlorophyll-rich regions of the western basin (i.e. the deep convection region and the core of the eddies in the Alboran Sea) and 0.15(0.05) μg l^{-1} elsewhere in the western (eastern) basin.

In conclusion, though the aforementioned discrepancies between mCHL and oCHL, the model is able to track the location of: i) most of the major productive areas (except the missing regions for which an explanation has already been put forward, ii) a well-marked Liguro-Provencal bloom, which is, nevertheless, more ~~intense~~ intensive and more ~~expanded~~ extensive in the model, iii) a clearly visible weakly productive northern current (NC), and iv) a patch with high chlorophyll concentrations in the Rhodes Gyre.

A2.2 Seasonal surface variability

To further study the seasonal variability of surface chorophyll, we used (for the satellite and model derived chlorophyll concentrations) the metric ΔChl defined as follows :

$$\Delta Chl = \frac{\max(Chl_{\text{year}})}{\text{median}(Chl_{\text{year}})} \tag{A1}$$

Since chlorophyll time distribution does not follow a normal law, this indicator is ~~likely~~ probably more relevant than the mean and the standard deviation. Moreover, since it is applied to ~~a climatology~~ climatological data of chlorophyll outputs, extreme values have already been smoothed. High values of ΔChl can therefore be related to a strong seasonal variability, while low values, typically < 2, can be associated with a constant signal (Fig. 20).

For both model and satellite, the seasonal signal is particularly ~~important~~ strong in the Liguro-Provencal sub-basin ($\Delta Chl > 10$) and the Algerian Coast (ΔChl_{sat} about 8, ΔChl_{mod} above 10). ΔChl is broadly above 6 for the model and 4 for satellite data in the western basin west of 9°W. In the Tyrrhenian Sea, ΔChl is close to zero for the model, except for the area along the Italian Coast, while ΔChl for satellite data, it is above 3, with a maximum value around 6.

In the eastern basin, model ΔChl is almost nil everywhere except in the Rhodes Gyre (> 10) and in the Adriatic Sea where two patches of values above 10 can be seen. ~~This is consistent with~~ oCHL values ~~which~~ are also low, except in the south ~~Levantine~~ Ionian basin (where $\Delta Chl \approx$ ~~about~~ 2), ~~in~~ the Rhodes Gyre ~~(> 6)~~ and ~~in~~ the Gulf of Gabes ($\Delta Chl > 6$). In the Adriatic sea, a patch of values of ΔChl above 3 is visible in the south.

Using SeaWiFS and MODIS surface chlorophyll data from 1998 to 2010 and ~~the~~ statistical work from D'Ortenzio and Ribera d'Alcalà (2009), Lavigne et al. (2013) identified 9 different regions on the basis of the seasonality of the chlorophyll signal. These regions are consistent with ~~the ones~~ those emerging from the present study. The north-west bloom region is associated with the region of the highest values of ΔChl_{mod} and ΔChl_{sat}. The Algerian region is characterized by relatively high ΔChl values, while the intermittent Rhodes Gyre region is identified as highly variable in the present study according to satellite data and model outputs. The distinction between the ~~South and North~~ southern and northern Ionian basins in the bioregionalization, also visible satellite ΔChl is however absent in the model ΔChl.

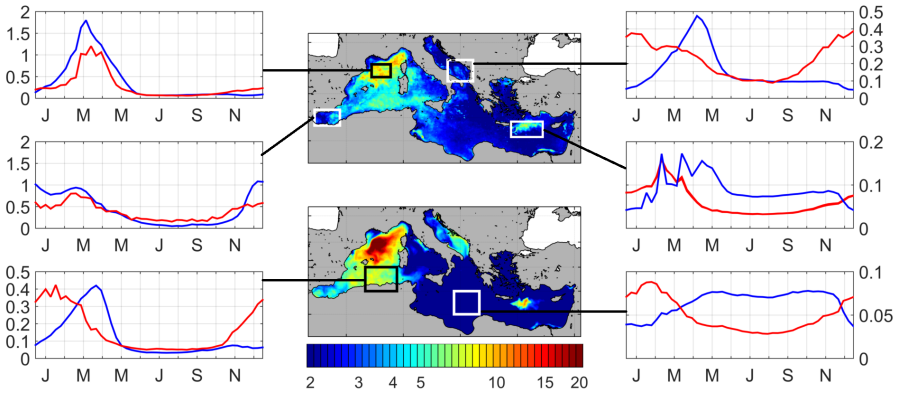

Figure 20. Maps of the ratio ΔChl (Eq. A1) between annual maximum and annual median for satellite (top) and model (bottom) chlorophyll surface concentrations over the 2002-2011 period. A climatology of oCHL (red lines) and mCHL (blue lines) over the same period is also plotted for the most representative regions.

The comparison of modeled and observed time series (climatological data ~~climatology~~ over the 2000-2011 period) provides ~~an~~ additional information on the modeli's ability to reproduce surface chlorophyll seasonal variations. Though the model values of the central eastern basin are within the range of observations in the open sea (see Fig. 19), the highest discrepancy in the seasonal signal is observed in the oligotrophic region of the Levantine basin: the mCHL seasonal signal is in phase opposition with that of oCHL, ~~'s one,~~ and the maximum mCHL ~~are~~ is obtained in summer-autumn against winter for oCHL. Comparison between models ~~intercomparison~~ is beyond the scope of this paper, however comparisons with former simulations (Lazzari et al., 2012; Mattia et al., 2013) can ~~give~~ offer some information. It is noteworthy that results from Mattia et al. (2013) showed a ~~more important~~ greater bias in the eastern basin than in the western basin, with higher annual concentrations compared to satellite measurements. However, the maximum of surface chlorophyll in the eastern basin was simulated in winter (as for satellite chlorophyll) in Mattia et al. (2013). This is also the case in the simulation ~~runned~~ run by Lazzari et al. (2012), however summer concentrations seemed to be underestimated in that case. This shortcoming can however be largely relativized by the fact that the mean surface chlorophyll in summer-autumn does not differ significantly from the satellite measurement. Furthermore, surface chlorophyll in the model is estimated as the mean over the first 10 m of the water column, and therefore includes part of the chlorophyll gradient towards the Deep Chlorophyll Maximum (DCM) which is shallower than that ~~the~~ observed ~~one~~ in the eastern basin during the stratification period (results not shown though the same bias is observed at the DyFaMed site, see Appendix A2.3). Finally, the summer functioning of the surface layer is well reproduced by the model : small phytoplankton are largely dominant and maintain their activity ~~thanks to~~ because of the microbial loop (Siokou-Frangou et al., 2010).

A shift in chlorophyll maximum can also be seen in the south of the western basin, with an earlier and longer bloom in oCHL than in mCHL. This could be partly due to the ~~already~~ aforementioned ~~model~~ tendency of the model to exagerate the isolation of the surface Atlantic waters from the rest of the water column, thus delaying the input of nutrients from deep water through winter convection. Finally, in the Adriatic Sea, a delayed input of nutrients from deep waters combined with the presence of two eddies with high core mCHL values in winter and mostly in spring that are not observed on oCHL (the position of the two eddies can be seen on the primary production map in Fig. 22), ~~likely~~ probably explains the shift between oCHL and mCHL. Conversely, in regions associated with high nutrient inputs (Ligurian Sea, Alboran Sea) the temporal ~~evolution~~ pattern of change of surface chlorophyll is reproduced by the model but concentrations are overestimated during the bloom in the deep convection region, ~~likely~~ probaly due to ~~a~~ too ~~intense~~ intensive winter mixing (Beuvier, 2011).

A2.3 Vertical variability

At the DyFaMed station, ~~a~~ strong seasonal variability in chlorophyll concentrations can be observed in both model outputs and in situ data (Marty et al., 2002; Marty and Chiavérini, 2010). Chlorophyll data (oCHL) and modeled ~~ones~~ data (mCHL) are mutually consistent ~~with each other~~ as shown in Fig. 21: they both show a bloom occurring in late February early March after the period of maximum mixing (mid February in this area), and characterized by high chlorophyll concentrations ~~inside~~ within the mixing layer (down to 150 m depth). A second less intense and shallower bloom often follows in April, characterized by chlorophyll concentrations above 1.5 μg l^{-1} in both model outputs and observations. During summer, surface concentrations are at their lowest level with values of mChl and oChl often below 0.1 μg l^{-1}, while their maximum values are observed in early spring.

Following April, a DCM is visible in both observations and model, though it is shallower in the model and its intensity decreases more rapidly than in observations (see Fig. 21-top).

However, when looking at the two chlorophyll contributors of the model, it appears that the position of the DCM associated with large phytoplankton is close to that ~~the~~ observed. ~~one.~~ This means that the difference in the DCM depth is ~~likely~~ probably due to the underestimation of large phytoplankton concentrations at depth by the model during summer, that may be inferred by the already identified underestimation by the model of nutrient stocks in the intermediate layer (see section A1.1).

A3 Primary production

In the following section, mIPP refers to the modeled integrated Gross Primary Production, i.e. to the total amount of inorganic carbon fixed by the two phytoplankton groups integrated over the water column. The equivalent for observations will be referred to as oIPP.

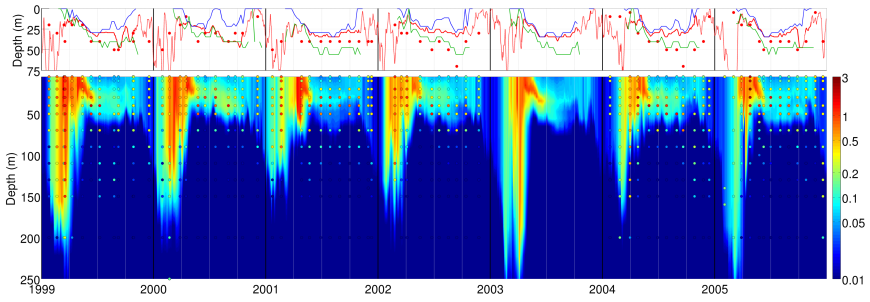

Figure 21. Patterns of change over time ~~evolution~~ of vertical concentrations of chlorophyll (μg l^{-1}) at the DyFaMed site, with model outputs in shaded colors and in situ data (Marty et al., 2008) in colored dots. ~~On~~ Top, the depth of chlorophyll maximum is represented with red dots for in situ data and the red line for the model. Depths of maximum chlorophyll for small phytoplankton (blue) and large plankton (green) are also plotted.

A3.1 Spatial variability

The mean annual mIPP ~~of~~ for the whole basin over the 2000-2012 period equals 82 gC m^{-2} y^{-1}, which is within the range of published values (see Table 3). In this table, the studies by Bosc et al. (2004) and Uitz et al. (2012) ~~studies~~ both show quite similar oIPP spatial distributions despite the two analyses having been conducted during different periods (1997-2001 for Bosc et al. (2004) and 1998-2007 for Uitz et al. (2012)). IPP calculated by Bosc et al. (2004) tend to overestimate observations, particularily in ultra-oligotrophic regions ~~, but~~ while IPP from Uitz et al. (2012) does not show a trend of error. In the different geographical regions defined in Bosc et al. (2004) and reported in Tab. 3, mIPP is mostly within the range defined by the two aforementioned studies. More importantly, the hierarchy in terms of IPP values between the different regions is ~~similar between~~ the same for the model and the satellite products. ~~In the western basin, the level of productivity of the different regions is the same, with the exception of the Algero-Provencal basin which is the less productive in both satellite products.~~

mIPP values in the Mediterranean Sea range between 35.4 and 270 gC m^{-2} y^{-1}, showing a strong spatial heterogeneity (see Fig. 22a). A gradient in mIPP is observed from west to east : the western basin production is almost twice that of the eastern basin, which is coherent with the dissimilarity in chlorophyll and nutrients already mentioned. This ratio is also coherent with the oIPP values derived from in situ measurements (Moutin and Raimbault, 2002), but higher than that found using ~~the~~ satellite data (Uitz et al., 2012; Bosc et al., 2004) or another model (Lazzari et al., 2012).

Figure 22b shows that, except in the regions that benefit from permanent or episodic nutrient inputs from the deep sea (i.e. the deep convection region in the Liguro-Provencal sub-basin, eddies in the Alboran, Adriatic Seas and the Rhodes Gyre region), mIPP is mostly due to small phytoplankton ~~in all~~ throughout the Mediterranean Basin. In the eastern basin, the proportion of IPP due to small

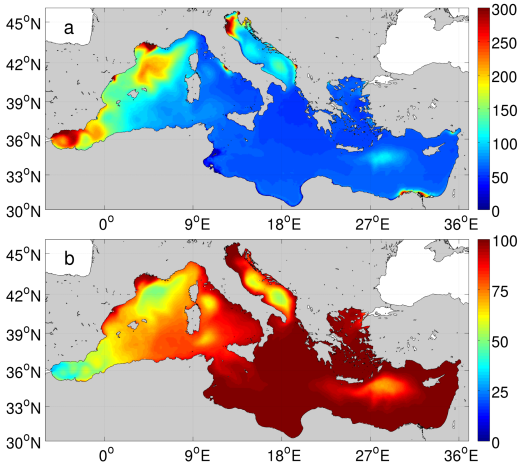

Figure 22. (a) Annual gross primary production calculated over the 2000-2012 period and integrated ~~along~~ through the whole water column, in gC m^{-2} y^{-1}, (b) proportion of production due to small phytoplankton group, in % .

phytoplankton is close to 100% everywhere, except in the Levantine basin in the region of the Rhodes Gyre. These results are consistent with in situ studies (Siokou-Frangou et al., 2010; MERMEX-group, 2011).

A3.2 Seasonal variability

In addition to satellite data, in situ oIPP measured at the DyFaMed station between 2002 and 2006 (Marty et al., 2008) were used for comparison with mIPP (Fig. 23). The model and observations show very similar patterns, with a maximum in March-April, and a slight decrease from July to December. The correlation between mIPP and oIPP is ~~significative~~ significant as suggested by the right panel in Fig. 23, and does not show any bias though the model fails ~~in reproducing~~ to reproduce the highest oIPP values.

Table 3. Integrated gross primary production ~~in~~ (IPP in gC m^{-2} y^{-1}) for the different regions defined by Bosc et al. (2004) and for ~~of~~ the whole Mediterranean Basin. ~~Sea~~. mIPP values calculated by the model ~~and~~ are compared to IPP values derived from the following references: (a) Bosc et al. (2004), (b) Uitz et al. (2012) (c) Antoine et al. (1995), (d) Lazzari et al. (2012), and (e) Sournia (1973). References (a) to (c) refer to satellite data, (d) to another modeling study, and (e) to a climatology of ^{14}C measurements

Region	Model (mIPP)	(a)	(b)	(c)	(d)	(e)
Alboran Sea	222	150	230			
Gulf of Lion	182	97	194			
Balearic Sea	145	80	167			
Algero-Provencal basin	123	78	153			
Ligurian Sea	109	80	165			
Algerian basin	107	78	163			
Adriatic Sea	102	71	182			
Tyrrhenian Sea	66	67	137			
South Levantine basin	65	59	105			
North Levantine basin	63	60	106			
South Ionian Sea	60	61	115			
North Ionian Sea	55	63	126			
Mediterranean Basin	82	68	136	156	98	80-90

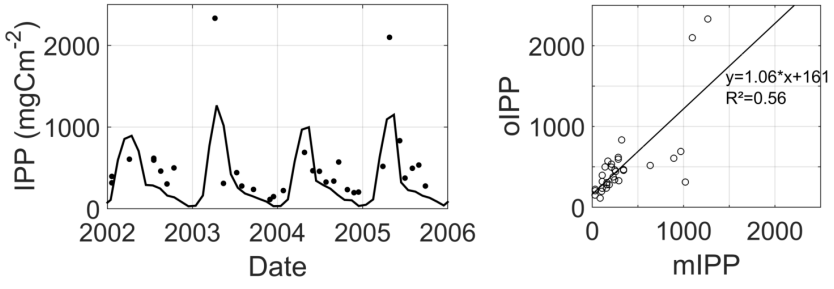

Figure 23. Patterns of change over time ~~Time evolution~~ of monthly integrated gross primary production (IPP) in mg C^{-2} d^{-1}. oIPP correspond to 0-100 m in situ measurements extracted from the DyFaMed database (dots) and mIPP correspond to the 0-100 m IPP provided by the model during the same period (black line). oIPP were converted to daily gross primary production according to the Moutin et al. (1999) method.

A4 Dissolved organic carbon

Regular measurements of total DOC (i.e. including refractory (RDOC) and semi-refractory (SR-DOC) pools) performed at the DyFaMed site (Avril, 2002), were used for comparison. Since the model only provides the labile and semi-labile DOC pools, the in situ DOC concentration measured in deep water ($>$ 1000 m), which can be considered as refractory DOC, has been added to the model DOC output. Moreover, since our run does not cover the period of the in situ data, we decided to work on a ~~climatology~~ climatological survey of DOC vertical profiles: bi-monthly mean, ~~maximal and minimal~~ maximum and minimum DOC values were calculated and compared (Fig. 24).

At the DyFaMed grid point, mDOC stock is underestimated ~~over~~ throughout the whole water column during winter. Then, mDOC and oDOC increase during spring (April-May), but only near ~~close to~~ the surface for mDOC. In summer, the mDOC and oDOC values remain high in the upper layers, and finally decrease in autumn. If these seasonal variations are well reproduced by the model, high differences can however be seen between mDOC and oDOC. If we first focus on the 0-100 m layer, DOC concentrations and seasonal variations of both the model and observations are ~~maximal~~ at a maximum at the surface, but from spring to autumn, mDOC is higher than oDOC near the surface (roughly in the 0-50 m layer), and lower between 50 and 100 m depth, resulting in higher vertical DOC gradients in the model. The same discrepancy can also be evidenced (mostly in the western basin) from the comparison between mDOC and oDOC during the BOUM cruise that took place in summer (Fig. 25). The overestimated near-surface DOC concentrations may be attributable to an excessive P-limitation in the model, ~~likely~~ probably due to too low phosphate deep concentrations (see also ~~the Discussion~~ section 4.3 for the description of the DOC accumulation process under P depletion). The shallower and underestimated DCM as compared to that ~~the~~ measured ~~one~~ (see section A2.3) may also partly explain ~~part of~~ the discrepancy since photosynthesis rates are underestimated. As a consequence, the excess of newly synthetized carbon through photosynthesis which fuels the DOC pool is probably ~~likely~~ underestimated in the region of the modeled DCM and even below. ~~the modeled DCM. A t~~ Too easy access for bacteria to SLDOC, resulting in ~~an~~ overcomsuption of DOC by nutrient-replete bacteria, is another possible explanation of this bias.

mDOC concentrations are systematically lower than those of oDOC ~~ones~~ beyond 100 m depth. The latter argument relative to SLDOC access by bacteria could also partly explain the systematically underestimated mDOC concentrations below 100 m depth. Again, this model failure is also observed ~~in~~ during the BOUM cruise (Fig. 25).

~~However, t~~ The comparison between oDOC and mDOC requires the addition of an unknown DOC component, namely the semi-refractory and the refractory pools, to the mDOC value. It is indeed generally assumed that both these pools are constant across the water column and that they correspond to the deep DOC concentration (i.e. 40 μM at DyFaMed station), but this is a clear source of bias, especially below 100 m depth where the SRDOC concentrations are significant ~~is significative~~ and may vary, as suggested in Santinelli et al. (2010).

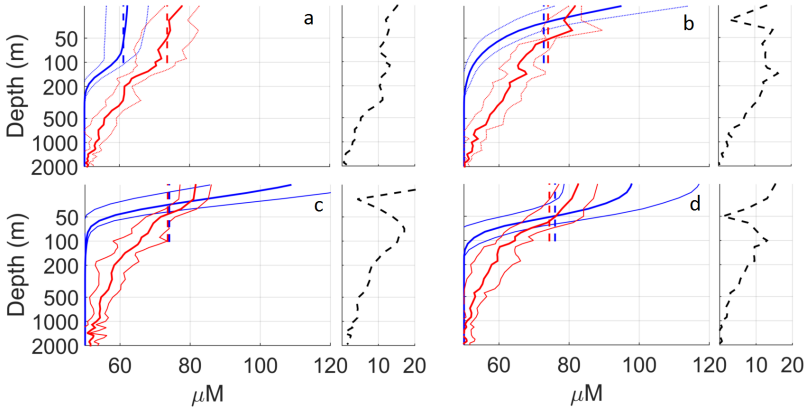

Figure 24. Vertical profiles of total DOC (μmol l^{-1}) at DyFaMed site (a) in winter, (b) spring, (c) summer and (d) autumn. mDOC are weekly averaged outputs. Blue and red lines respectively refer to modeled (mDOC) and measured (oDOC) DOC. Thick lines represent the mean of DOC over the period, while thin lines represent the standard deviation for each depth. oDOC and mDOC respectively cover the 1991-1993 (Avril, 2002) and the 2000-2012 simulation period. The dotted lines in the right panels represent the mean absolute bias between oDOC and mDOC.

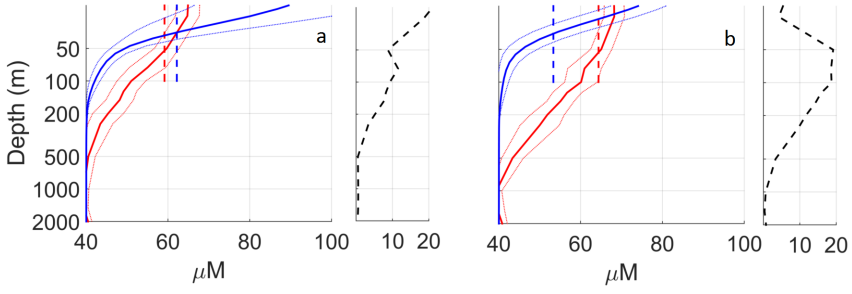

Figure 25. Vertical profiles of total DOC (μmol l^{-1}) during the BOUM cruise. mDOC are weekly averaged outputs over the whole BOUM section. Blue and red lines respectively refer to modeled (mDOC) and measured (oDOC) DOC. Thick lines represent the mean of DOC over the period, while thin lines represent the standard deviation for each depth. The dotted lines in the right panels represent the mean absolute bias between oDOC and mDOC.

The fact that the modeled 0-100 m integrated stocks are quite similar to the measured ones (though the slight underestimation in the eastern basin during the BOUM cruise since DOC accumulation has not yet reached its maximum value in summer) is however an essential point as regards the DOC export at 100 m.

Finally, the Taylor diagram presented in Fig. 26 ~~summerize~~ summarizes the numerous comparisons between model outputs and the DyFaMed station observations ~~that have been~~ undertaken in the present study.

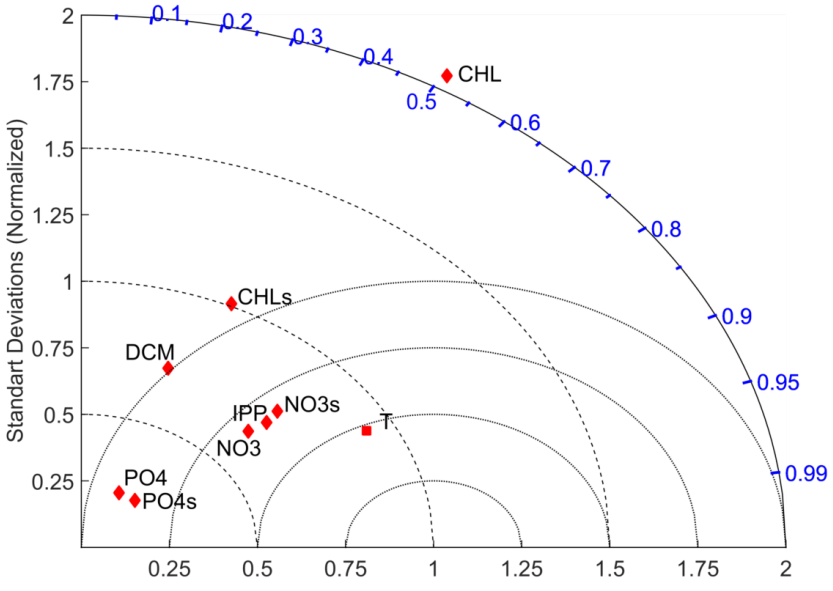

Figure 26. Taylor diagram of simulated and observed variables in the 0-100 m layer. Model outputs and in situ data are taken at the same depth and time. PO4s, NO3s and CHLs are surface concentrations of phosphate, nitrate and chlorophyll respectively. T refers to temperature. Chlorophyll concentrations are log-transformed.